Elsevier Editorial System(tm) for International Journal of Engineering Science
Manuscript Draft

Manuscript Number: IJES-D-10-00660

Title: A finite element model based on a coupled refined high-order global-local theory for static electromechanical response of smart multilayered/sandwich beams

Article Type: Full Length Article

Keywords: Finite element; piezoelectric; Laminated composite beams; Global-local theory; Transverse shear and normal stresses; Non-homogenous shear stress boundary conditions; Electric unknowns.

Corresponding Author: Dr bahram beheshti, Ph.D.

Corresponding Author's Institution:

First Author: Mojtaba Lezgy-Nazargah, Ph.D. Candidate

Order of Authors: Mojtaba Lezgy-Nazargah, Ph.D. Candidate; bahram beheshti, Ph.D.

Abstract: In the present study, a coupled refined high-order global-local theory is developed for predicting fully coupled behavior of smart multilayered/sandwich beams under electromechanical conditions. The proposed theory considers effects of transverse normal stress and transverse flexibility which is important for beams including soft cores or beams with drastic material properties changes through depth. Effects of induced transverse normal strains through the piezoelectric layers are also included in this study. In the presence of non-zero in-plane electric field component, all the kinematic and stress continuity conditions are satisfied at layer interfaces. In addition, for the first time, conditions of non-zero shear and normal tractions are satisfied even while the bottom or the top layer of the beam is piezoelectric
A combination of polynomial and exponential expressions with a layerwise term containing first order differentiation of electrical unknowns is used to introduce the in-plane displacement field. Also, the transverse displacement field is formulated utilizing a combination of continuous piecewise fourth-order polynomial with a layerwise representation of electrical unknowns. Finally, a quadratic electric potential is used across the thickness of each piezoelectric layer.
It is worthy to note that in the proposed shear locking-free finite element formulation, the number of mechanical unknowns is independent of the number of layers. Excellent correlation has been found between the results obtained from the proposed formulation for thin and thick piezoelectric beams with those resulted from the three-dimensional theory of piezoelasticity. Moreover, the proposed finite element model is computationally economic.

Dear Professor Kachanov,
The respected Editor-in-Chief,
International Journal of Engineering Science

Please kindly find our attached paper entitled ***"A finite element model based on a coupled refined high-order global-local theory for static electromechanical response of smart multilayered/sandwich beams"*** that is intended to be submitted to *International Journal of Engineering Science* as a *Research paper*, with many thanks.

The submitted paper is an original one which has neither previously, nor simultaneously, in whole or in part been submitted anywhere else.

Yours Sincerely,
S.Bahram Beheshti-Aval
Assistant Professor
Research and Development Deputy
Faculty of Civil Engineering
K.N. Toosi University of Technoogy, Tehran-Iran
E-mail addresses: *sb_beheshti@yahoo.com* and *beheshti@kntu.ac.ir*

***Title page with author information**

A finite element model based on a coupled refined high-order global-local theory for static electromechanical response of smart multilayered/sandwich beams

M. Lezgy-Nazargah[a], S.B. Beheshti-Aval[b]

[a]*Ph.D. Candidate, Civil Engineering Faculty, K.N. Toosi University of Technology, Tehran, Iran.*
Email:m.lezgy.n@gmail.com

[b]*Assistant Professor, Civil Engineering Faculty, K.N. Toosi University of Technology, Tehran, Iran.*
Fax: 0098(21)88779476, Tel: 0098(21)88786215, Email: beheshti@kntu.ac.ir and sb_beheshti@yahoo.com

A finite element model based on a coupled refined high-order global-local theory for static electromechanical response of smart multilayered/sandwich beams

Abstract

In the present study, a coupled refined high-order global-local theory is developed for predicting fully coupled behavior of smart multilayered/sandwich beams under electromechanical conditions. The proposed theory considers effects of transverse normal stress and transverse flexibility which is important for beams including soft cores or beams with drastic material properties changes through depth. Effects of induced transverse normal strains through the piezoelectric layers are also included in this study. In the presence of non-zero in-plane electric field component, all the kinematic and stress continuity conditions are satisfied at layer interfaces. In addition, for the first time, conditions of non-zero shear and normal tractions are satisfied even while the bottom or the top layer of the beam is piezoelectric

A combination of polynomial and exponential expressions with a layerwise term containing first order differentiation of electrical unknowns is used to introduce the in-plane displacement field. Also, the transverse displacement field is formulated utilizing a combination of continuous piecewise fourth-order polynomial with a layerwise representation of electrical unknowns. Finally, a quadratic electric potential is used across the thickness of each piezoelectric layer.

It is worthy to note that in the proposed shear locking-free finite element formulation, the number of mechanical unknowns is independent of the number of layers. Excellent correlation has been found between the results obtained from the proposed formulation for thin and thick piezoelectric beams with those resulted from the three-dimensional theory of piezoelasticity. Moreover, the proposed finite element model is computationally economic.

Keywords: Finite element; piezoelectric; Laminated composite beams; Global-local theory; Transverse shear and normal stresses; Non-homogenous shear stress boundary conditions; electric unknowns.

1. Introduction

Future engineering research is inclined toward structures that are able to sense, respond and minimize the effects of the applied disturbance on them. This class of structures is generally called smart structures. Piezoelectric materials have been widely used in the form of sensors and actuators in order to self-respond to structures. Thanks to small dimensions, it is possible to use many piezoelectric patches as sensors and actuators, without causing significant changes in dynamic properties of the main structure. In the application of sensors, mechanically induced deformations can be determined by measuring the induced electrical potential, whereas in the application of actuators, deformations can be controlled by introducing an appropriate electric potential. A comprehensive overview on applications of smart structures can be found in Chopra [1] and Gaudenzi [2].

Various mathematical models developed for structures containing piezoelectric sensors and actuators can be classified into two broad categories including induced strain models and coupled electromechanical models. The induced strain models use approximate theories in order to incorporate external forces associated with the piezoelectric actuators. The electric potential is neglected as a state variable in the formulation; therefore these models cannot capture the coupled mechanical and electrical responses and are only limited to predict the actuator behavior of piezoelectric materials (e.g., Crawley and de Luis [3], Tzou and Gadre [4], Wang and Rogers [5], Sung et al. [6]). Compared to the induced strain models, the coupled electromechanical models provide a more consistent representation of both the sensor and actuator responses of piezoelectric materials, incorporating both the displacements and the electric potentials as the state variables in the formulation. An overview on the modeling of piezoelectric structures is given in Benjeddou [7], and Saravanos and Heyliger [8].

The most accurate approach for coupled electromechanical analysis of the piezoelectric laminated structures is solving the governing differential equations of the three-dimensional (3D) theory of piezoelasticity (e.g., Brooks and Heyliger [9], Ray et al. [10-11]). However, development of these solutions is a difficult task and the resulted solution cannot be expressed in a closed form for the general cases of arbitrary geometry, boundary and loading conditions. Piezoelectric 3D finite element was proposed by Allik and Hughes [12], Tzou and Tseng [13], and Xu et al. [14]. However, the cost of the 3D finite element

analysis is relatively high, and it will become a problem when piezoelectric layers are thin compared to the structure size.

These drawbacks encouraged researchers to employ the two-dimensional (2D) models, prescribing variations of the displacement components and electric potential in the transverse direction. In the available 2D theories in the literature, the electric potential in the piezoelectric layers is mostly modeled by a layerwise approach (Reddy [15]). Concerning the mechanical displacement fields, 2D models can be classified into three broad groups: global or equivalent single layer theories (ESLT), local theories (e.g., layer-wise (LWT) theories), and global-local theories. In the following paragraphs these groups have been adequately reviewed.

In ESLT, the number of unknowns is independent of the number of layers, but continuity of transverse shear stresses is often violated at the layer interfaces. Thus, in some circumstances, classical (Hwang and Park [16]), Reissner-Mindlin-type first-order shear-deformation (Suleman and Venkaya [17], Sheikh et al. [18], Kogl and Bucalem [19-20]), and third-order shear deformation theories (Chee et al. [21], Jiang and Li [22], Shu [23], Thornburgh and Chattopadhyay [24], Fukunaga et al. [25], Mitchell and Reddy [26]) which are variants of the ESLT, may lead to inaccurate results.

In order to overcome the shortcoming of the ESLT, the idea of LWT or discrete-layer theory were presented by some researchers (Heyliger and Saravanos [27], Saravanos and Heyliger [28], Saravanos et al. [29], Kusculuoglu et al. [30], Garcia Lage et al. [31-32], Robaldo et al. [33], Tzou and Ye [34]). The displacement field across the thickness of each ply was approximated by a piecewise continuous function. In spite of the fact that LWT reduces the restrictions of ESLT, in these types of theories the number of unknowns are dependent on the number of the layers which in turn, increases the computational cost of the analysis. In order to improve the accuracy of ESLT while avoiding the computational burden of the LWT, zigzag (ZZ) theories were proposed by some researchers. These theories are able to reproduce piecewise continuous displacement and transverse stress fields in the thickness direction of the laminated structures. Ambartsumyan [35] is pioneer in these types of approaches and many extensions have been proposed to extend Ambartsumyan's work to generally laminated configurations. ZZ theories were used and developed by researcher such as Whitney [36], Icardi [37-38], Reissner [39], Murakami [40-41], Carrera [42-43] (see [44]). Oh and Cho [45] proposed a third order ZZ model for electromechanical problems of multilayer plates. Kapuria [46], Kapuria et al. [47], and Kapuria and Alam [48] introduced an efficient coupled ZZ theory for the static and dynamic analysis of piezoelectric laminated\sandwich beams based on third order ZZ approximations. Polit and Touratier [49], and Dau et al. [50] presented a ZZ theory for the analysis of the laminated plates\shells based on sine function. The extension of this ZZ theory to the piezoelectric effect was carried out by Ossadzow-David and Touratier [51], and Fernandes and Pouget [52] using an analytical approach. By introducing a layer refinement in the kinematics, Vidal and Polit [53] enriched the ZZ sinus model and introduced a family of sinus finite elements for the analysis of rectangular laminated beams. The coupling with the piezoelectric effect is provided by Beheshti-Aval and Lezgy-Nazargah [54-55]. For the most recent works on piezoelectric ZZ models, readers can refer to D'Ottavio and Kröplin [56], and Carrera and Nali [57].

Based on the double superposition of the local components of the in-plane displacements on the global ones, Li and Liu [58] proposed the first global-local laminate theory. Using this theory, the in-plane stresses and transverse shear stresses can be well estimated from the constitutive equations. Shariyat [59] extended the double superposition theory of Li and Liu, and proposed a generalized global-local higher order theory for the composite laminates. This generalized global-local higher order theory satisfies the transverse shear and normal stresses continuity at the interfaces. Lezgy-Nazargah et al. [60-61] introduced a computationally low cost refined global-local theory for the analysis of multilayered\sandwich beams based on an exponential function. In addition to ensure continuity conditions of the displacements and the transverse shear stresses at the layer interfaces, the non-uniform non-homogenous boundary conditions of the transverse shear stresses on the upper and lower surfaces of the beam are also satisfied in the works of these researchers. Zhen and Wanji [62] have extended the global-local laminate theory of Li and Liu for the electromechanical analysis of laminated piezoelectric plates. An excellent review in theories and computational models for laminated piezoelectric beams, plates, and shells has been provided by Saravanos and Heyligher [8].

Most of the studies on the analysis of laminated structures containing piezoelectric layers neglect the in-plane electric field components. Due to direct piezoelectric effect or applying non-uniform actuation potential along longitudinal direction (e.g., in using segmented piezoelectric actuator layers), these electric field components are not zero and should be considered in the analysis. In some limited studies which the non-zero in-plane electric field components have been considered in the formulation, the boundary conditions of the transverse shear stresses at the top and bottom surfaces of the piezoelectric layers are not exactly satisfied [21-22, 54]. In addition to the aforementioned drawback, the available laminated piezoelectric beam/plate theories either do not consider the transverse flexibility or do not impose the continuity conditions of the

transverse normal stresses at the interfaces [45-46]. However, the transverse normal stresses and strains and the transverse flexibility have important roles in the analysis of such structures, especially those with soft cores.

To overcome restrictions of the available theories, in the present study, a coupled refined high-order global-local laminate theory is developed based on the double superposition hypothesis for the static analysis of piezoelectric laminated/sandwich composite beams. In the presence of non-zero longitudinal electric field, the presented theory not only satisfies the continuity conditions of the transverse shear stresses at the top and bottom surfaces of the piezoelectric layers but also the non-homogenous shear traction conditions are exactly satisfied. The boundary conditions of normal tractions are also fulfilled on the upper and lower surfaces of the beam. Besides, continuity conditions of the displacement components, transverse normal stresses, and the transverse normal stress gradient at the layer interfaces are satisfied. This novel coupled refined global-local theory is also able to capture the transverse normal strains induced through the piezoelectric layers. With the exception of the coupled discrete layer theory of Saravanos and Heyliger [8, 27-29] and coupled ZZ theory of Kapuria [46-48], all of the theories described above have discarded the transverse strains due to electric potential, while these strains have significant effects on the electromechanical response of piezoelectric laminated structures under electrical loadings. To the best knowledge of the authors, this work is the first numerical experience for the analysis of smart laminated composite and sandwich beams including both electric transverse strains and transverse flexibility effects.

In the proposed model, the in-plane displacement component is described by a combination of polynomial and exponential expressions with a layerwise term which contains first order differentiation of electrical unknowns. A combination of continuous piecewise fourth-order polynomial with a layerwise representation of electrical unknowns is assumed for the transverse displacement component. Concerning the electric part, a quadratic electric potential has been considered across the thickness direction of the piezoelectric layers. Having some novel features, the present model is computationally significantly economic and has finally one mechanical independent generalized unknown parameter more than FSDT.

Based on the proposed model, a three nodded shear locking-free beam element is employed. The element has C^0-continuity except for in-plane variations of the transverse deflection which has C^1. The virtual work principle leads to a derivation that could include dynamic analysis. However, in this study only static problems have been considered. Various validation examples are examined using a written computer code whose algorithm is based on the present model. The obtained numerical results exhibit a good agreement with the 3D exact piezoelasticity solutions and the coupled 3D finite element (ABAQUS) results.

2. Mathematical formulation

2.1. Geometry and coordinate system

The considered piezoelectric beam is a prismatic one with a rectangular uniform cross section of height *h* and width *b*. The beam is made of N_l layers of different linearly elastic materials. Each layer may be piezoelectric (actuators/sensors) or non-piezoelectric. The geometric parameters of the laminated beam and the chosen Cartesian coordinate system (x, y, z) are shown in Fig. 1. As it may be noted from Fig. 1, the x, y and z axes are respectively along the length, width and thickness of the piezoelectric beam. Since it is intended to develop a global-local beam theory, transverse global and local coordinate systems shown in Fig. 2 are chosen for the present piezoelectric beam model.

2.2. Constitutive coupled equations

In this model the non-piezoelectric materials is assumed to be orthotropic and the general type of piezoelectric materials is 'orthorhombic-class *mm2*'. Concerning this assumption, the constitutive equations of piezoelectric materials in their global material coordinate system can be expressed as:

$$\begin{Bmatrix} \sigma_{xx} \\ \sigma_{yy} \\ \sigma_{zz} \\ \tau_{yz} \\ \tau_{xz} \\ \tau_{xy} \end{Bmatrix} = \begin{bmatrix} c_{11} & c_{12} & c_{13} & 0 & 0 & c_{16} \\ c_{12} & c_{22} & c_{23} & 0 & 0 & c_{26} \\ c_{13} & c_{23} & c_{33} & 0 & 0 & c_{36} \\ 0 & 0 & 0 & c_{44} & c_{45} & 0 \\ 0 & 0 & 0 & c_{45} & c_{55} & 0 \\ c_{16} & c_{26} & c_{36} & 0 & 0 & c_{66} \end{bmatrix} \begin{Bmatrix} \varepsilon_{xx} \\ \varepsilon_{yy} \\ \varepsilon_{zz} \\ \gamma_{yz} \\ \gamma_{xz} \\ \gamma_{xy} \end{Bmatrix} - \begin{bmatrix} 0 & 0 & e_{31} \\ 0 & 0 & e_{32} \\ 0 & 0 & e_{33} \\ e_{14} & e_{24} & 0 \\ e_{15} & e_{25} & 0 \\ 0 & 0 & e_{36} \end{bmatrix} \begin{Bmatrix} E_x \\ E_y \\ E_z \end{Bmatrix} \tag{1}$$

$$\begin{Bmatrix} D_x \\ D_y \\ D_z \end{Bmatrix} = \begin{bmatrix} 0 & 0 & 0 & e_{14} & e_{15} & 0 \\ 0 & 0 & 0 & e_{24} & e_{25} & 0 \\ e_{31} & e_{32} & e_{33} & 0 & 0 & e_{36} \end{bmatrix} \begin{Bmatrix} \varepsilon_{xx} \\ \varepsilon_{yy} \\ \varepsilon_{zz} \\ \gamma_{yz} \\ \gamma_{xz} \\ \gamma_{xy} \end{Bmatrix} + \begin{bmatrix} \chi_{11} & \chi_{12} & 0 \\ \chi_{12} & \chi_{22} & 0 \\ 0 & 0 & \chi_{33} \end{bmatrix} \begin{Bmatrix} E_x \\ E_y \\ E_z \end{Bmatrix}$$

(2)

In a piezoelectric laminated/sandwich beam with small width, the following assumptions are made:

$$\sigma_{yy} \cong 0, \quad \tau_{yz} \cong 0, \quad \tau_{xy} \cong 0, \quad E_y \cong 0 \tag{3}$$

Using the conditions (3) and using the static condensation procedure, the constitutive relations (1) and (2) could be expressed as:

$$\begin{aligned} \boldsymbol{\sigma} &= \overline{\boldsymbol{C}}\boldsymbol{\varepsilon} - \bar{\boldsymbol{e}}^{\boldsymbol{T}}\boldsymbol{E} \\ \boldsymbol{D} &= \bar{\boldsymbol{e}}\boldsymbol{\varepsilon} + \bar{\boldsymbol{\chi}}\boldsymbol{E} \end{aligned} \tag{4}$$

where

$$\boldsymbol{\sigma} = \begin{Bmatrix} \sigma_{xx} \\ \sigma_{zz} \\ \tau_{xz} \end{Bmatrix} \quad , \quad \boldsymbol{\varepsilon} = \begin{Bmatrix} \varepsilon_{xx} \\ \varepsilon_{zz} \\ \gamma_{xz} \end{Bmatrix} \quad , \quad \boldsymbol{D} = \begin{Bmatrix} D_x \\ D_z \end{Bmatrix} \quad , \quad \boldsymbol{E} = \begin{Bmatrix} E_x \\ E_z \end{Bmatrix}$$

$$\overline{\boldsymbol{C}} = \begin{bmatrix} \bar{c}_{11} & \bar{c}_{13} & 0 \\ \bar{c}_{13} & \bar{c}_{33} & 0 \\ 0 & 0 & \bar{c}_{55} \end{bmatrix} = \begin{bmatrix} c_{11} & c_{13} & 0 \\ c_{13} & c_{33} & 0 \\ 0 & 0 & c_{55} \end{bmatrix} - \begin{bmatrix} c_{16} & 0 & c_{12} \\ c_{36} & 0 & c_{23} \\ 0 & c_{45} & 0 \end{bmatrix} \begin{bmatrix} c_{66} & 0 & c_{26} \\ 0 & c_{44} & 0 \\ c_{26} & 0 & c_{22} \end{bmatrix}^{-1} \begin{bmatrix} c_{16} & c_{36} & 0 \\ 0 & 0 & c_{45} \\ c_{12} & c_{23} & 0 \end{bmatrix}$$

$$\bar{\boldsymbol{e}} = \begin{bmatrix} 0 & 0 & \bar{e}_{15} \\ \bar{e}_{31} & \bar{e}_{33} & 0 \end{bmatrix} = \begin{bmatrix} 0 & 0 & e_{15} \\ e_{31} & e_{33} & 0 \end{bmatrix} - \begin{bmatrix} 0 & e_{14} & 0 \\ e_{36} & 0 & e_{32} \end{bmatrix} \begin{bmatrix} c_{66} & 0 & c_{26} \\ 0 & c_{44} & 0 \\ c_{26} & 0 & c_{22} \end{bmatrix}^{-1} \begin{bmatrix} c_{16} & c_{36} & 0 \\ 0 & 0 & c_{45} \\ c_{12} & c_{23} & 0 \end{bmatrix}$$

$$\bar{\boldsymbol{\chi}} = \begin{bmatrix} \bar{\chi}_{11} & 0 \\ 0 & \bar{\chi}_{33} \end{bmatrix} = \begin{bmatrix} \chi_{11} & 0 \\ 0 & \chi_{33} \end{bmatrix} + \begin{bmatrix} 0 & e_{14} & 0 \\ e_{36} & 0 & e_{32} \end{bmatrix} \begin{bmatrix} c_{66} & 0 & c_{26} \\ 0 & c_{44} & 0 \\ c_{26} & 0 & c_{22} \end{bmatrix}^{-1} \begin{bmatrix} 0 & e_{36} \\ e_{14} & 0 \\ 0 & e_{32} \end{bmatrix}$$

2.3. Approximation of electric potential

Based on the successful experience of Kogl and Bucalem [19-20], in this study the following quadratic electric potential has been considered across the thickness direction of the *k-th* piezoelectric layer:

$$\phi^k(x,y,z,t) = L_1^k(z)\phi_b^k(x,t) + L_3^k(z)\phi_c^k(x,t) + L_2^k(z)\phi_t^k(x,t) \tag{5}$$

where $\phi_b^k(x,t)$, $\phi_c^k(x,t)$ and $\phi_t^k(x,t)$ denote the electric potential at the bottom, center and top of the *k-th* piezoelectric layer, respectively. $L_j^k(z)$ $(j = 1,2,3)$ are the interpolation functions as follows:

$$L_1^k(z) = -\frac{1}{2}\bar{z}_k(1-\bar{z}_k) \ , \ L_3^k(z) = (1+\bar{z}_k)(1-\bar{z}_k) \ , \ L_2^k(z) = \frac{1}{2}\bar{z}_k(1+\bar{z}_k) \tag{6}$$

where $\bar{z}_k = a_k z - b_k$, $a_k = \dfrac{2}{z_{k+1} - z_k}$, $b_k = \dfrac{z_{k+1} + z_k}{z_{k+1} - z_k}$

The electric field components can be related to the electric potential using the following relations:

$$\boldsymbol{E}^k = \begin{bmatrix} E_x^k \\ E_z^k \end{bmatrix} = \begin{Bmatrix} -\dfrac{\partial \phi^k}{\partial x} \\ -\dfrac{\partial \phi^k}{\partial z} \end{Bmatrix} = -\begin{bmatrix} L_1^k(z)\dfrac{d}{dx} & L_3^k(z)\dfrac{d}{dx} & L_2^k(z)\dfrac{d}{dx} \\ \dfrac{dL_1^k}{dz} & \dfrac{dL_2^k}{dz} & \dfrac{dL_3^k}{dz} \end{bmatrix} \begin{Bmatrix} \phi_b^k \\ \phi_c^k \\ \phi_t^k \end{Bmatrix} \tag{7}$$

2.4. Approximation of displacement and strain fields

In the present study, the following refined high-order global-local displacement field is employed ($k=1,2,....,N_l$) [61]:

$$
\begin{aligned}
u^k(x,y,z,t) &= u_0(x,t) - z\,w_0(x,t)_{,x} + ze^{-2(z/h)^2}[\theta(x,t)+w_0(x,t)_{,x}] + \bar{u}_L^k(x,z,t) + \hat{u}_L^k(x,z,t) \\
w^k(x,y,z,t) &= w_0(x,t) + z\,w_1(x,t) + z^2\,w_2(x,t) + z^3\,w_3(x,t) + z^4\,w_4(x,t) \\
&\quad + \sum_{j=1}^{k-1}\psi_j(x,t)\,(z-z_{j+1})H(z-z_{j+1}) + \sum_{j=1}^{k-1}\Psi_j(x,t)\,(z-z_{j+1})^2 H(z-z_{j+1})
\end{aligned}
\tag{8}
$$

where H is Heaviside's function. The functions $u(x,y,z,t)$ and $w(x,y,z,t)$ represent the horizontal (in-plane) and vertical (transverse) displacement components, respectively. The $u_0(x,t)$, $w_0(x,t)$, $w_1(x,t)$, $w_2(x,t)$, $w_3(x,t)$ and $w_4(x,t)$ are global displacement parameters of the reference layer (e.g., the first layer). t is the time and $\theta(x,t)$ denotes the shear-bending rotation around the y axis. $\psi_j(x,t)$ and $\Psi_j(x,t)$ are functions to be determined as to fulfill the transverse normal stress and stress gradient continuity conditions at the laminate interfaces. The local components $\bar{u}_L^k$ and $\hat{u}_L^k$ can be chosen based on the layerwise variations concept. Therefore, if they are chosen as combinations of the Legendre polynomial to simplify the numerical integration process, one may write:

$$
\bar{u}_L^k(x,z,t) = \bar{z}_k\,u_1^k(x,t) + \frac{3\bar{z}_k^2-1}{2}\,u_2^k(x,t) \tag{9}
$$

$$
\hat{u}_L^k(x,z,t) = \frac{5\bar{z}_k^3-3\bar{z}_k}{2}\,u_3^k(x,t) \tag{10}
$$

Local variations of the transverse displacement component are represented by the two summations appeared in Eq. (8), employing a discrete-layer concept. The continuity conditions of the displacement components at the laminate interfaces should be satisfied. Due to using a layerwise description for the local term, the transverse displacement component satisfies the kinematic continuity condition automatically. By imposing the continuity conditions on the in-plane displacement component, the following two equations are resulted:

$$
\bar{u}_L^k = \bar{u}_L^{k-1} \quad , \quad k=2,...,N_l \tag{11}
$$

$$
\hat{u}_L^k = \hat{u}_L^{k-1} \quad , \quad k=2,...,N_l \tag{12}
$$

Eqs. (11) and (12) lead to the following equations:

$$
u_2^k = u_1^{k-1} + u_2^{k-1} + u_1^k \tag{13}
$$

$$
u_3^k = (-1)^{k-1}u_3^1 \tag{14}
$$

Since ZZ models based on constant transverse displacement assumption are able to estimate the transverse shear stresses of the piezoelectric multilayered structures accurately [51, 62], the simplifying assumption $w(x,y,z,t) = w_0(x,,t)$ is used in the computation of the transverse shear stress only to avoid the computational complexity. Hence, the transverse shear stress of the *k-th* layer may be determined from the following equation:

$$
\begin{aligned}
\tau_{xz}^{(k)}(z) &= G_k(e^{-2(z/h)^2} - 4(\frac{z}{h})^2 e^{-2(z/h)^2})(\theta + w_{0,x}) + G_k a_k u_1^k + 3G_k\bar{z}_k a_k u_2^k \\
&\quad + G_k(-\frac{3}{2}a_k + \frac{15}{2}a_k\bar{z}_k^2)u_3^k + \bar{e}_{15}^k(L_1^k(z)\,(\phi_b^k)_{,x} + L_3^k(z)\,(\phi_c^k)_{,x} + L_2^k(z)\,(\phi_t^k)_{,x})
\end{aligned}
\tag{15}
$$

where $G_k = \bar{c}_{55}^{(k)}$ is the transverse shear modulus of the *k-th* layer. By imposing the transverse shear stress continuity condition at the mutual interfaces of the adjacent layers, the following recursive condition is obtained:

$$
\begin{aligned}
&G_k(e^{-2(z_k/h)^2} - 4(\frac{z_k}{h})^2 e^{-2(z_k/h)^2})(\theta + w_{0,x}) + G_k a_k u_1^k - 3G_k a_k u_2^k + 6G_k a_k u_3^k \\
&+ \bar{e}_{15}^k(L_1^k(z_k)\,(\phi_b^k)_{,x} + L_3^k(z_k)\,(\phi_c^k)_{,x} + L_2^k(z_k)\,(\phi_t^k)_{,x}) = \\
&\quad G_{k-1}(e^{-2(z_k/h)^2} - 4(\frac{z_k}{h})^2 e^{-2(z_k/h)^2})(\theta + w_{0,x}) + G_{k-1}a_{k-1}u_1^{k-1} + 3G_{k-1}a_{k-1}u_2^{k-1} + 6G_{k-1}a_{k-1}u_3^{k-1} \\
&\quad + \bar{e}_{15}^{k-1}(L_1^{k-1}(z_k)\,(\phi_b^{k-1})_{,x} + L_3^{k-1}(z_k)\,(\phi_c^{k-1})_{,x} + L_2^{k-1}(z_k)\,(\phi_t^{k-1})_{,x})
\end{aligned}
\tag{16}
$$

Furthermore, the boundary conditions of the prescribed values of the shear tractions (that are generally non-zero values) on the top and bottom surfaces of the piezoelectric laminated/sandwich beam should be satisfied. Thus, the following two boundary conditions are obtained:

$$\tau_{xz}^{(1)}(z=-\frac{h}{2}) = G_1 a_1 u_1^1 - 3G_1 a_1 u_2^1 + 6G_1 a_1 u_3^1 + \bar{e}_{15}^1 (L_1^1(z_1)\ (\phi_b^1)_{,x} + L_3^1(z_1)\ (\phi_c^1)_{,x} + L_2^1(z_1)\ (\phi_t^1)_{,x}) = X^-(x,t) \tag{17}$$

$$\tau_{xz}^{(N_l)}(z=\frac{h}{2}) = G_{N_l} a_{N_l} u_1^{N_l} + 3G_{N_l} a_{N_l} u_2^{N_l} + 6G_{N_l} a_{N_l} u_3^{N_l} + \bar{e}_{15}^{N_l} (L_1^{N_l}(z_{N_l+1})\ (\phi_b^{N_l})_{,x} + L_3^{N_l}(z_{N_l+1})\ (\phi_c^{N_l})_{,x} + L_2^{N_l}(z_{N_l+1})\ (\phi_t^{N_l})_{,x}) = X^+(x,t) \tag{18}$$

where $X^-(x,t)$ and $X^+(x,t)$ are the prescribed shear tractions of the bottom and top surfaces of the beam, respectively. By using of Eqs. (13) and (16), the following recursive equations are obtained:

$$u_1^k = F_1^k(\theta + w_{0,x}) + F_2^k u_1^{k-1} + F_3^k u_2^{k-1} + F_4^k u_3^k + F_5^k (\phi_b^k)_{,x} + F_6^k (\phi_c^k)_{,x} + F_7^k (\phi_t^k)_{,x} + F_8^k (\phi_b^{k-1})_{,x} + F_9^k (\phi_c^{k-1})_{,x} + F_{10}^k (\phi_t^{k-1})_{,x} \tag{19}$$

$$u_2^k = H_1^k(\theta + w_{0,x}) + H_2^k u_1^{k-1} + H_3^k u_2^{k-1} + H_4^k u_3^k + H_5^k (\phi_b^k)_{,x} + H_6^k (\phi_c^k)_{,x} + H_7^k (\phi_t^k)_{,x} + H_8^k (\phi_b^{k-1})_{,x} + H_9^k (\phi_c^{k-1})_{,x} + H_{10}^k (\phi_t^{k-1})_{,x} \tag{20}$$

where the coefficients F_j^k and H_j^k are ($j = 1, 2, ..., 10$):

$$F_1^k = \frac{(e^{-2(z_k/h)^2} - 4(z_k/h)^2 e^{-2(z_k/h)^2})(G_k - G_{k-1})}{2G_k a_k}, \quad H_1^k = F_1^k$$

$$F_2^k = \frac{(-G_{k-1}a_{k-1} - 3G_k a_k)}{2G_k a_k}, \quad H_2^k = \frac{(-G_{k-1}a_{k-1} - G_k a_k)}{2G_k a_k}$$

$$F_3^k = \frac{(-3G_{k-1}a_{k-1} - 3G_k a_k)}{2G_k a_k}, \quad H_3^k = \frac{(-3G_{k-1}a_{k-1} - G_k a_k)}{2G_k a_k}$$

$$F_4^k = \frac{(6G_{k-1}a_{k-1} + 6G_k a_k)}{2G_k a_k}, \quad H_4^k = F_4^k$$

$$F_5^k = \frac{\bar{e}_{15}^k L_1^k(z_k)}{2G_k a_k}, \quad H_5^k = F_5^k$$

$$F_6^k = \frac{\bar{e}_{15}^k L_3^k(z_k)}{2G_k a_k}, \quad H_6^k = F_6^k$$

$$F_7^k = \frac{\bar{e}_{15}^k L_2^k(z_k)}{2G_k a_k}, \quad H_7^k = F_7^k$$

$$F_8^k = -\frac{\bar{e}_{15}^{k-1} L_1^{k-1}(z_k)}{2G_k a_k}, \quad H_8^k = F_8^k$$

$$F_9^k = -\frac{\bar{e}_{15}^{k-1} L_3^{k-1}(z_k)}{2G_k a_k}, \quad H_9^k = F_9^k$$

$$F_{10}^k = -\frac{\bar{e}_{15}^{k-1} L_2^{k-1}(z_k)}{2G_k a_k}, \quad H_{10}^k = F_{10}^k \tag{21}$$

Substituting Eq. (14) into Eq. (17) yields:

$$u_3^k = \frac{(-1)^{k-1}}{6G_1 a_1} X^- + \frac{(-1)^k}{6} u_1^1 + \frac{(-1)^{k-1}}{2} u_2^1 + (-1)^k \frac{\bar{e}_{15}^1 L_1^1(z_1)}{6G_1 a_1} (\phi_b^1)_{,x} + (-1)^k \frac{\bar{e}_{15}^1 L_3^1(z_1)}{6G_1 a_1} (\phi_c^1)_{,x} + (-1)^k \frac{\bar{e}_{15}^1 L_2^1(z_1)}{6G_1 a_1} (\phi_t^1)_{,x} \tag{22}$$

The above equation expresses u_3^k in terms of u_1^1, u_2^1, X^-, $(\phi_b^1)_{,x}$, $(\phi_c^1)_{,x}$ and $(\phi_t^1)_{,x}$. Substituting Eq. (22) into the recursive Eqs. (19) and (20) relates u_1^k and u_2^k to u_1^1, u_2^1, $(\theta + w_{0,x})$, X^-, $(\phi_b^i)_{,x}$, $(\phi_c^i)_{,x}$ and

$(\phi_t^i)_{,x}$ where $i=1,2,...,PN_l$ and PN_l denotes the number of piezoelectric layers. After calculating $u_1^{N_l}$, $u_2^{N_l}$ and $u_3^{N_l}$ from the recursive Eqs. (19), (20) and (22), respectively and substituting them into Eq. (18), u_2^1 can be eliminated. Thus, Eqs. (19), (20) and (22) can be rewritten as:

$$
\begin{aligned}
u_1^k(x,t) &= \alpha_1^k(\theta(x,t)+w_0(x,t)_{,x})+\beta_1^k u_1^1(x,t)\\
&\quad+\delta_1^k X^+(x,t)+\lambda_1^k X^-(x,t)+\sum_{i=1}^{PN_l}\left(\kappa_{1i}^k\phi_b^i(x,t)_{,x}+\mu_{1i}^k\phi_c^i(x,t)_{,x}+\vartheta_{1i}^k\phi_t^i(x,t)_{,x}\right)\\
u_2^k(x,t) &= \alpha_2^k(\theta(x,t)+w_0(x,t)_{,x})+\beta_2^k u_1^1(x,t)\\
&\quad+\delta_2^k X^+(x,t)+\lambda_2^k X^-(x,t)+\sum_{i=1}^{PN_l}\left(\kappa_{2i}^k\phi_b^i(x,t)_{,x}+\mu_{2i}^k\phi_c^i(x,t)_{,x}+\vartheta_{2i}^k\phi_t^i(x,t)_{,x}\right)\\
u_3^k(x,t) &= \alpha_3^k(\theta(x,t)+w_0(x,t)_{,x})+\beta_3^k u_1^1(x,t)\\
&\quad+\delta_3^k X^+(x,t)+\lambda_3^k X^-(x,t)+\sum_{i=1}^{PN_l}\left(\kappa_{3i}^k\phi_b^i(x,t)_{,x}+\mu_{3i}^k\phi_c^i(x,t)_{,x}+\vartheta_{3i}^k\phi_t^i(x,t)_{,x}\right)
\end{aligned}
\tag{23}
$$

where coefficients $\alpha_1^k,\alpha_2^k,\alpha_3^k,\beta_1^k,\beta_2^k,\beta_3^k,\delta_1^k,\delta_2^k,\delta_3^k,\lambda_1^k,\lambda_2^k,\lambda_3^k,\kappa_{1i}^k,\kappa_{2i}^k,\kappa_{3i}^k,\mu_{1i}^k,\mu_{2i}^k,\mu_{3i}^k,\vartheta_{1i}^k,\vartheta_{2i}^k,\vartheta_{3i}^k$ are obtained from the procedure described above. These coefficients are only dependent on the material properties and the global coordinates of the layers.

The transverse normal stress and stress gradient in the *k-th* layer are determined from the following equations:

$$
\begin{aligned}
\sigma_{zz}^{(k)} &= \bar{c}_{13}^{(k)}\varepsilon_{xx}^{(k)}+\bar{c}_{33}^{(k)}\varepsilon_{zz}^{(k)}-\bar{e}_{33}^{(k)}E_z^{(k)}\\
&= \bar{c}_{13}^{(k)}(u_{0,x}-zw_{0,xx}+(\theta_{,x}+w_{,xx})J(z)+T(z)u_{1,x}^1+P(z)(X^+)_{,x}+R(z)(X^-)_{,x}\\
&\qquad+\sum_{i=1}^{PN_l}(O_{1i}^{elec}(z)(\phi_b^i)_{,xx}+O_{2i}^{elec}(z)(\phi_c^i)_{,xx}+O_{3i}^{elec}(z)(\phi_t^i)_{,xx}))\\
&\quad+\bar{c}_{33}^{(k)}(w_1+2zw_2+3z^2w_3+4z^3w_4+\sum_{j=1}^{k-1}\psi_j\ H(z-z_{j+1})+2\sum_{j=1}^{k-1}\Psi_j(z-z_{j+1})H(z-z_{j+1}))\\
&\quad+\bar{e}_{33}^{(k)}(\frac{dL_1^k(z)}{dz}\phi_b^k+\frac{dL_3^k(z)}{dz}\phi_c^k+\frac{dL_2^k(z)}{dz}\phi_t^k)
\end{aligned}
\tag{24}
$$

$$
\begin{aligned}
\sigma_{zz,z}^{(k)} &= \bar{c}_{13}^{(k)}(-w_{0,xx}+(\theta_{,x}+w_{0,xx})J(z)_{,z}+T(z)_{,z}u_{1,x}^1+P(z)_{,z}(X^+)_{,x}+R(z)_{,z}(X^-)_{,x}\\
&\qquad+\sum_{i=1}^{PN_l}(O_{1i}^{elec}(z)_{,z}(\phi_b^i)_{,xx}+O_{2i}^{elec}(z)_{,z}(\phi_c^i)_{,xx}+O_{3i}^{elec}(z)_{,z}(\phi_t^i)_{,xx}))\\
&\quad+\bar{c}_{33}^{(k)}(2w_2+6zw_3+12z^2w_4+2\sum_{j=1}^{k-1}\Psi_j H(z-z_{j+1}))\\
&\quad+\bar{e}_{33}^{(k)}(\frac{d^2L_1^k(z)}{dz^2}\phi_b^k+\frac{d^2L_3^k(z)}{dz^2}\phi_c^k+\frac{d^2L_2^k(z)}{dz^2}\phi_t^k)
\end{aligned}
\tag{25}
$$

where

$$J(z)=ze^{-2(z/h)^2}+\sum_{k=1}^{N_l}(\bar{z}_k\alpha_1^k+(-\frac{1}{2}+\frac{3\bar{z}_k^2}{2})\alpha_2^k+(-\frac{3\bar{z}_k}{2}+\frac{5\bar{z}_k^3}{2})\alpha_3^k)(H(z-z_k)-H(z-z_{k+1}))$$

$$T(z)=\sum_{k=1}^{N_l}(\bar{z}_k\beta_1^k+(-\frac{1}{2}+\frac{3\bar{z}_k^2}{2})\beta_2^k+(-\frac{3\bar{z}_k}{2}+\frac{5\bar{z}_k^3}{2})\beta_3^k)\times(H(z-z_k)-H(z-z_{k+1}))$$

$$P(z)=\sum_{k=1}^{N_l}(\bar{z}_k\delta_1^k+(-\frac{1}{2}+\frac{3\bar{z}_k^2}{2})\delta_2^k+(-\frac{3\bar{z}_k}{2}+\frac{5\bar{z}_k^3}{2})\delta_3^k)\times(H(z-z_k)-H(z-z_{k+1}))$$

$$R(z)=\sum_{k=1}^{N_l}(\bar{z}_k\lambda_1^k+(-\frac{1}{2}+\frac{3\bar{z}_k^2}{2})\lambda_2^k+(-\frac{3\bar{z}_k}{2}+\frac{5\bar{z}_k^3}{2})\lambda_3^k)\times(H(z-z_k)-H(z-z_{k+1}))$$

$$O_{1i}^{elec}(z)=\sum_{k=1}^{N_l}(\bar{z}_k\kappa_{1i}^k+(-\frac{1}{2}+\frac{3\bar{z}_k^2}{2})\kappa_{2i}^k+(-\frac{3\bar{z}_k}{2}+\frac{5\bar{z}_k^3}{2})\kappa_{3i}^k)\times(H(z-z_k)-H(z-z_{k+1}))$$

$$O_{2i}^{elec}(z)=\sum_{k=1}^{N_l}(\bar{z}_k\mu_{1i}^k+(-\frac{1}{2}+\frac{3\bar{z}_k^2}{2})\mu_{2i}^k+(-\frac{3\bar{z}_k}{2}+\frac{5\bar{z}_k^3}{2})\mu_{3i}^k)\times(H(z-z_k)-H(z-z_{k+1}))$$

$$O_{3i}^{elec}(z)=\sum_{k=1}^{N_l}(\bar{z}_k\vartheta_{1i}^k+(-\frac{1}{2}+\frac{3\bar{z}_k^2}{2})\vartheta_{2i}^k+(-\frac{3\bar{z}_k}{2}+\frac{5\bar{z}_k^3}{2})\vartheta_{3i}^k)\times(H(z-z_k)-H(z-z_{k+1})) \quad (26)$$

and $H(z)$ denotes Heaviside's function. Continuity of $\sigma_{zz,z}$ and σ_{zz} must be fulfilled at N_l-1 interfaces:

$$\sigma_{zz,z}^{(k+1)}(z_{k+1})=\sigma_{zz,z}^{(k)}(z_{k+1}) \quad , \quad k=1,2,...,N_l-1 \quad (27)$$

$$\sigma_{zz}^{(k+1)}(z_{k+1})=\sigma_{zz}^{(k)}(z_{k+1}) \quad , \quad k=1,2,...,N_l-1 \quad (28)$$

From the recursive Eqs. (27) and (28), $\psi_k(x,t)$ and $\Psi_k(x,t)$ will have the following form ($k=1,2,...,N_l-1$):

$$\begin{aligned}\Psi_k &= A_1^k w_{0,xx}+A_2^k w_2+A_3^k w_3+A_4^k w_4+A_5^k\theta_{,x}+A_6^k(u_1^1)_{,x}+A_7^k(X^+)_{,x}+A_8^k(X^-)_{,x}\\ &+\sum_{i=1}^{PN_l}(A_{3+6i}^k\phi_b^i+A_{4+6i}^k\phi_c^i+A_{5+6i}^k\phi_t^i+A_{6+6i}^k(\phi_b^i)_{,xx}+A_{7+6i}^k(\phi_c^i)_{,xx}+A_{8+6i}^k(\phi_t^i)_{,xx})\end{aligned} \quad (29)$$

$$\begin{aligned}\psi_k &= B_1^k w_{0,xx}+B_2^k w_1+B_3^k w_2+B_4^k w_3+B_5^k w_4+B_6^k(u_0)_{,x}+B_7^k\theta_{,x}+B_8^k(u_1^1)_{,x}+B_9^k(X^+)_{,x}+B_{10}^k(X^-)_{,x}\\ &+\sum_{i=1}^{PN_l}(B_{5+6i}^k\phi_b^i+B_{6+6i}^k\phi_c^i+B_{7+6i}^k\phi_t^i+B_{8+6i}^k(\phi_b^i)_{,xx}+B_{9+6i}^k(\phi_c^i)_{,xx}+B_{10+6i}^k(\phi_t^i)_{,xx})\end{aligned} \quad (30)$$

Moreover, the boundary conditions of the transverse normal stress and transverse normal stress gradient on the upper and lower faces should be satisfied:

$$\sigma_{zz,z}^{(N_l)}(z_{N_l+1})=\sigma_{zz,z}^{(1)}(z_1)=0 \quad (31)$$

$$\sigma_{zz}^{(1)}(z_1)=Z^-(x,t) \quad , \quad \sigma_{zz}^{(N_l)}(z_{N_l+1})=Z^+(x,t) \quad (32)$$

where $Z^-(x,t)$ and $Z^+(x,t)$ are the distributed lateral loads acting on the bottom and top surfaces of the beam, respectively. From Eqs. (31) and (32), the unknowns w_1, w_2, w_3 and w_4 can be expressed in terms of $u_{0,x}$, $w_{0,xx}$, $\theta_{,x}$, $(u_1^1)_{,x}$, $(X^+)_{,x}$, $(X^-)_{,x}$, Z^+, Z^-, ϕ_b^i, ϕ_c^i, ϕ_t^i, $(\phi_b^i)_{,xx}$, $(\phi_c^i)_{,xx}$ and $(\phi_t^i)_{,xx}$ $(i=1,2,...,PN_l)$:

$$\begin{aligned}w_1(x,t) &= \Theta_{11}^1(u_0)_{,x}+\Theta_{12}^1 w_{0,xx}+\Theta_{13}^1\theta_{,x}+\Theta_{14}^1(u_1^1)_{,x}+\Theta_{15}^1(X^+)_{,x}+\Theta_{16}^1(X^-)_{,x}+\Theta_{17}^1Z^++\Theta_{18}^1Z^-\\ &+\sum_{i=1}^{PN_l}(\Theta_{13+6i}^1\phi_b^i+\Theta_{14+6i}^1\phi_c^i+\Theta_{15+6i}^1\phi_t^i+\Theta_{16+6i}^1(\phi_b^i)_{,xx}+\Theta_{17+6i}^1(\phi_c^i)_{,xx}+\Theta_{18+6i}^1(\phi_t^i)_{,xx})\end{aligned} \quad (33)$$

$$\begin{aligned}w_2(x,t) &= \Theta_{21}^2(u_0)_{,x}+\Theta_{22}^2 w_{0,xx}+\Theta_{23}^2\theta_{,x}+\Theta_{24}^2(u_1^1)_{,x}+\Theta_{25}^2(X^+)_{,x}+\Theta_{26}^2(X^-)_{,x}+\Theta_{27}^2Z^++\Theta_{28}^2Z^-\\ &+\sum_{i=1}^{PN_l}(\Theta_{23+6i}^2\phi_b^i+\Theta_{24+6i}^2\phi_c^i+\Theta_{25+6i}^2\phi_t^i+\Theta_{26+6i}^2(\phi_b^i)_{,xx}+\Theta_{27+6i}^2(\phi_c^i)_{,xx}+\Theta_{28+6i}^2(\phi_t^i)_{,xx})\end{aligned} \quad (34)$$

$$\begin{aligned}w_3(x,t) &= \Theta_{31}^3(u_0)_{,x}+\Theta_{32}^3 w_{0,xx}+\Theta_{33}^3\theta_{,x}+\Theta_{34}^3(u_1^1)_{,x}+\Theta_{35}^3(X^+)_{,x}+\Theta_{36}^3(X^-)_{,x}+\Theta_{37}^3Z^++\Theta_{38}^3Z^-\\ &+\sum_{i=1}^{PN_l}(\Theta_{33+6i}^3\phi_b^i+\Theta_{34+6i}^3\phi_c^i+\Theta_{35+6i}^3\phi_t^i+\Theta_{36+6i}^3(\phi_b^i)_{,xx}+\Theta_{37+6i}^3(\phi_c^i)_{,xx}+\Theta_{38+6i}^3(\phi_t^i)_{,xx})\end{aligned} \quad (35)$$

$$\begin{aligned}w_4(x,t) &= \Theta_{41}^4(u_0)_{,x}+\Theta_{42}^4 w_{0,xx}+\Theta_{43}^4\theta_{,x}+\Theta_{44}^4(u_1^1)_{,x}+\Theta_{45}^4(X^+)_{,x}+\Theta_{46}^4(X^-)_{,x}+\Theta_{47}^4Z^++\Theta_{48}^4Z^-\\ &+\sum_{i=1}^{PN_l}(\Theta_{43+6i}^4\phi_b^i+\Theta_{44+6i}^4\phi_c^i+\Theta_{45+6i}^4\phi_t^i+\Theta_{46+6i}^4(\phi_b^i)_{,xx}+\Theta_{47+6i}^4(\phi_c^i)_{,xx}+\Theta_{48+6i}^4(\phi_t^i)_{,xx})\end{aligned} \quad (36)$$

By substituting Eqs. (33) to (36) into Eqs. (29) and (30), $\psi_k(x,t)$ and $\Psi_k(x,t)$ can be rewritten as follows ($k=1,2,...,N_l-1$):

$$\begin{aligned}\Psi_k(x,t) &= C_1^k(u_0)_{,x}+C_2^k w_{0,xx}+C_3^k\theta_{,x}+C_4^k(u_1^1)_{,x}+C_5^k(X^+)_{,x}+C_6^k(X^-)_{,x}+C_7^kZ^++C_8^kZ^-\\ &+\sum_{i=1}^{PN_l}(C_{3+6i}^k\phi_b^i+C_{4+6i}^k\phi_c^i+C_{5+6i}^k\phi_t^i+C_{6+6i}^k(\phi_b^i)_{,xx}+C_{7+6i}^k(\phi_c^i)_{,xx}+C_{8+6i}^k(\phi_t^i)_{,xx})\end{aligned} \quad (37)$$

$$\begin{aligned}\psi_k(x,t) &= D_1^k(u_0)_{,x}+D_2^k w_{0,xx}+D_3^k\theta_{,x}+D_4^k(u_1^1)_{,x}+D_5^k(X^+)_{,x}+D_6^k(X^-)_{,x}+D_7^kZ^++D_8^kZ^-\\ &+\sum_{i=1}^{PN_l}(D_{3+6i}^k\phi_b^i+D_{4+6i}^k\phi_c^i+D_{5+6i}^k\phi_t^i+D_{6+6i}^k(\phi_b^i)_{,xx}+D_{7+6i}^k(\phi_c^i)_{,xx}+D_{8+6i}^k(\phi_t^i)_{,xx})\end{aligned} \quad (38)$$

At this stage, all the mechanical unknowns of the displacement fields (Eq. 8) are determined in terms of four independent mechanical unknown parameters u_0, w_0, θ and u_1^1, and electrical unknowns ϕ_b^i, ϕ_c^i and ϕ_t^i

$(i=1,2,...,PN_l)$. Therefore, the final displacement fields of the proposed coupled refined high-order global-local theory can be written as:

$$u = u_0 - zw_{0,x} + (\theta + w_{0,x})J(z) + T(z)u_1^1 + P(z)(X^+) + R(z)(X^-) + \sum_{i=1}^{PN_l}(O_{1i}^{elec}(z)(\phi_b^i)_{,x} + O_{2i}^{elec}(z)(\phi_c^i)_{,x} + O_{3i}^{elec}(z)(\phi_t^i)_{,x})$$

$$w^k(x,y,z,t) = w_0(x,t) + \Delta_1^k(z)u_{0,x} + \Delta_2^k(z)w_{0,xx} + \Delta_3^k(z)\theta_{,x} + \Delta_4^k(z)(u_1^1)_{,x} + \Delta_5^k(z)(X^+)_{,x} + \Delta_6^k(z)(X^-)_{,x} + \Delta_7^k(z)Z^+ + \Delta_8^k(z)Z^- + \sum_{i=1}^{PN_l}(\Delta_{3+6i}^k\phi_b^i + \Delta_{4+6i}^k\phi_c^i + \Delta_{5+6i}^k\phi_t^i + \Delta_{6+6i}^k(\phi_b^i)_{,xx} + \Delta_{7+6i}^k(\phi_c^i)_{,xx} + \Delta_{8+6i}^k(\phi_t^i)_{,xx}) \quad (39)$$

where

$$\Delta_1^k(z) = \Theta_{11}^1 z + \Theta_{21}^2 z^2 + \Theta_{31}^3 z^3 + \Theta_{41}^4 z^4 + \sum_{j=1}^{k-1} D_1^j (z-z_{j+1})H(z-z_{j+1}) + \sum_{j=1}^{k-1} C_1^j (z-z_{j+1})^2 H(z-z_{j+1})$$

$$\Delta_2^k(z) = \Theta_{12}^1 z + \Theta_{22}^2 z^2 + \Theta_{32}^3 z^3 + \Theta_{42}^4 z^4 + \sum_{j=1}^{k-1} D_2^j (z-z_{j+1})H(z-z_{j+1}) + \sum_{j=1}^{k-1} C_2^j (z-z_{j+1})^2 H(z-z_{j+1})$$

$$\Delta_3^k(z) = \Theta_{13}^1 z + \Theta_{23}^2 z^2 + \Theta_{33}^3 z^3 + \Theta_{43}^4 z^4 + \sum_{j=1}^{k-1} D_3^j (z-z_{j+1})H(z-z_{j+1}) + \sum_{j=1}^{k-1} C_3^j (z-z_{j+1})^2 H(z-z_{j+1})$$

$$\Delta_4^k(z) = \Theta_{14}^1 z + \Theta_{24}^2 z^2 + \Theta_{34}^3 z^3 + \Theta_{44}^4 z^4 + \sum_{j=1}^{k-1} D_4^j (z-z_{j+1})H(z-z_{j+1}) + \sum_{j=1}^{k-1} C_4^j (z-z_{j+1})^2 H(z-z_{j+1})$$

$$\Delta_5^k(z) = \Theta_{15}^1 z + \Theta_{25}^2 z^2 + \Theta_{35}^3 z^3 + \Theta_{45}^4 z^4 + \sum_{j=1}^{k-1} D_5^j (z-z_{j+1})H(z-z_{j+1}) + \sum_{j=1}^{k-1} C_5^j (z-z_{j+1})^2 H(z-z_{j+1})$$

$$\Delta_6^k(z) = \Theta_{16}^1 z + \Theta_{26}^2 z^2 + \Theta_{36}^3 z^3 + \Theta_{46}^4 z^4 + \sum_{j=1}^{k-1} D_6^j (z-z_{j+1})H(z-z_{j+1}) + \sum_{j=1}^{k-1} C_6^j (z-z_{j+1})^2 H(z-z_{j+1})$$

$$\Delta_7^k(z) = \Theta_{17}^1 z + \Theta_{27}^2 z^2 + \Theta_{37}^3 z^3 + \Theta_{47}^4 z^4 + \sum_{j=1}^{k-1} D_7^j (z-z_{j+1})H(z-z_{j+1}) + \sum_{j=1}^{k-1} C_7^j (z-z_{j+1})^2 H(z-z_{j+1})$$

$$\Delta_8^k(z) = \Theta_{18}^1 z + \Theta_{28}^2 z^2 + \Theta_{38}^3 z^3 + \Theta_{48}^4 z^4 + \sum_{j=1}^{k-1} D_8^j (z-z_{j+1})H(z-z_{j+1}) + \sum_{j=1}^{k-1} C_8^j (z-z_{j+1})^2 H(z-z_{j+1})$$

$$\Delta_{3+6i}^k(z) = \Theta_{13+6i}^1 z + \Theta_{23+6i}^2 z^2 + \Theta_{33+6i}^3 z^3 + \Theta_{43+6i}^4 z^4 + \sum_{j=1}^{k-1} D_{3+6i}^j (z-z_{j+1})H(z-z_{j+1}) + \sum_{j=1}^{k-1} C_{3+6i}^j (z-z_{j+1})^2 H(z-z_{j+1})$$

$$\Delta_{4+6i}^k(z) = \Theta_{14+6i}^1 z + \Theta_{24+6i}^2 z^2 + \Theta_{34+6i}^3 z^3 + \Theta_{44+6i}^4 z^4 + \sum_{j=1}^{k-1} D_{4+6i}^j (z-z_{j+1})H(z-z_{j+1}) + \sum_{j=1}^{k-1} C_{4+6i}^j (z-z_{j+1})^2 H(z-z_{j+1})$$

$$\Delta_{5+6i}^k(z) = \Theta_{15+6i}^1 z + \Theta_{25+6i}^2 z^2 + \Theta_{35+6i}^3 z^3 + \Theta_{45+6i}^4 z^4 + \sum_{j=1}^{k-1} D_{5+6i}^j (z-z_{j+1})H(z-z_{j+1}) + \sum_{j=1}^{k-1} C_{5+6i}^j (z-z_{j+1})^2 H(z-z_{j+1})$$

$$\Delta_{6+6i}^k(z) = \Theta_{16+6i}^1 z + \Theta_{26+6i}^2 z^2 + \Theta_{36+6i}^3 z^3 + \Theta_{46+6i}^4 z^4 + \sum_{j=1}^{k-1} D_{6+6i}^j (z-z_{j+1})H(z-z_{j+1}) + \sum_{j=1}^{k-1} C_{6+6i}^j (z-z_{j+1})^2 H(z-z_{j+1})$$

$$\Delta_{7+6i}^k(z) = \Theta_{17+6i}^1 z + \Theta_{27+6i}^2 z^2 + \Theta_{37+6i}^3 z^3 + \Theta_{47+6i}^4 z^4 + \sum_{j=1}^{k-1} D_{7+6i}^j (z-z_{j+1})H(z-z_{j+1}) + \sum_{j=1}^{k-1} C_{7+6i}^j (z-z_{j+1})^2 H(z-z_{j+1})$$

$$\Delta_{8+6i}^k(z) = \Theta_{18+6i}^1 z + \Theta_{28+6i}^2 z^2 + \Theta_{38+6i}^3 z^3 + \Theta_{48+6i}^4 z^4 + \sum_{j=1}^{k-1} D_{8+6i}^j (z-z_{j+1})H(z-z_{j+1}) + \sum_{j=1}^{k-1} C_{8+6i}^j (z-z_{j+1})^2 H(z-z_{j+1}) \quad (40)$$

Using Cauchy's definition of the strain tensor, the in-plane, transverse shear and normal strain components may be calculated based on the proposed coupled global-local description of the displacement field as:

$$\varepsilon_{xx} = u_{0,x} - zw_{0,xx} + (\theta_{,x} + w_{0,xx})J(z) + T(z)u^1_{1,x} + P(z)(X^+)_{,x} + R(z)(X^-)_{,x} + \sum_{i=1}^{PN_l}(O^{elec}_{1i}(z)(\phi^i_b)_{,xx} + O^{elec}_{2i}(z)(\phi^i_c)_{,xx} + O^{elec}_{3i}(z)(\phi^i_t)_{,xx})$$

$$\varepsilon_{zz} = \Delta^k_1(z)_{,z}\, u_{0,x} + \Delta^k_2(z)_{,z}\, w_{0,xx} + \Delta^k_3(z)_{,z}\, \theta_{,x} + \Delta^k_4(z)_{,z}\,(u^1_1)_{,x} + \Delta^k_5(z)_{,z}\,(X^+)_{,x} + \Delta^k_6(z)_{,z}\,(X^-)_{,x} + \Delta^k_7(z)_{,z}\, Z^+ \Delta^k_8(z)_{,z}\, Z^- + \sum_{i=1}^{PN_l}((\Delta^k_{3+6i})_{,z}\,\phi^i_b + (\Delta^k_{4+6i})_{,z}\,\phi^i_c + (\Delta^k_{5+6i})_{,z}\,\phi^i_t + (\Delta^k_{6+6i})_{,z}\,(\phi^i_b)_{,xx} + (\Delta^k_{7+6i})_{,z}\,(\phi^i_c)_{,xx} + (\Delta^k_{8+6i})_{,z}\,(\phi^i_t)_{,xx})$$

$$\gamma_{xz} = (\theta + w_{0,x})J(z)_{,z} + T(z)_{,z}\, u^1_1 + P(z)_{,z}\, X^+ + R(z)_{,z}\, X^- + \sum_{i=1}^{PN_l}(O^{elec}_{1i}(z)_{,z}\,(\phi^i_b)_{,x} + O^{elec}_{2i}(z)_{,z}\,(\phi^i_c)_{,x} + O^{elec}_{3i}(z)_{,z}\,(\phi^i_t)_{,x}) \tag{41}$$

Since the functions $u(x,y,z,t)$ and $w(x,y,z,t)$ are coupled in the strain energy expression, it is expected that the presented coupled refined global-local theory compensates to some extent for the simplifying assumption $w(x,y,z,t) = w_0(x,,t)$ used only in the computation of the transverse shear stress.

3. Finite element model

In this section, a finite element representation of the displacement filed description given in Eq. (39) is introduced using appropriate shape functions and nodal variables. It can be seen that the expression of the strain energy (Eq. (41)) contains the second-order differentiation operators of w_0. Moreover, for more accurate results, the slope continuity of w_0 should be guaranteed. For these reasons, in-plane variations of w_0 should be C^1-continuous. Therefore, compatible Hermite cubic shape functions are employed to interpolate the in-plane variations of the transverse displacement component w_0. The rotation θ can be C^0-continuous but it is interpolated by quadratic Lagrangian shape functions to ensure obtaining more accurate results. Furthermore, if an identical order is adopted for the shape functions of both $w_{0,x}$ and θ parameters in the relevant transverse shear strain components, the shear locking phenomenon may be avoided due to using a consistent displacement field [53, 60-61]. Finally, u_0, u^1_1, X^+, X^-, Z^+, Z^-, ϕ^i_b, ϕ^i_c and ϕ^i_t may be interpolated using Lagrangian quadratic shape functions. The proposed piezoelectric beam element as well as its nodal degrees of freedom is shown in Fig. 3. As shown in this figure, the beam element has three nodes with a variable number of electric potential degrees of freedom at each node. In addition to the displacement and electrical unknown parameters, the transverse shear and normal stresses of the top and bottom layers are defined at the nodal points of the element. Therefore, interlaced discretization meshes are employed to present a mixed formulation (in the global sense). Based on Eqs. (5), (7), (39) and (41), the electric potential, displacements, strain and electric field components may be expressed in the following matrices form:

$$\begin{bmatrix}\boldsymbol{u}\\ \boldsymbol{\varphi}\end{bmatrix} = \begin{bmatrix}\boldsymbol{A}_{uu} & \boldsymbol{A}_{u\varphi}\\ \boldsymbol{0} & \boldsymbol{A}_{\varphi\varphi}\end{bmatrix}\begin{bmatrix}\boldsymbol{u}_u\\ \boldsymbol{u}_\varphi\end{bmatrix} \quad , \quad \begin{bmatrix}\boldsymbol{\varepsilon}\\ \boldsymbol{E}\end{bmatrix} = \begin{bmatrix}\boldsymbol{L}_{uu} & \boldsymbol{L}_{u\varphi}\\ \boldsymbol{0} & \boldsymbol{L}_{\varphi\varphi}\end{bmatrix}\begin{bmatrix}\boldsymbol{u}_u\\ \boldsymbol{u}_\varphi\end{bmatrix} \tag{42}$$

where $\boldsymbol{u} = \begin{bmatrix} u & w\end{bmatrix}^T$, $\boldsymbol{u}_u = \begin{bmatrix} u_0 & w_0 & \theta & u^1_1 & X^+ & X^- & Z^+ & Z^-\end{bmatrix}^T$, $\boldsymbol{\varphi} = \begin{bmatrix}\phi^i\end{bmatrix}^T$, $\boldsymbol{u}_{\boldsymbol{\varphi}} = \begin{bmatrix}\phi^i_b & \phi^i_c & \phi^i_t\end{bmatrix}^T$, $\boldsymbol{\varepsilon} = \begin{bmatrix}\varepsilon_{xx} & \varepsilon_{zz} & \gamma_{xz}\end{bmatrix}^T$, $\boldsymbol{E} = \begin{bmatrix}E_x & E_z\end{bmatrix}^T$, and

$$\boldsymbol{A}_{uu} = \begin{bmatrix} 1 & -z\dfrac{d}{dx} + J(z) & J(z) & T(z) & P(z) & R(z) & 0 & 0\\ \Delta^k_1(z)\dfrac{d}{dx} & 1 + \Delta^k_2(z)\dfrac{d^2}{dx^2} & \Delta^k_3(z)\dfrac{d}{dx} & \Delta^k_4(z)\dfrac{d}{dx} & \Delta^k_5(z)\dfrac{d}{dx} & \Delta^k_6(z)\dfrac{d}{dx} & \Delta^k_7(z) & \Delta^k_8(z)\end{bmatrix}$$

$$\boldsymbol{A}_{u\varphi} = \begin{bmatrix} O^{elec}_{1i}(z)\dfrac{d}{dx} & O^{elec}_{2i}(z)\dfrac{d}{dx} & O^{elec}_{3i}(z)\dfrac{d}{dx}\\ \Delta^k_{3+6i}(z) + \Delta^k_{6+6i}(z)\dfrac{d^2}{dx^2} & \Delta^k_{4+6i}(z) + \Delta^k_{7+6i}(z)\dfrac{d^2}{dx^2} & \Delta^k_{5+6i}(z) + \Delta^k_{8+6i}(z)\dfrac{d^2}{dx^2}\end{bmatrix}$$

$$\boldsymbol{A}_{\varphi\varphi}=\left[L^i_1(z)\quad L^i_3(z)\quad L^i_2(z)\right]$$

$$\boldsymbol{L}_{uu}=\begin{bmatrix} \frac{d}{dx} & -z\frac{d^2}{dx^2}+J(z)\frac{d}{dx} & J(z)\frac{d}{dx} & T(z)\frac{d}{dx} & P(z)\frac{d}{dx} & R(z)\frac{d}{dx} & 0 & 0 \\ \Delta^k_1(z)_{,z}\frac{d}{dx} & \Delta^k_2(z)_{,z}\frac{d^2}{dx^2} & \Delta^k_3(z)_{,z}\frac{d}{dx} & \Delta^k_4(z)_{,z}\frac{d}{dx} & \Delta^k_5(z)_{,z}\frac{d}{dx} & \Delta^k_6(z)_{,z}\frac{d}{dx} & \Delta^k_7(z)_{,z} & \Delta^k_8(z)_{,z} \\ 0 & J(z)_{,z}\frac{d}{dx} & J(z)_{,z} & T(z)_{,z} & P(z)_{,z} & R(z)_{,z} & 0 & 0 \end{bmatrix}$$

$$\boldsymbol{L}_{u\varphi}=\begin{bmatrix} O^{elec}_{1i}(z)\frac{d^2}{dx^2} & O^{elec}_{2i}(z)\frac{d^2}{dx^2} & O^{elec}_{3i}(z)\frac{d^2}{dx^2} \\ \Delta^k_{3+6i}(z)_{,z}+\Delta^k_{6+6i}(z)_{,z}\frac{d^2}{dx^2} & \Delta^k_{4+6i}(z)_{,z}+\Delta^k_{7+6i}(z)_{,z}\frac{d^2}{dx^2} & \Delta^k_{5+6i}(z)_{,z}+\Delta^k_{8+6i}(z)_{,z}\frac{d^2}{dx^2} \\ O^{elec}_{1i}(z)_{,z}\frac{d}{dx} & O^{elec}_{2i}(z)_{,z}\frac{d}{dx} & O^{elec}_{3i}(z)_{,z}\frac{d}{dx} \end{bmatrix}$$

$$\boldsymbol{L}_{\varphi\varphi}=-\begin{bmatrix} L^i_1(z)\frac{d}{dx} & L^i_3(z)\frac{d}{dx} & L^i_2(z)\frac{d}{dx} \\ \frac{dL^i_1(z)}{dz} & \frac{dL^i_3(z)}{dz} & \frac{dL^i_2(z)}{dz} \end{bmatrix}$$

The vector of displacement and electric potential components $\boldsymbol{u}_u$ and $\boldsymbol{u}_\varphi$ may be expressed in terms of the mechanical and electrical nodal variables vectors $\boldsymbol{u}^e_u$ and $\boldsymbol{u}^e_\varphi$ as follows:

$$\begin{bmatrix}\boldsymbol{u}_u\\ \boldsymbol{u}_\varphi\end{bmatrix}=\begin{bmatrix}\boldsymbol{N}_{uu} & \boldsymbol{0}\\ \boldsymbol{0} & \boldsymbol{N}_{\varphi\varphi}\end{bmatrix}\begin{bmatrix}\boldsymbol{u}^e_u\\ \boldsymbol{u}^e_\varphi\end{bmatrix} \tag{43}$$

where

$$\boldsymbol{u}^e_u=\Big\{(u_0)_1\quad (w_0)_1\quad \theta_1\quad (w_{0,x})_1\quad (u^1_1)_1\quad (X^+)_1\quad (X^-)_1\quad (Z^+)_1\quad (Z^-)_1\quad (u_0)_3\quad \theta_3\quad (u^1_1)_3$$
$$(X^+)_3\quad (X^-)_3\quad (Z^+)_3\quad (Z^-)_3\quad (u_0)_2\quad (w_0)_2\quad \theta_2\quad (w_{0,x})_2\quad (u^1_1)_2\quad (X^+)_2\quad (X^-)_2\quad (Z^+)_2\quad (Z^-)_2\Big\}^T$$

$$\boldsymbol{u}^e_\phi=\Big\{(\phi^i_b)_1\quad (\phi^i_c)_1\quad (\phi^i_t)_1\quad (\phi^i_b)_3\quad (\phi^i_c)_3\quad (\phi^i_t)_3\quad (\phi^i_b)_2\quad (\phi^i_c)_2\quad (\phi^i_t)_2\Big\}^T$$

$$\boldsymbol{N}_u=\begin{bmatrix} \overline{N}_1 & 0 & 0 & 0 & 0 & 0 & 0 & 0 & 0 & \overline{N}_3 & 0 & 0 & 0 \\ 0 & N_1 & 0 & Nd_1 & 0 & 0 & 0 & 0 & 0 & 0 & 0 & 0 & 0 \\ 0 & 0 & \overline{N}_1 & 0 & 0 & 0 & 0 & 0 & 0 & 0 & \overline{N}_3 & 0 & 0 \\ 0 & 0 & 0 & 0 & \overline{N}_1 & 0 & 0 & 0 & 0 & 0 & 0 & \overline{N}_3 & 0 \\ 0 & 0 & 0 & 0 & 0 & \overline{N}_1 & 0 & 0 & 0 & 0 & 0 & 0 & \overline{N}_3 \\ 0 & 0 & 0 & 0 & 0 & 0 & \overline{N}_1 & 0 & 0 & 0 & 0 & 0 & 0 \\ 0 & 0 & 0 & 0 & 0 & 0 & 0 & \overline{N}_1 & 0 & 0 & 0 & 0 & 0 \\ 0 & 0 & 0 & 0 & 0 & 0 & 0 & 0 & \overline{N}_1 & 0 & 0 & 0 & 0 \end{bmatrix}$$

$$\begin{bmatrix} 0 & 0 & 0 & \overline{N}_2 & 0 & 0 & 0 & 0 & 0 & 0 & 0 & 0 \\ 0 & 0 & 0 & 0 & N_2 & 0 & Nd_2 & 0 & 0 & 0 & 0 & 0 \\ 0 & 0 & 0 & 0 & 0 & \overline{N}_2 & 0 & 0 & 0 & 0 & 0 & 0 \\ 0 & 0 & 0 & 0 & 0 & 0 & 0 & \overline{N}_2 & 0 & 0 & 0 & 0 \\ 0 & 0 & 0 & 0 & 0 & 0 & 0 & 0 & \overline{N}_2 & 0 & 0 & 0 \\ \overline{N}_3 & 0 & 0 & 0 & 0 & 0 & 0 & 0 & 0 & \overline{N}_2 & 0 & 0 \\ 0 & \overline{N}_3 & 0 & 0 & 0 & 0 & 0 & 0 & 0 & 0 & \overline{N}_2 & 0 \\ 0 & 0 & \overline{N}_3 & 0 & 0 & 0 & 0 & 0 & 0 & 0 & 0 & \overline{N}_2 \end{bmatrix}$$

$$\boldsymbol{N}_{\varphi\varphi}=\begin{bmatrix}\overline{N}_1 & 0 & 0 & \overline{N}_3 & 0 & 0 & \overline{N}_2 & 0 & 0\\ 0 & \overline{N}_1 & 0 & 0 & \overline{N}_3 & 0 & 0 & \overline{N}_2 & 0\\ 0 & 0 & \overline{N}_1 & 0 & 0 & \overline{N}_3 & 0 & 0 & \overline{N}_2\end{bmatrix}$$

in which $\overline{N}_i$ $(i=1,2,3)$ are the Lagrangian quadratic shape functions defined as:

$$\overline{N}_1\equiv\overline{N}_1(\xi)=-\xi\,(1-\xi)/2\,,\qquad \overline{N}_2\equiv\overline{N}_2(\xi)=\xi\,(1+\xi)/2\,,\qquad \overline{N}_3\equiv\overline{N}_3(\xi)=(1+\xi)\,(1-\xi) \tag{44}$$

and the Hermitian shape functions are:

$$N_1=N_1(\xi)=\frac{1}{4}(1-\xi)^2(2+\xi)\,,\quad N_2=N_2(\xi)=\frac{1}{4}(2-\xi)(1+\xi)^2$$

$$Nd_1=Nd_1(\xi)=\frac{l_e}{8}(1-\xi)^2(1+\xi)\,,\quad Nd_2=Nd_2(\xi)=-\frac{l_e}{8}(1-\xi)(1+\xi)^2 \tag{45}$$

where ξ is the natural coordinate and l_e denotes the length of the element. Using Eqs. (42) and (43), the displacements, electric potential, strain and electric field vectors may be expressed as follows:

$$\begin{bmatrix}\boldsymbol{u}\\ \boldsymbol{\varphi}\end{bmatrix}=\begin{bmatrix}\boldsymbol{A}_{uu} & \boldsymbol{A}_{u\varphi}\\ \boldsymbol{0} & \boldsymbol{A}_{\varphi\varphi}\end{bmatrix}\begin{bmatrix}\boldsymbol{u}_u\\ \boldsymbol{u}_\varphi\end{bmatrix}=\begin{bmatrix}\boldsymbol{A}_{uu} & \boldsymbol{A}_{u\varphi}\\ \boldsymbol{0} & \boldsymbol{A}_{\varphi\varphi}\end{bmatrix}\begin{bmatrix}\boldsymbol{N}_{uu} & \boldsymbol{0}\\ \boldsymbol{0} & \boldsymbol{N}_{\varphi\varphi}\end{bmatrix}\begin{bmatrix}\boldsymbol{u}_u^e\\ \boldsymbol{u}_\varphi^e\end{bmatrix}=\mathscr{N}\,\boldsymbol{u}^e \tag{46}$$

$$\begin{bmatrix}\boldsymbol{\varepsilon}\\ \boldsymbol{E}\end{bmatrix}=\begin{bmatrix}\boldsymbol{L}_{uu} & \boldsymbol{L}_{u\varphi}\\ \boldsymbol{0} & \boldsymbol{L}_{\varphi\varphi}\end{bmatrix}\begin{bmatrix}\boldsymbol{u}_u\\ \boldsymbol{u}_\varphi\end{bmatrix}=\begin{bmatrix}\boldsymbol{L}_{uu} & \boldsymbol{L}_{u\varphi}\\ \boldsymbol{0} & \boldsymbol{L}_{\varphi\varphi}\end{bmatrix}\begin{bmatrix}\boldsymbol{N}_{uu} & \boldsymbol{0}\\ \boldsymbol{0} & \boldsymbol{N}_{\varphi\varphi}\end{bmatrix}\begin{bmatrix}\boldsymbol{u}_u^e\\ \boldsymbol{u}_\varphi^e\end{bmatrix}=\mathscr{B}\;\boldsymbol{u}^e \tag{47}$$

In Eq. (46), $\mathscr{N}$ denotes displacements and electric potential interpolation matrix. Strains and electric fields interpolation matrix is represented with $\mathscr{B}$.

The principle of virtual work is employed to extract governing equations of the piezoelectric beam element. According to this principle, for a piezoelectric medium of volume Ω and regular boundary surface Γ, one may write [7]:

$$\begin{aligned}\delta\Pi=\delta U-\delta W=&-\int_\Omega\boldsymbol{\delta\varepsilon}^T\boldsymbol{\sigma}\,d\Omega+\int_\Gamma\boldsymbol{\delta u}^T\boldsymbol{F}_S\,d\Gamma+\int_\Omega\boldsymbol{\delta u}^T\boldsymbol{F}_V\,d\Omega-\int_\Omega\rho\boldsymbol{\delta u}^T\ddot{\boldsymbol{u}}\,d\Omega\\&+\int_\Omega\delta\boldsymbol{E}^T\boldsymbol{D}\,d\Omega-\int_\Gamma\overline{Q}\,\delta\boldsymbol{\varphi}\,d\Gamma-\int_\Omega\overline{q}\,\delta\boldsymbol{\varphi}\,d\Omega=0\end{aligned} \tag{48}$$

where $\boldsymbol{F}_S$, $\boldsymbol{F}_V$, $\overline{q}$, $\overline{Q}$ and ρ are surface force vector, mechanical body force vector, electrical body charge, surface charge and mass density, respectively. $\delta\boldsymbol{u}$ and $\delta\boldsymbol{\varphi}$ are admissible virtual displacement and potential. Substituting Eqs. (4), (46) and (47) into Eq. (48), and assembling the element equations yields the following general dynamic equation of motion:

$$\boldsymbol{M}\ddot{\boldsymbol{q}}(t)+\boldsymbol{K}\boldsymbol{q}(t)=\boldsymbol{F}(t) \tag{49}$$

The matrices and vectors in the above equation are mass matrix $\boldsymbol{M}=\int_\Omega\rho\mathscr{N}^T\mathscr{N}\,d\Omega$, elastic matrix $\boldsymbol{K}=\int_\Omega\mathscr{B}^T\begin{bmatrix}\overline{\boldsymbol{C}} & -\overline{\boldsymbol{e}}^{\boldsymbol{T}}\\ \overline{\boldsymbol{e}} & \overline{\boldsymbol{\chi}}\end{bmatrix}\mathscr{B}\,d\Omega$, and loads vector $\boldsymbol{F}(t)=\int_\Omega\mathscr{N}^T\begin{bmatrix}\boldsymbol{F}_V\\ \overline{q}\end{bmatrix}d\Omega+\int_\Gamma\mathscr{N}^T\begin{bmatrix}\boldsymbol{F}_S\\ \overline{Q}\end{bmatrix}d\Gamma$. Eq. (49) can be partitioned and arranged as:

$$\begin{bmatrix}\boldsymbol{M}_{qq} & \boldsymbol{M}_{q\varphi}\\ \boldsymbol{M}_{\varphi q} & \boldsymbol{M}_{\varphi\varphi}\end{bmatrix}\begin{bmatrix}\ddot{\boldsymbol{q}}_u(t)\\ \ddot{\boldsymbol{q}}_\varphi(t)\end{bmatrix}+\begin{bmatrix}\boldsymbol{K}_{qq} & \boldsymbol{K}_{q\varphi}\\ \boldsymbol{K}_{\varphi q} & \boldsymbol{K}_{\varphi\varphi}\end{bmatrix}\begin{bmatrix}\boldsymbol{q}_u(t)\\ \boldsymbol{q}_\varphi(t)\end{bmatrix}=\begin{bmatrix}\boldsymbol{F}_u(t)\\ \boldsymbol{F}_\varphi(t)\end{bmatrix} \tag{50}$$

where $\boldsymbol{q}_u(t)$ and $\boldsymbol{q}_\varphi(t)$ are the vector of mechanical degrees of freedom and electrical degrees of freedom, respectively.

4. Numerical results and discussions

To assess the performance and the validity of the developed coupled theory, some examples of piezoelectric sandwich and laminated beams have been analyzed using the presented finite element model. The results of the present finite element are compared with the 3D exact piezoelasticity solution [9] and the 3D finite element (ABAQUS) results. The present numerical results are obtained from a MATLAB program whose algorithm is based on the theoretical formulation described in the previous section. The program

allows any element at any layer can be made of different materials (piezoelectric or non-piezoelectric). Note that the polarization of the piezoelectric materials is aligned in the transverse direction of each piezoelectric layer unless stated otherwise.

4.1. Example 1

A simply supported piezoelectric laminated beam with length to thickness ratio $S(L/h)=4$ (thick beam), $S=10$ (moderately thick beam) and $S=100$ (thin beam) is analyzed using the present coupled theory. This beam has the lamination scheme [$pz/0^\circ/90^\circ/90^\circ/0^\circ$] which pz indicates the piezoelectric layer. The substrate of the beam is made of graphite-epoxy with the following properties:

$(E_L, E_T, G_{LT}, G_{TT}) = (181, 10.3, 7.17, 2.87)\,GPa, \quad (\nu_{LT}, \nu_{TT}) = (0.28, 0.33)$

L and *T* denote directions parallel and transverse to the fibers, respectively. The piezoelectric layer is made of PZT-5A with the following properties:

$(E_{11}, E_{22}, E_{33}, G_{12}, G_{23}, G_{31}) = (61.0, 61.0, 53.2, 22.6, 21.1, 21.1)\,GPa$,

$(\nu_{12}, \nu_{13}, \nu_{23}) = (0.35, 0.38, 0.38)$,

$(d_{31}, d_{32}, d_{33}, d_{15}, d_{24}) = (-171, -171, 374, 584, 584)\times 10^{-12} m/V$,

$(\chi_{11}, \chi_{22}, \chi_{33}) = (1.53, 1.53, 1.50)\times 10^{-8}\, F/m$

The ratio of the piezoelectric thickness layer to the laminate thickness *h* is assumed to be 0.1. All layers of the substrate are assumed to have equal thickness. The interface of the piezoelectric layer with the substrate is assumed to be zero potential.

4.1.1. Sensor case. A sinusoidal pressure $p(x) = -p_0 \sin(\pi x/L)$ has been applied on the top surface of the simply supported beam. Due to the symmetry, only half of the beam is modeled. Results of the mesh convergence study are shown in Table 1 for *S=10*. This table shows that the convergence rate of the proposed finite element model is very high. A mesh with 2 elements gives excellent results in the prediction of deflection of the beam. Only 8 elements are adequate to predict the induced sensory potential, in-plane displacement and stress components. However, for the analysis of the problem, the beam was mathematically divided into 15 beam elements of equal lengths and five layers. The obtained numerical results are normalized as follows:

$(\bar{u}, \bar{w}) = 100(u, w/S)E_T/hS^3 p_0, \quad (\bar{\sigma}_{xx}, \bar{\sigma}_{zz}, \bar{\tau}_{xz}) = (\sigma_{xx}/S^2, \sigma_{zz}, \tau_{xz}/S)/p_0, \quad \bar{\phi} = 10^4 \phi E_T d_T / hS^2 p_0$

with $d_T = 374\times 10^{-12} CN^{-1}$.

The normalized numerical results for deflection, in-plane displacement, transverse shear and normal stresses, the induced potential at the sensory layer and in-plane stress are given in Table 2 for three values of length to thickness ratio $S=4$, $S=10$ and $S=100$. The variation of the normalized stress and displacement components through the thickness ($S=4$ and $S=10$) are shown in Fig. 4 and Fig. 5. The distribution of the normalized induced potential across the sensory layer is also shown in these figures. The transverse normal stresses have been calculated using two different methods: (i) employing the constitutive equations; (ii) integrating the elasticity equilibrium equations in terms of the stress components, across the thickness of laminates. Results of these two approaches are denoted by (C) and (E), respectively. The transverse shear stresses have been obtained by integrating the stress equilibrium equation through the thickness of laminates at the post-processing level.

For deflection, the present model gives results with the error less than 4.21%, whatever the length to thickness ratio. The model predicts the in-plane displacement and in-plane stress at top face of thin to moderately thick laminated beams with the error less than 2.62% and 5.72% respectively. The transverse shear and normal stress distributions obtained from the present model are in excellent agreement with the exact solution for both thin and thick laminated beams. It can be seen that the present theory unlike most of available similar theories, is able to predict the transverse normal stress well from constitutive equations. The coupled proposed theory is also capable of predicting the induced sensory potential with very good accuracy for thin to moderately thick laminated beams. The error in the predicted sensory potential is only 3.7% for moderately thick beams. The error approach zero for thin beams.

Variations of the normalized deflection calculated at the middle of the sensory composite beam versus the aspect ratio are shown in Fig. 6. Comparison of the present results with results of the exact piezoelasticity solution reveals that the present beam element is free of shear locking. These results show that the developed finite element model performs well in the prediction of the sensory behavior of thick and thin laminated beams.

4.1.2. Actuator case. An actuating potential $\phi(x) = \phi_0 \sin(\pi x / L)$ has been applied on the top surface of the simply supported beam. Table 3 shows the results of the mesh convergence test for *S=10*. Similar to the sensor case, the convergence rate of the present finite element is very high. Although a mesh with 8 elements adequately analyzes the problem, the layered substrate composite beam and its piezoelectric layer were divided into 15 beam elements of equal lengths and five layers. The obtained numerical results are normalized as follows:

$$(\tilde{u}, \tilde{w}) = 10(u, w/S) S d_T \phi_0, \quad (\tilde{\sigma}_{xx}, \tilde{\sigma}_{zz}, \tilde{\tau}_{xz}) = (\sigma_{xx}/10, S^2\sigma_{zz}, S\tau_{xz})h/Y_T d_T \phi_0, \quad \tilde{D}_z = D_z h/100 E_T d_T^2 \phi_0$$

The normalized numerical results for the transverse electric displacement, stress and displacement components are compared in Table 4 for length to thickness ratios $S = 4$, $S = 10$ and $S = 100$. Through-the-thickness distributions of $\tilde{w}$, $\tilde{u}$, $\tilde{\sigma}_{xx}$, $\tilde{\sigma}_{zz}$, $\tilde{\tau}_{xz}$ and $\tilde{D}_z$ for thick and moderately thick beams are shown in Fig. 7 and Fig. 8. The model predicts the in-plane displacement, deflection and in-plane stresses of thin to moderately thick laminated beams with the error less than 5%. For transverse electric displacement, the present theory gives results with the maximum error of 0.52% , whatever the length to thickness ratio. Similar to the sensor model, the transverse shear stresses distributions deduced from the present model are in excellent agreement with the exact solution; even for the very thick beam $S = 4$ (the error is less than 5%). The developed theory is also able to predict the transverse normal stresses of both thin and thick active laminated beams with good accuracy (the maximum error is 10.15%).

Considering the various values for the aspect ratio, the normalized deflection of the active composite beam is shown in Fig. 9 along with the exact piezoelasticity solutions. It can be inferred from this figure that the present finite element does not suffer from shear locking. These results demonstrate that the presented model is efficient in predicting the actuator behavior of thick and thin laminated beams.

4.1.3. Coupled electrical-mechanical loading case. In this case, both actuating potential $\phi(x) = \phi_0 \sin(\pi x / L)$ and sinusoidal pressure $p(x) = -p_0 \sin(\pi x / L)$ have been applied simultaneously on the top surface of the thick simply supported beam (*S=4*). The obtained numerical results are normalized as follows:

$$(\hat{\sigma}_{xx}, \hat{\sigma}_{zz}, \hat{\tau}_{xz}) = (\sigma_{xx}/S^2, \sigma_{zz}, \tau_{xz}/S)/p_0, \quad \hat{D}_z = D_z h/100 E_T d_T^2 \phi_0$$

In Fig. 10, distributions of $\hat{\sigma}_{xx}$, $\hat{\sigma}_{zz}$, $\hat{\tau}_{xz}$ and $\hat{D}_z$ across the thickness direction are depicted. Once more, the results of the present finite element based on the coupled refined high-order global-local theory are correlated well with the exact solutions. The model estimates the in-plane stress and transverse electric displacement with the maximum error of 8.76% and 0.31%, respectively. For transverse shear and normal stresses, the error is respectively less than 7.02% and 5.50%.

4.2. Example 2

Geometry, material properties, boundary and loading conditions of the smart laminated composite beam of the present example are the same as those of the previous example. The only difference is the lay-up of the considered beam which in this example is [$pz/0^\circ/90^\circ/0^\circ/90^\circ$].

4.2.1. Sensor case. Through-the-thickness distributions of $\bar{w}$, $\bar{u}$, $\bar{\sigma}_{xx}$, $\bar{\sigma}_{zz}$, $\bar{\tau}_{xz}$ and $\bar{\phi}$ obtained from the present coupled refined high-order global-local theory for the sensory thick and moderately thick beams are compared in Fig. 11 and Fig. 12 with the exact piezoelasticity solution. Similar comparison for these quantities is presented in Table 5 for the aspect ratios $S = 4$, $S = 10$ and $S = 100$. It is observed from Fig. 11 and Fig. 12 that the prediction of the transverse shear and normal stresses using the present finite element model is agree very well with the exact piezoelasticity solution for both thin and thick beams. For the central deflection $\bar{w}$ and the in-plane displacement $\bar{u}$ at the top face of the thick beam (*S=4*), the maximum percent error in the present results is 6.49 and 5.92, respectively. In case of thin to moderately thick beams, the prediction of the induced electric potential through the thickness by the present model agrees very well to those of the exact solutions (the maximum percent discrepancy is 6.94). The discrepancies are more remarkable for *S=4* that is of less practical importance. The error of the predicted in-plane stress in the sensor layer of the thick beams is less than 3.50%.

4.2.2. Actuator case. Results correspondent to this case study are discussed in Figs. 13-14 and Table 6. It is observed from these results that the present coupled theory has captured through-the-thickness variations of $\tilde{\tau}_{xz}$ and $\tilde{D}_z$ quite well even for the thick active laminated beams. Due to the inclusion of the transverse normal strains induced through the actuator layer, the prediction of $\tilde{w}$ from the present finite element model has also good correlation with the exact solutions. In case of thick beams, the present theory estimates the in-

plane stress of the actuator layer with the error less than 4.50%. The model also predicts the in-plane displacement and transverse normal stresses of thin to moderately thick active laminated beams with the maximum error 2.27% and 0.84%, respectively.

4.3. Example 3

As a final example, a soft core sandwich beam with a piezoelectric layer bonded to its top is considered. In this case, results of majority of the available theories may become unreliable due to neglecting the effects of the non-zero shear tractions and longitudinal electric field, and ignoring continuity conditions of the transverse shear and normal stress components at the conjunctions of piezoelectric layers. In this regard, a cantilever smart sandwich beam with length $L=10cm$, cross section width $b=1cm$, and height $h=1cm$ is considered. Thickness of the piezoelectric layer and face sheets are *0.1h* and thickness of the soft core is assumed to be *0.7h*. The face sheets are made of graphite-epoxy with the following material properties:

$(E_{11}, E_{22}, E_{33}, G_{12}, G_{13}, G_{23}) = (131.1,\ 6.9,\ 6.9,\ 3.588,\ 3.588,\ 2.3322)\,GPa$, $(\nu_{12}, \nu_{13}, \nu_{23}) = (0.32,\ 0.32, 0.49)$

The material properties of the soft core are:

$(E_{11}, E_{22}, E_{33}, G_{12}, G_{13}, G_{23}) = (0.2208,\ 0.2001,\ 2760,\ 16.56,\ 545.1,\ 455.4)\,MPa$

$(\nu_{12}, \nu_{13}, \nu_{23}) = (0.99,\ 0.00003, 0.00003)$

Similar to the previous examples, the piezoelectric layer is made of PZT-5A. The interface of the piezoelectric layer with the substrate is also grounded (zero potential). Since no exact 3D piezoelasticity solution is available for the considered example, a coupled 3D finite element analysis was performed in ABAQUS with a very refined mesh, using the 20-node piezoelectric solid element (C3D20RE).

4.3.1. Sensor case. The smart sandwich beam is subjected to distributed uniform pressures $Z^{+}=-50N/m^2$ and $Z^{-}=50N/m^2$, and shear tractions $X^{+}=250N/m^2$ and $X^{-}=-250N/m^2$ on its top and bottom surfaces, respectively (Fig. 15). In order to analyze the problem, the beam was mathematically divided into 20 beam elements of equal lengths. In Fig. 16, through-the-thickness distributions of the in-plane stress, induced sensory electric potential and displacement components are shown. It may be observed that the depicted in-plane displacement component based on the present formulation is in excellent agreement with the coupled 3D finite element results. The error in present finite element results is 12.73% for the in-plane stress, up to 14.07% for the sensory electric potential and 5.61% for the transverse displacement. The thickness variations of transverse shear and normal stresses at different sections of the sensory sandwich beam are plotted in Fig. 17. The proposed finite element model predicts the transverse shear stresses of the sensory sandwich beam with an error less than 4%. Moreover, the transverse normal stresses predicted from both the equilibrium and constitutive equations have also good agreement with those extracted from the coupled 3D finite element analysis. These results confirm the accuracy of the proposed formulation in the prediction of the sensory behavior of sandwich beams.

4.3.2. Actuator case. In this case, the cantilever piezoelectric sandwich beam is subjected to the actuating potential $\phi(x)=\sin(\pi x/L)$ on its top surface. Results correspondent to this case study are plotted in Fig. 18. As shown in Fig. 18, the prediction of the deflection by the present finite element agrees well with the results of ABAQUS due to the inclusion of the effects of both the transverse flexibility and electrical transverse normal strains. The model predicts the maximum deflection of the active sandwich beam with the error less than 1%. Moreover, the depicted in-plane displacement component based on the present theory has an excellent agreement with the coupled 3D finite element results. The model estimates the in-plane and transverse shear stresses with the maximum error of 15.24% and 8.55%, respectively. Concerning the transverse electric displacement, the coupled refined global-local theory yields very accurate results with respect to ABAQUS, with a maximum error of 1.23%. The effectiveness of the present theory in the prediction of the active behavior of smart sandwich beams is confirmed through these results.

5. Conclusions

A computationally economic and accurate coupled refined global-local finite element model is presented for static response of piezoelectric laminated composite and sandwich beams. Contrary to most of the available theories, all the kinematic and stress boundary conditions are satisfied at the interfaces of the piezoelectric layers with the non-zero longitudinal electric field. Moreover, both electrical transverse normal strains and transverse flexibility are taken into account for the first time in the present theory. Unlike the

available laminated piezoelectric composite beam models, the non-uniform non-zero shear and normal traction boundary conditions on the top and bottom surfaces of the beam are satisfied for any electrical boundary conditions. The describing expression of the in-plane displacement of the beam contains a high-order polynomial, an exponential expression and a layerwise term containing first order differentiation of electrical unknowns. The transverse displacement is introduced using a combination of continuous piecewise fourth-order polynomial with a layerwise representation of electrical unknowns. A quadratic electric potential is also assumed in the piezoelectric layers. In the proposed finite element formulation, the mechanical number of the unknown parameters is very small and is independent of the number of the layers. Besides, the shear locking phenomenon does not appear in the presented smart beam element.

In order to verify the accuracy of the proposed finite element formulation, some comparisons have been made with the results obtained from the coupled 3D finite element (ABAQUS) analysis and 3D theory of piezoelasticity. To this end, various electro-mechanical bending tests for piezoelectric laminated/sandwich beams with different geometric parameters, stacking sequences, boundary conditions, and number of layers are considered. The comparisons show that the presented coupled finite element formulation, besides its advantages of low computational time due to using small number of the unknown parameters is sufficiently accurate in the modeling of thin and thick piezoelectric composite and sandwich beams under different mechanical and electrical loading conditions.

References

[1] I. Chopra, Review of state of art of smart structures and integrated systems, AIAA J. 40(11) (2002) 2145–2187.

[2] P. Gaudenzi, Smart Structures: Physical behavior, mathematical modeling and applications, John Wiley & Sons, 2009.

[3] E.F. Crawley, J. de Luis, Use of piezoelectric actuators as element of intelligent structures, AIAA J. 25 (1987) 1373-1385.

[4] H.S. Tzou, M. Gadre, Theoretical analysis of a multi-layered thin shell coupled with piezoelectric shell actuators for distributed vibration controls, J. Sound Vib. 132 (1989) 433-450.

[5] B.T. Wang, C.A. Rogers, Laminate plate theory for spatially distributed induced strain actuators, J. Compos. Mater. 25(4) (1991) 433-452.

[6] C.K. Sung, T.F. Chen, S.G. Chen, Piezoelectric modal sensor/actuator design for monitoring /generating flexural and torsional vibrations of cylindrical shells, J. Sound Vib. 118 (1996) 48-55.

[7] A. Benjeddou, Advances in piezoelectric finite element modeling of adaptive structural elements: a survey, Comput. Struct. 76 (2000) 347-363.

[8] D.A. Saravanos, P.R. Heyliger, Mechanics and computational models for laminated piezoelectric beams, plates, and shells, Appl. Mech. Rev. 52(10) (1999) 305–320.

[9] S. Brooks, P. Heyliger, Static behavior of piezoelectric laminates with distributed and patched actuators, J. Intell. Mater. Syst. Struct. 5 (1994) 635-646.

[10] M.C. Ray, K.M. Rao, B. Samanta, Exact analysis of coupled electroelastic behavior of a piezoelectric plate under cylindrical bending, Comput. Struct. 45(4) (1992) 667-677.

[11] M.CH. Ray, K.M. Rao, B. Samanta, Exact solution for static analysis of an intelligent structure under cylindrical bending, Comput. Struct. 47(6) (1993) 1031-1042.

[12] H. Allik, T.J.R. Hughes, Finite element method for piezoelectric vibration, Int. J. Numer. Methods Eng. 2 (1970) 151-157.

[13] H.S. Tzou, C.I. Tseng, Distributed piezoelectric sensor/actuator design for dynamic measurement /control of distributed parameter systems: a piezoelectric finite element approach, J. Sound Vib. 138 (1) (1990) 17-34.

[14] K.M. Xu, A.K. Noor, Y. Tang, Three-dimensional solutions for coupled thermo-electro-elastic response of multi-layered plates, Comput. Meth. Appl. Mech. Eng. 126 (1995) 355-371.

[15] J.N. Reddy, An evaluation of equivalent-single-layer and layerwise theories of composite laminates, Compos. Struct. 25(1-4) (1993) 21-35.

[16] W.S. Hwang, H.C. Park, Finite element modeling of piezoelectric sensors and actuators, AIAA J. 31 (1993) 930–937.

[17] A. Suleman, and V.B. Venkaya, A simple finite element formulation for a laminated composite plate with piezoelectric layers, J. Intell. Mater. Syst. Struct. 6 (1995) 776-782.

[18] A.H. Sheikh, P. Topdar, S. Halder, An appropriate FE model for through thickness variation of displacement and potential in thin/moderately thick smart laminates, Compos. Struct. 51 (2001) 401–409.

[19] M. Kogl, M.L. Bucalem, A family of piezoelectric MITC plate elements, Comput. Struct. 83 (2005) 1277–1297.
[20] M. Kogl, M.L. Bucalem, Analysis of smart laminates using piezoelectric MITC plate and shell elements, Comput. Struct. 83 (2005) 1153–1163.
[21] C.Y.K. Chee, L. Tong, P.G. Steven, A mixed model for composite beams with piezoelectric actuators and sensors, Smart Mater. Struct. 8 (1999) 417–432.
[22] J.P. Jiang, D.X. Li, A new finite element model for piezothermoelastic composite beam, J. Sound Vib. 306 (2007) 849–864.
[23] X. Shu, Free-vibration of laminated piezoelectric composite plates based on an accurate theory, Compos. Struct. 67 (2005) 375-382.
[24] R.P. Thornburgh, and A. Chattopadhyay, Simultaneous modeling of mechanical and electrical response of smart composite structures, AIAA J. 40(8) (2002) 1603-1610.
[25] H. Fukunaga, N. Hu, G.X. Ren, Finite element modeling of adaptive composite structures using a reduced higher-order plate theory via penalty functions, Int. J. Solids Struct. 38 (2001) 8735-8752.
[26] J.A. Mitchell, J.N. Reddy, A refined plate theory for composite laminates with piezoelectric laminate, Int. J. Solids Struct. 32(16) (1995) 2345–2367.
[27] P.R. Heyliger, D.A. Saravanos, Coupled discrete-layer finite elements for laminated piezoelectric plates, Commun. Numer. Methods Eng. 10 (12) (1994) 971–981.
[28] D.A. Saravanos, P.R. Heyliger, Coupled layer-wise analysis of composite beams with embedded piezoelectric sensors and actuators, J. Intell. Mater. Syst. Struct. 6 (1995) 350–363.
[29] D.A. Saravanos, P.R. Heyliger, D.A. Hopkins, Layer-wise mechanics and finite element model for the dynamic analysis of piezoelectric composite plates, Int. J. Solids Struct. 34(3) (1997) 359–378.
[30] Z.K. Kusculuoglu, B. Fallahi, T.Y. Royston, Finite element model of a beam with a piezoelectric patch actuator, J. Sound Vib. 276 (2004) 27-44.
[31] R. Garcia Lage, C.M. Mota Soares, C.A. Mota Soares, J.N. Reddy, Analysis of adaptive plate structures by mixed layerwise finite elements, Compos. Struct. 66 (2004) 269-276.
[32] R. Garcia Lage, C.M. Mota Soares, C.A. Mota Soares, J.N. Reddy, Modeling of piezolaminated plates using layer-wise mixed finite element models, Comput. Struct. 82 (2004) 1849-1863.
[33] A. Robaldo, E. Carrera, A. Benjeddou, A unified formulation for finite element analysis of piezoelectric adaptive plates, Comput. Struct. 84 (2006) 1494-1505.
[34] H.S. Tzou, R. Ye, Analysis of piezoelastic structures with laminated piezoelectric triangle shell elements, AIAA J. 34 (1996) 110–115.
[35] S.A. Ambartsumyan, Theory of anisotropic plates, J. E. Ashton, Technomic, Stamford, CT, Translated from Russian by T. Cheron, 1969.
[36] J.M. Whitney, The effects of transverse shear deformation on the bending of laminated plates, J. Compos. Mater. 3 (1969) 534-547.
[37] U. Icardi, Higher-order zig-zag model for analysis of thick composite beams with inclusion of transverse normal stress and sublaminates approximations, Compos. Part B 32 (2001) 343-354.
[38] U. Icardi, A three-dimensional zig-zag theory for analysis of thick laminated beams, Compos. Struct. 52 (2001) 123-135.
[39] E. Reissner, On a mixed variational theorem and on a shear deformable plate theory, Int. J. Numer. Meth. Eng. 23 (1986) 193-198.
[40] H. Murakami, A laminated beam theory with interlayer slip, J. Appl. Mech. 51 (1984) 551-559.
[41] H. Murakami, Laminated composite plate theory with improved in-plane responses, J. Appl. Mech. 53 (1986) 661-666.
[42] E. Carrera, A study of transverse normal stress effects on vibration of multilayered plates and shells, J. Sound Vib. 225 (1999) 803-829.
[43] E. Carrera, Single-layer vs multi-layers plate modeling on the basis of Reissner's mixed theorem, AIAA J. 38 (2000) 342-343.
[44] E. Carrera, Historical review of zig-zag theories for multilayered plates and shells, Appl. Mech. Rev. 56 (2003) 287-308.
[45] J. Oh, M. Cho, A finite element based on cubic zig-zag plate theory for the prediction of thermo-electric-mechanical behaviors, Int. J. Solids Struct. 41(5-6) (2004) 1357-1375.
[46] S. Kapuria, An efficient coupled theory for multilayered beams with embedded piezoelectric sensory and active layers, Int. J. Solids Struct. 38 (2001) 9179-9199.
[47] S. Kapuria, P.C. Dumir, A. Ahmed, An efficient coupled layerwise theory for dynamic analysis of piezoelectric composite beams, J. Sound Vib. 261 (2003) 927-944.

[48] S. Kapuria, N. Alam, Efficient layerwise finite element model for dynamic analysis of laminated piezoelectric beams, Comput. Meth. Appl. Mech. Eng. 195 (2006) 2742-2760.
[49] O. Polit, M. Touratier, High-order triangular sandwich plate finite element for linear and non-linear analyses, Comput. Meth. Appl. Mech. Eng. 185(2-4) (2000) 305-324.
[50] F. Dau, O. Polit, M. Touratier, An efficient C^1 finite element with continuity requirements for multilayered/sandwich shell structures, Comput. Struct. 82(23-26) (2004) 1889-1899.
[51] C. Ossadzow-David, M. Touratier, A multilayered piezoelectric shell theory, Compos. Sci. Technol. 64 (2004) 2121-2137.
[52] A. Fernandes, J. Pouget, Analytical and numerical approaches to piezoelectric bimorph, Int. J. Solids Struct. 40 (2003) 4331-4352.
[53] P. Vidal, O. Polit, A family of sinus finite elements for the analysis of rectangular laminated beams, Compos. Struct. 84 (2008) 56-72.
[54] S.B. Beheshti-Aval, M. Lezgy-Nazargah, A finite element model for composite beams with piezoelectric layers using a sinus model, J. Mech. 26(2) (2010) 249-258.
[55] S.B. Beheshti-Aval, M. Lezgy-Nazargah, Assessment of velocity-acceleration feedback in optimal control of smart piezoelectric beams, Smart Struct. Syst. 6(8) (2010) 921-938.
[56] M. D'Ottavio, B. Kröplin, An extension of reissner mixed variational theorem to piezoelectric laminates, Mech. Adv. Mater. Struct. 13(2) (2006) 139-150.
[57] E. Carrera, P. Nali, Mixed piezoelectric plate elements with direct evaluation of transverse electric displacement, Int. J. Numer. Methods Eng. 80 (2009) 403-424.
[58] X. Li, D. Liu, Generalized laminate theories based on double superposition hypothesis, Int. J. Numer. Methods Eng. 40(7) (1997) 1197–1212.
[59] M. Shariyat, A generalized global–local high-order theory for bending and vibration analyses of sandwich plates subjected to thermo-mechanical loads, Int. J. Mech. Sci. 52 (2010) 495–514.
[60] M. Lezgy-Nazargah, S.B. Beheshti-Aval, M. Shariyat, A refined mixed global–local finite element model for bending analysis of multi- layered rectangular composite beams with small widths, Thin Walled Struct (2010) doi:10.1016/j.tws.2010.09.027.
[61] M. Lezgy-Nazargah, M. Shariyat, S.B. Beheshti-Aval, A refined high-order global- local theory for finite element bending and vibration analyses of the laminated composite beams, Acta Mech (2010) doi: 10.1007/s00707-010-0391-9.
[62] W. Zhen, C. Wanji, Refined triangular element for laminated elastic–piezoelectric plates, Compos. Struct. 78 (2007) 129–139.

Figures' legend:

Fig. 1. Geometric parameters of the smart laminated beam.
Fig. 2. Global and local coordinate systems of the piezoelectric laminated beam.
Fig. 3. (a) Mechanical and (b) electrical representation of the piezoelectric beam finite element.
Fig. 4. Through-the-thickness variations of $\overline{w}$, $\overline{u}$, $\overline{\sigma}_{xx}$, $\overline{\sigma}_{zz}$, $\overline{\tau}_{xz}$ and $\overline{\phi}$ for the sensory [$pz/0^\circ/90^\circ/90^\circ/0^\circ$] beam with S=4.
Fig. 5. Through-the-thickness variations of $\overline{w}$, $\overline{u}$, $\overline{\sigma}_{xx}$, $\overline{\sigma}_{zz}$, $\overline{\tau}_{xz}$ and $\overline{\phi}$ for the sensory [$pz/0^\circ/90^\circ/90^\circ/0^\circ$] beam with S=10.
Fig. 6. The normalized transverse deflection ($\overline{w}(0.5L,0)$) versus the aspect ratio for the sensory [$pz/0^\circ/90^\circ/90^\circ/0^\circ$] beam with S=4.
Fig. 7. Through-the-thickness variations of $\widetilde{w}$, $\widetilde{u}$, $\widetilde{\sigma}_{xx}$, $\widetilde{\sigma}_{zz}$, $\widetilde{\tau}_{xz}$ and $\widetilde{D}_z$ for the active [$pz/0^\circ/90^\circ/90^\circ/0^\circ$] beam with S=4.
Fig. 8. Through-the-thickness variations of $\widetilde{w}$, $\widetilde{u}$, $\widetilde{\sigma}_{xx}$, $\widetilde{\sigma}_{zz}$, $\widetilde{\tau}_{xz}$ and $\widetilde{D}_z$ for the active [$pz/0^\circ/90^\circ/90^\circ/0^\circ$] beam with S=10.
Fig. 9. The normalized transverse deflection ($\widetilde{w}(0.5L,0)$) versus the aspect ratio of the active [$pz/0^\circ/90^\circ/90^\circ/0^\circ$] beam with S=4.
Fig. 10. Through-the-thickness variations of $\hat{\sigma}_{xx}$, $\hat{\sigma}_{zz}$, $\hat{\tau}_{xz}$ and $\hat{D}_z$ for the thick [$pz/0^\circ/90^\circ/90^\circ/0^\circ$] beam under coupled electro-mechanical loadings (S=4).
Fig. 11. Through-the-thickness variations of $\overline{w}$, $\overline{u}$, $\overline{\sigma}_{xx}$, $\overline{\sigma}_{zz}$, $\overline{\tau}_{xz}$ and $\overline{\phi}$ for the

sensory [$pz/0^\circ/90^\circ/0^\circ/90^\circ$] beam with *S*=4.

Fig. 12. Through-the-thickness variations of $\bar{w}$, $\bar{u}$, $\bar{\sigma}_{xx}$, $\bar{\sigma}_{zz}$, $\bar{\tau}_{xz}$ and $\bar{\phi}$ for the sensory [$pz/0^\circ/90^\circ/0^\circ/90^\circ$] beam with *S*=10.

Fig. 13. Through-the-thickness variations of $\tilde{w}$, $\tilde{u}$, $\tilde{\sigma}_{xx}$, $\tilde{\sigma}_{zz}$, $\tilde{\tau}_{xz}$ and $\tilde{D}_z$ for the active [$pz/0^\circ/90^\circ/0^\circ/90^\circ$] beam with *S*=4.

Fig. 14. Through-the-thickness variations of $\tilde{w}$, $\tilde{u}$, $\tilde{\sigma}_{xx}$, $\tilde{\sigma}_{zz}$, $\tilde{\tau}_{xz}$ and $\tilde{D}_z$ for the active [$pz/0^\circ/90^\circ/0^\circ/90^\circ$] beam with *S*=10.

Fig. 15. Description of the geometry, boundary conditions, and loadings of the sensory sandwich beam.

Fig. 16. Variations of $w(m)$, $u(m)$, $\sigma_{xx}(N/m^2)$ and $\phi(V)$ through the thickness for the sensory sandwich beam.

Fig. 17. Through-the-thickness variations of $\tau_{xz}(N/m^2)$ and $\sigma_{zz}(N/m^2)$ at different sections of the sensory sandwich beam.

Fig. 18. Variations of $w(m)$, $u(m)$, $\sigma_{xx}(N/m^2)$, $\tau_{xz}(N/m^2)$ and $D_z(C/m^2)$ through the thickness of the active sandwich beam.

Tables' legend:

Table 1. Mesh convergence study for the sensory beam [$pz/0^\circ/90^\circ/90^\circ/0^\circ$] with $S=10$.

Table 2. Results for the sensory beam [$pz/0^\circ/90^\circ/90^\circ/0^\circ$] under the pressure load.

Table 3. Mesh convergence study for the actuated beam [$pz/0^\circ/90^\circ/90^\circ/0^\circ$] with $S=10$.

Table 4. Results for the actuated beam [$pz/0^\circ/90^\circ/90^\circ/0^\circ$] under sinusoidal electric potential.

Table 5. Results for the sensory beam [$pz/0^\circ/90^\circ/0^\circ/90^\circ$] under the pressure load.

Table 6. Results for the actuated beam [$pz/0^\circ/90^\circ/0^\circ/90^\circ$] under sinusoidal electric potential.

Fig. 1

Click here to download high resolution image

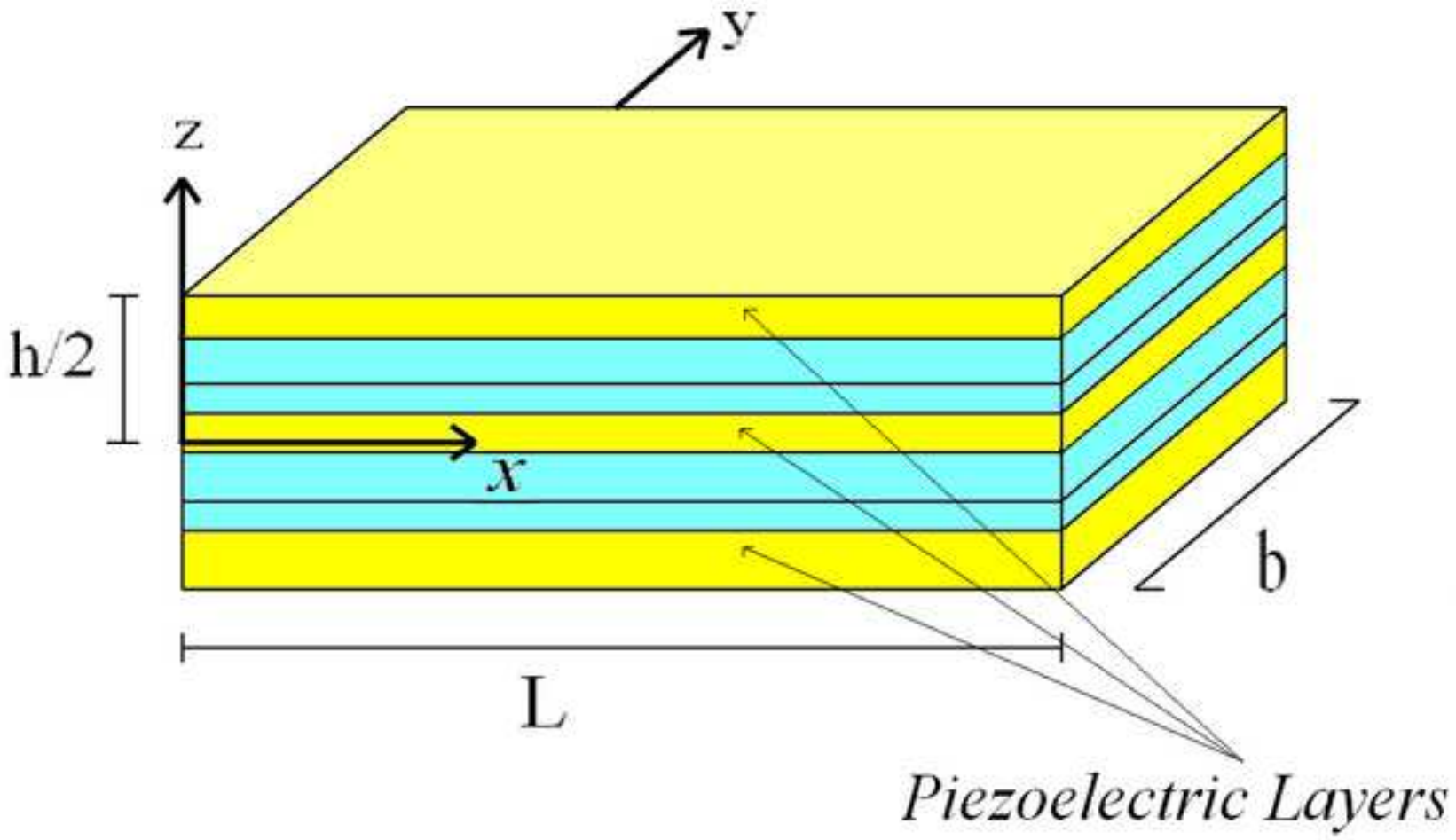

Fig. 2

Click here to download high resolution image

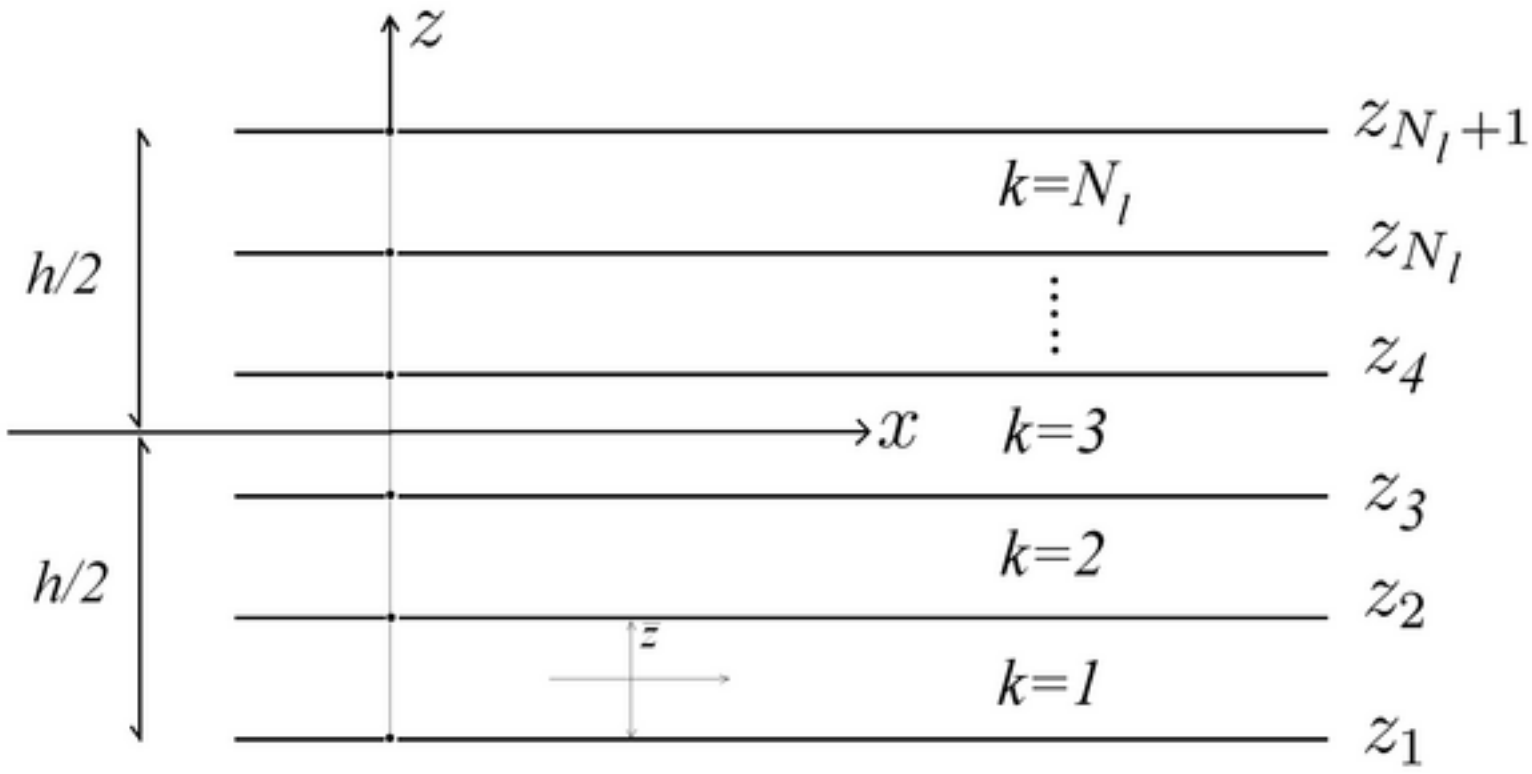

Fig. 3(a)
Click here to download high resolution image

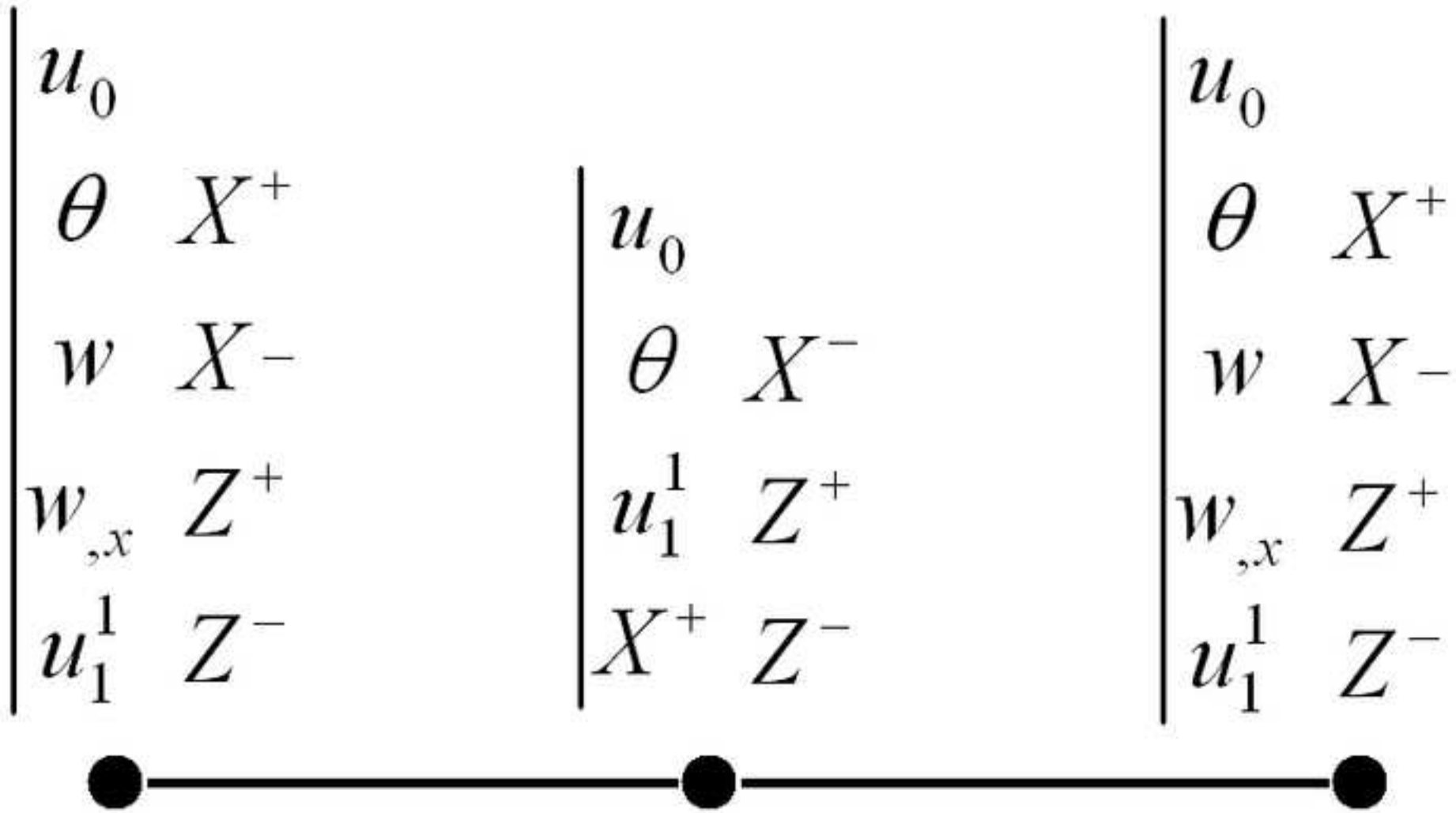

Fig. 3(b)

Click here to download high resolution image

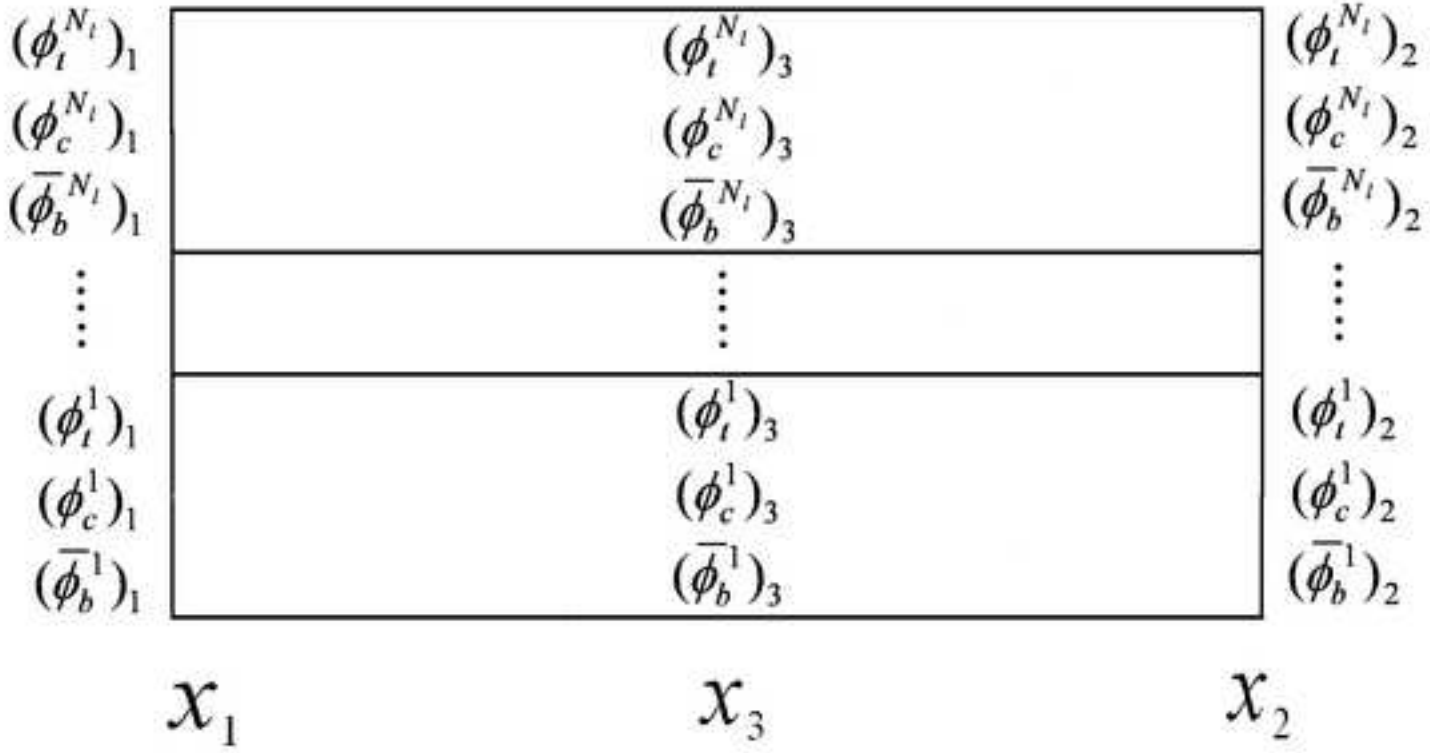

Fig. 4(a)
Click here to download high resolution image

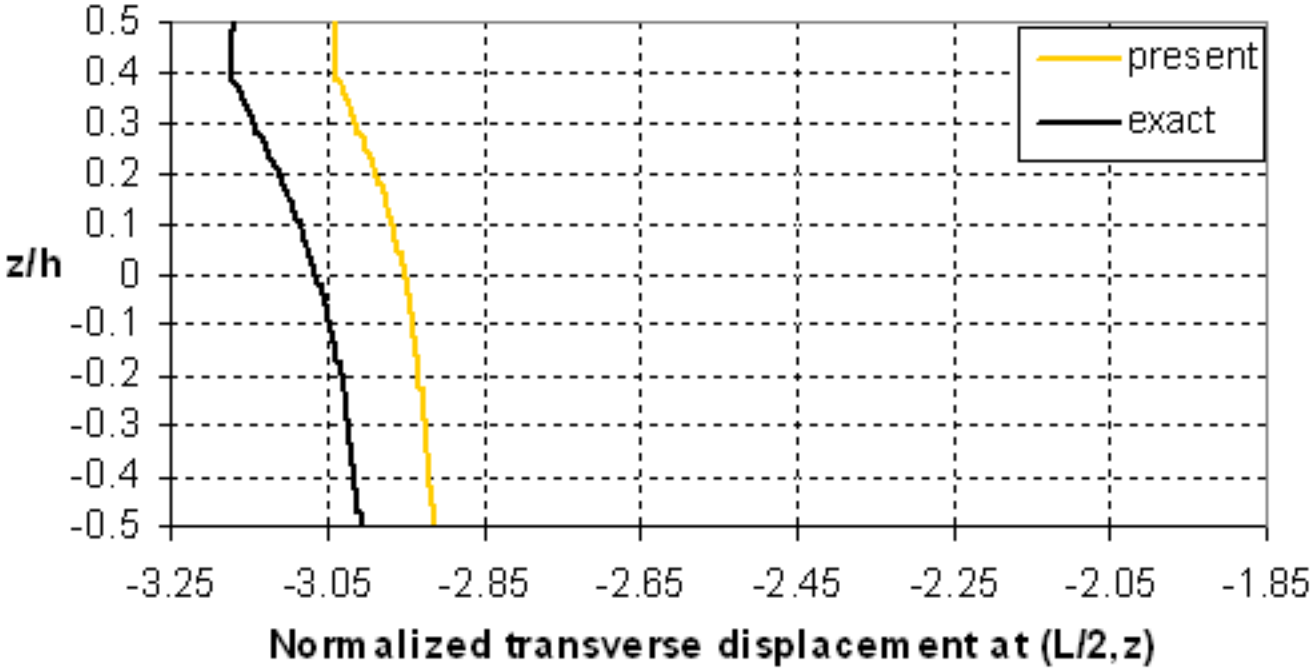

Fig. 4(b)
Click here to download high resolution image

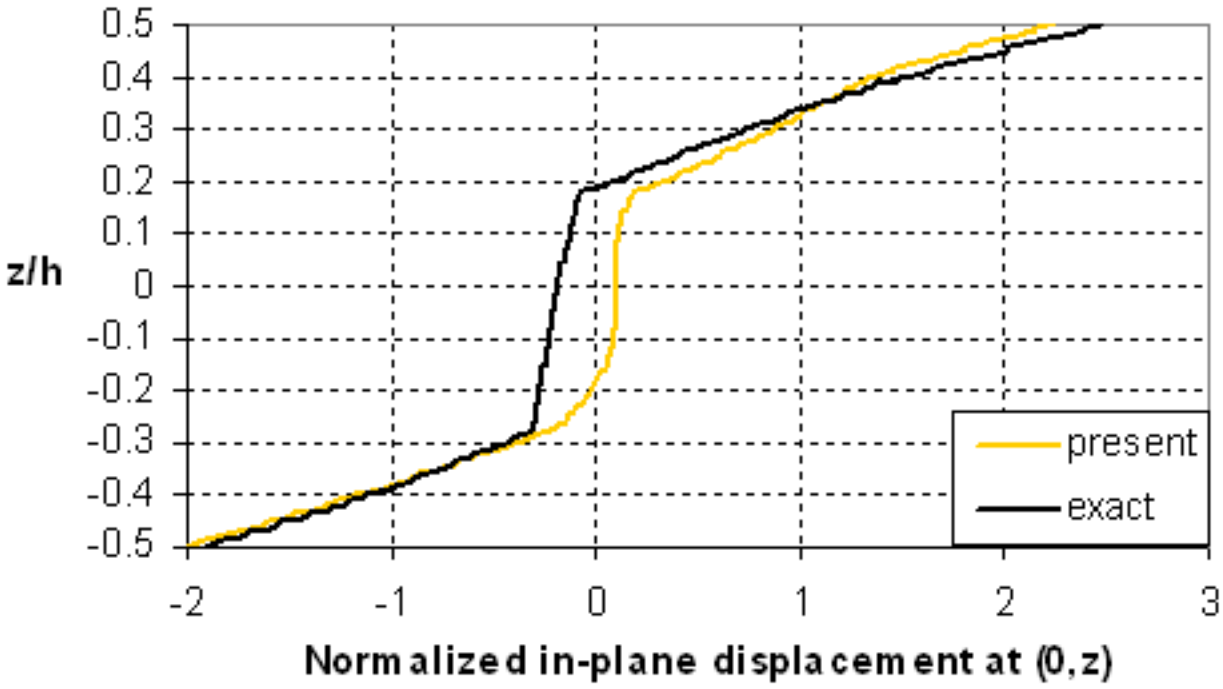

Fig. 4(c)
Click here to download high resolution image

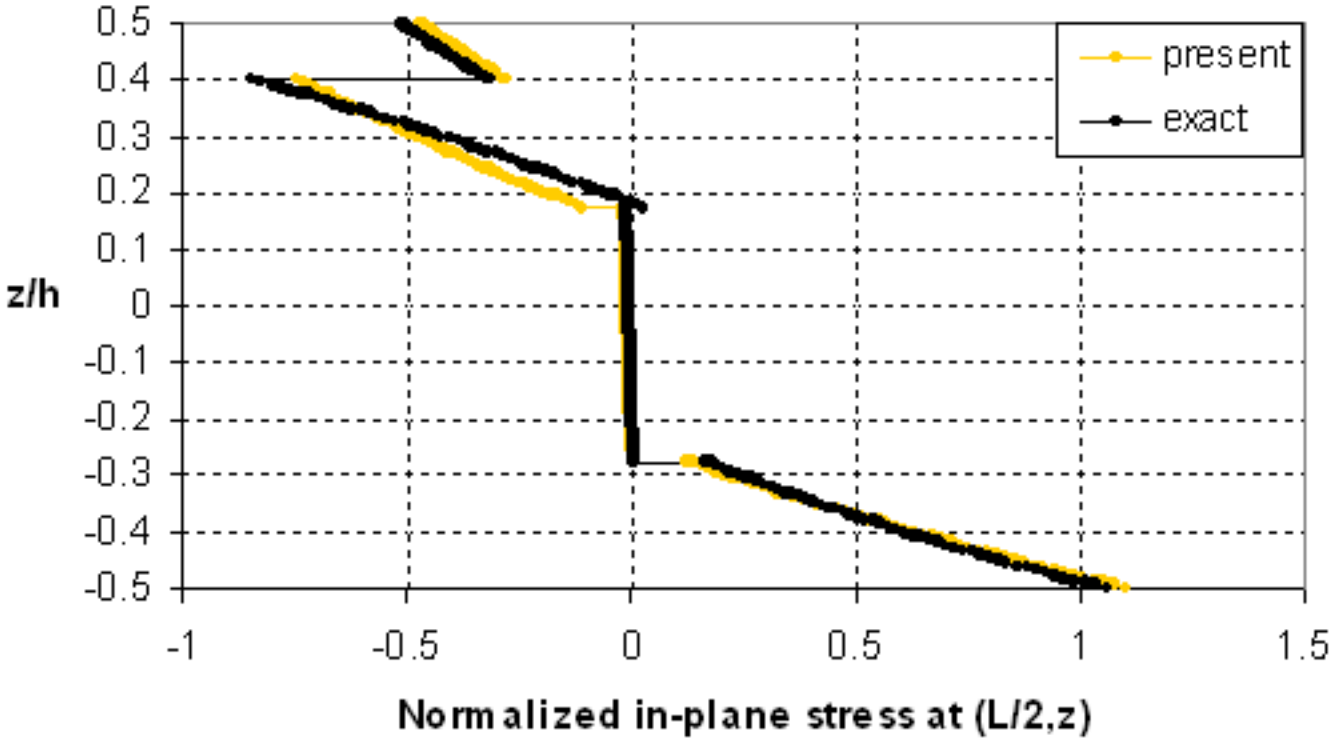

Fig. 4(d)
Click here to download high resolution image

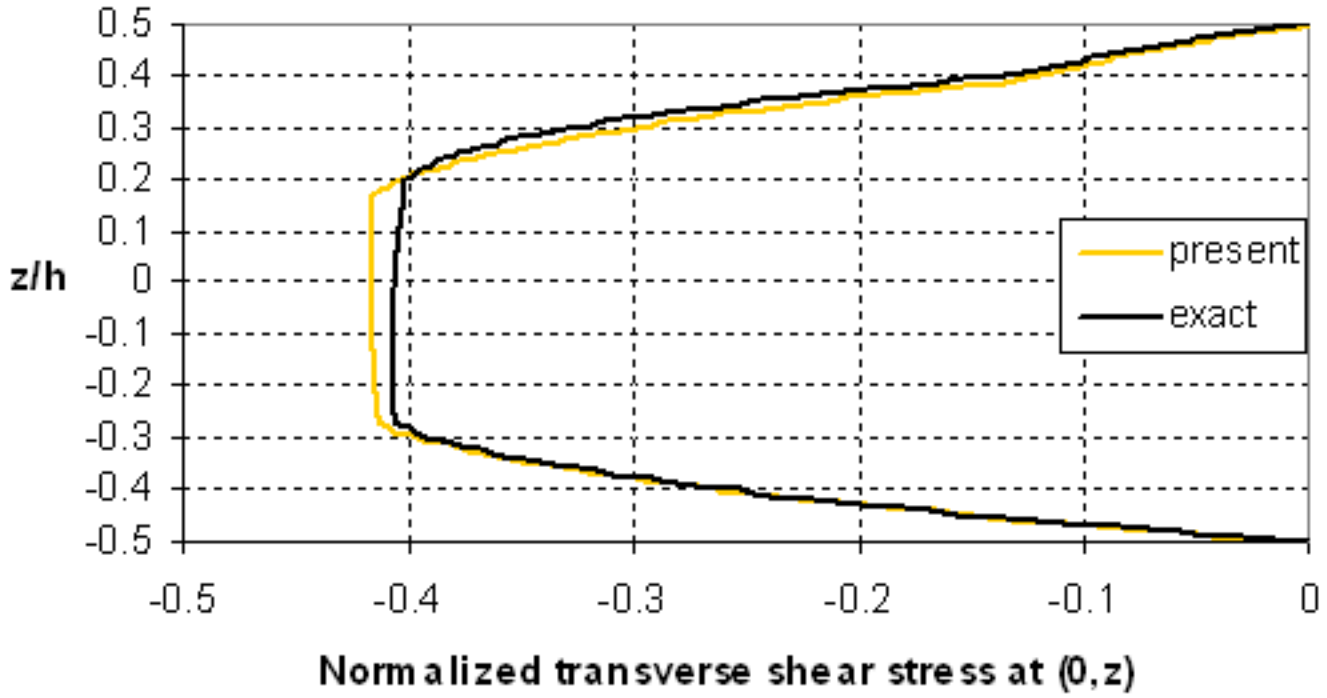

Fig. 4(e)
Click here to download high resolution image

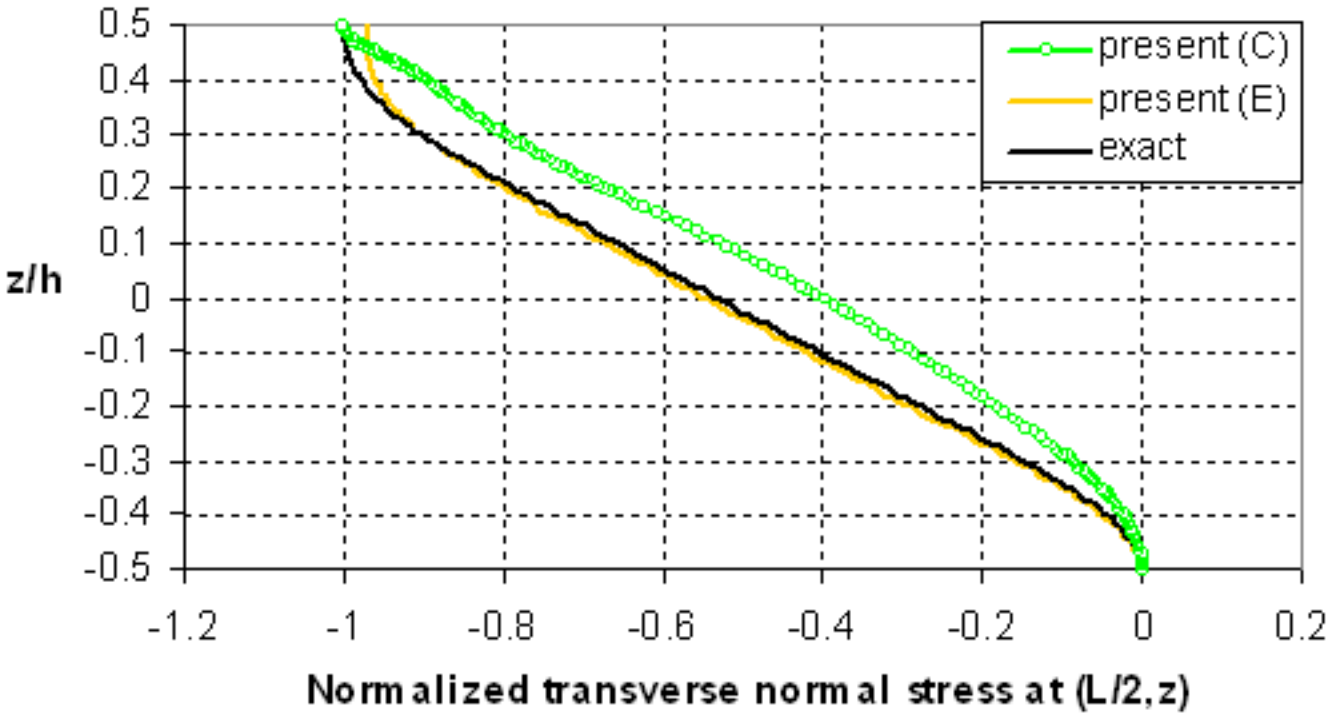

Fig. 4(f)
Click here to download high resolution image

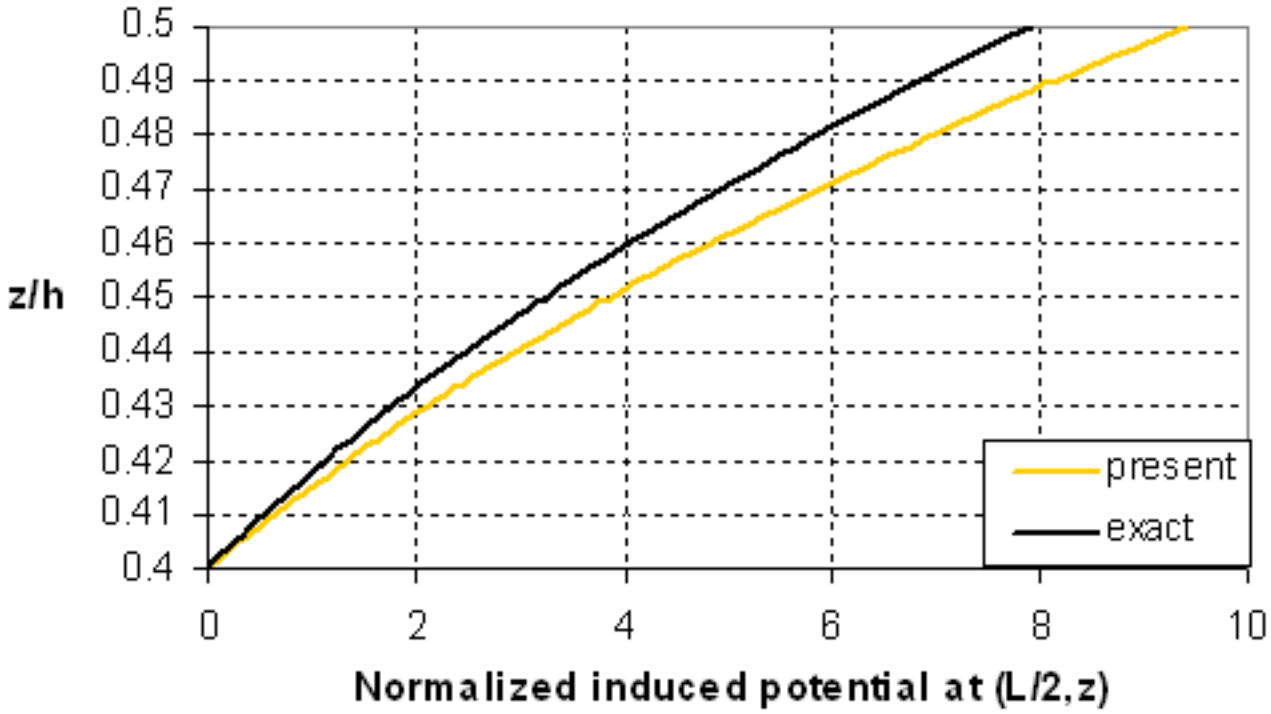

Fig. 5(a)
Click here to download high resolution image

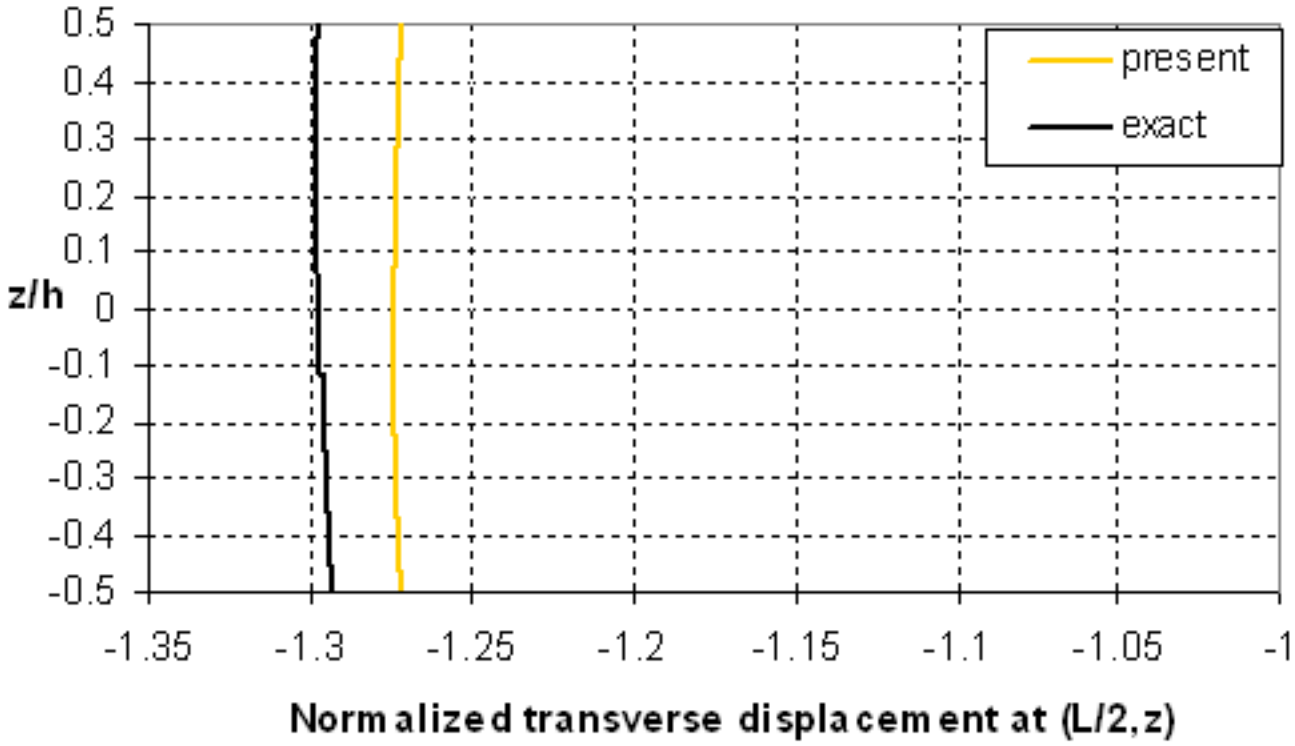

Fig. 5(b)
Click here to download high resolution image

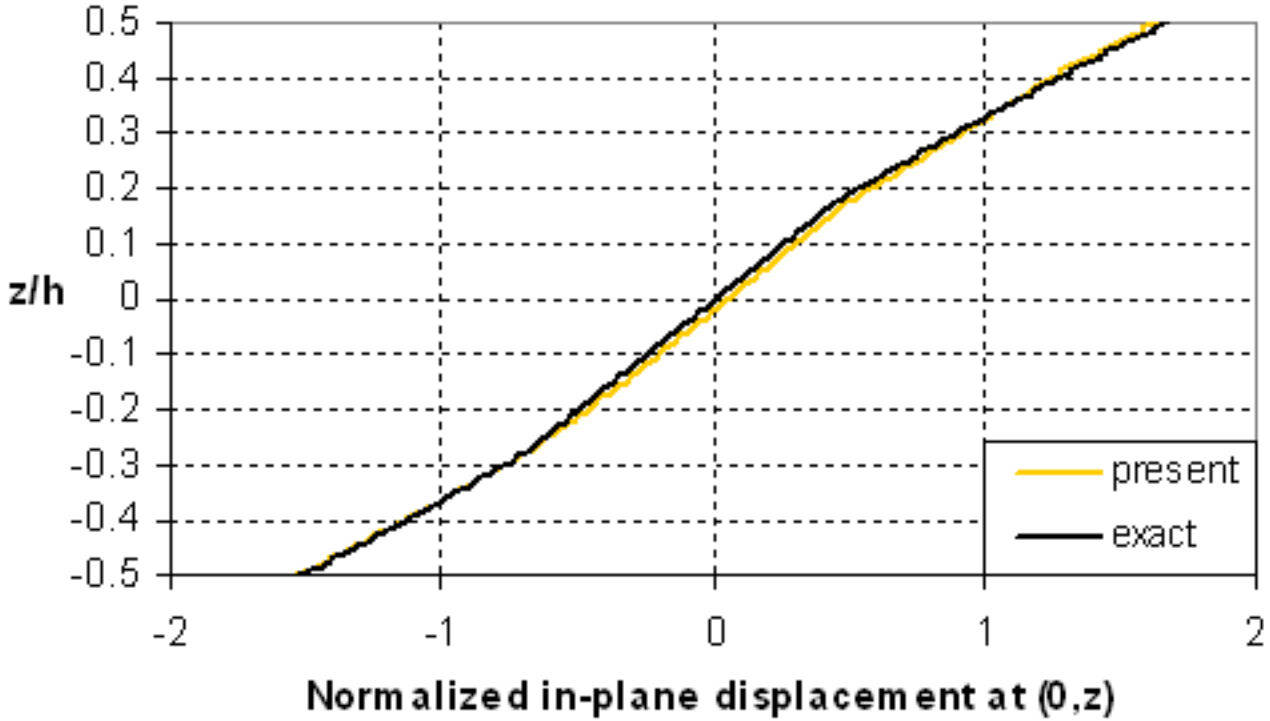

Fig. 5(c)
Click here to download high resolution image

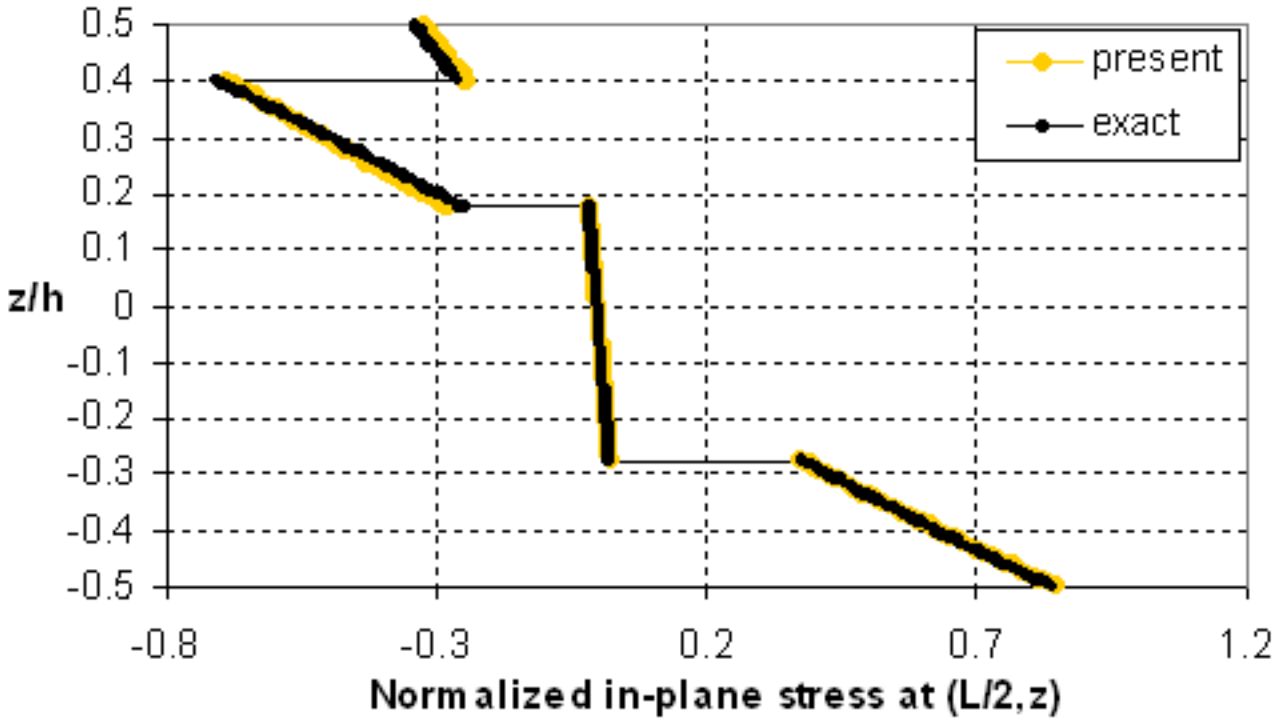

Fig. 5(d)
Click here to download high resolution image

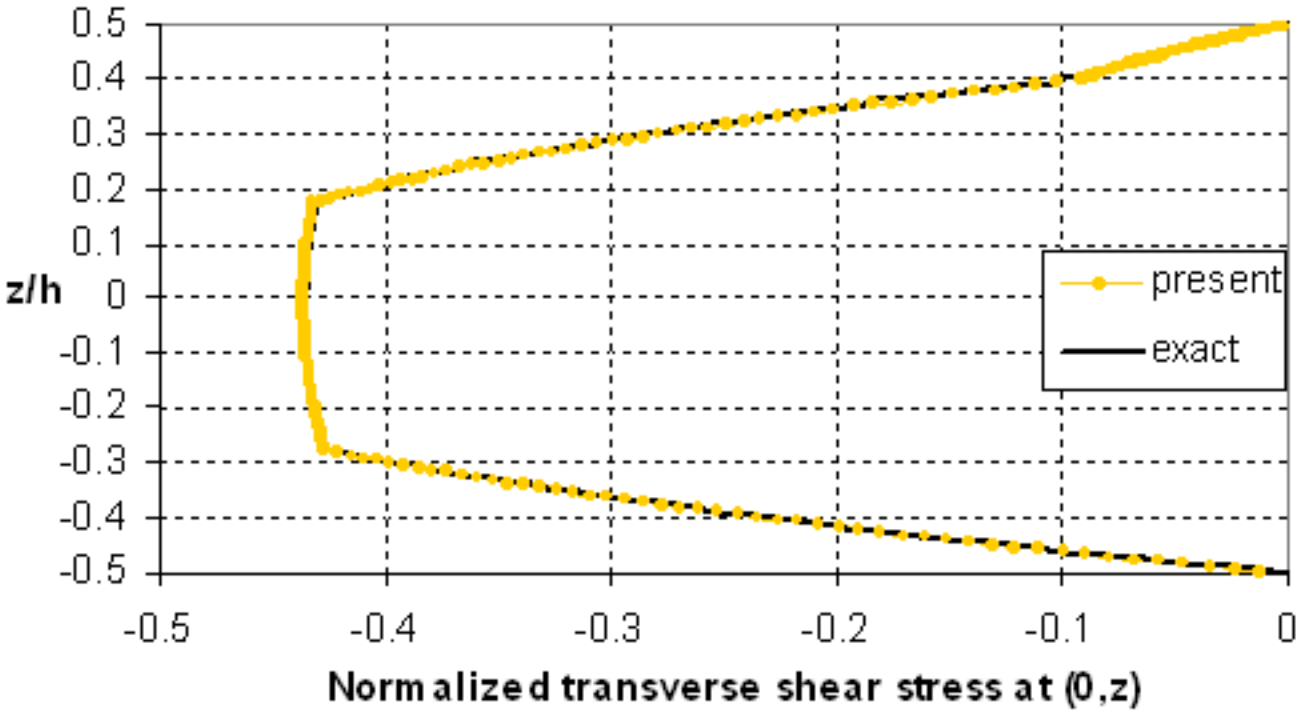

Fig. 5(e)
Click here to download high resolution image

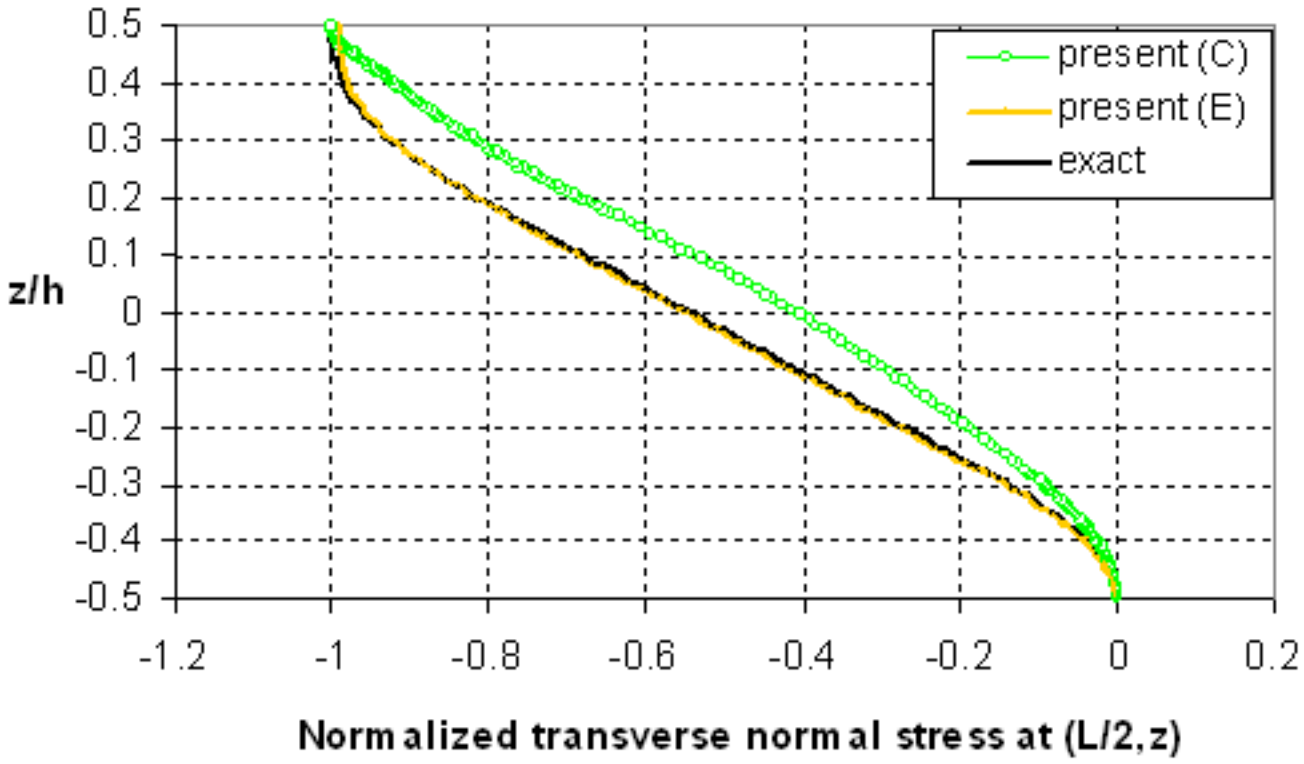

Fig. 5(f)
Click here to download high resolution image

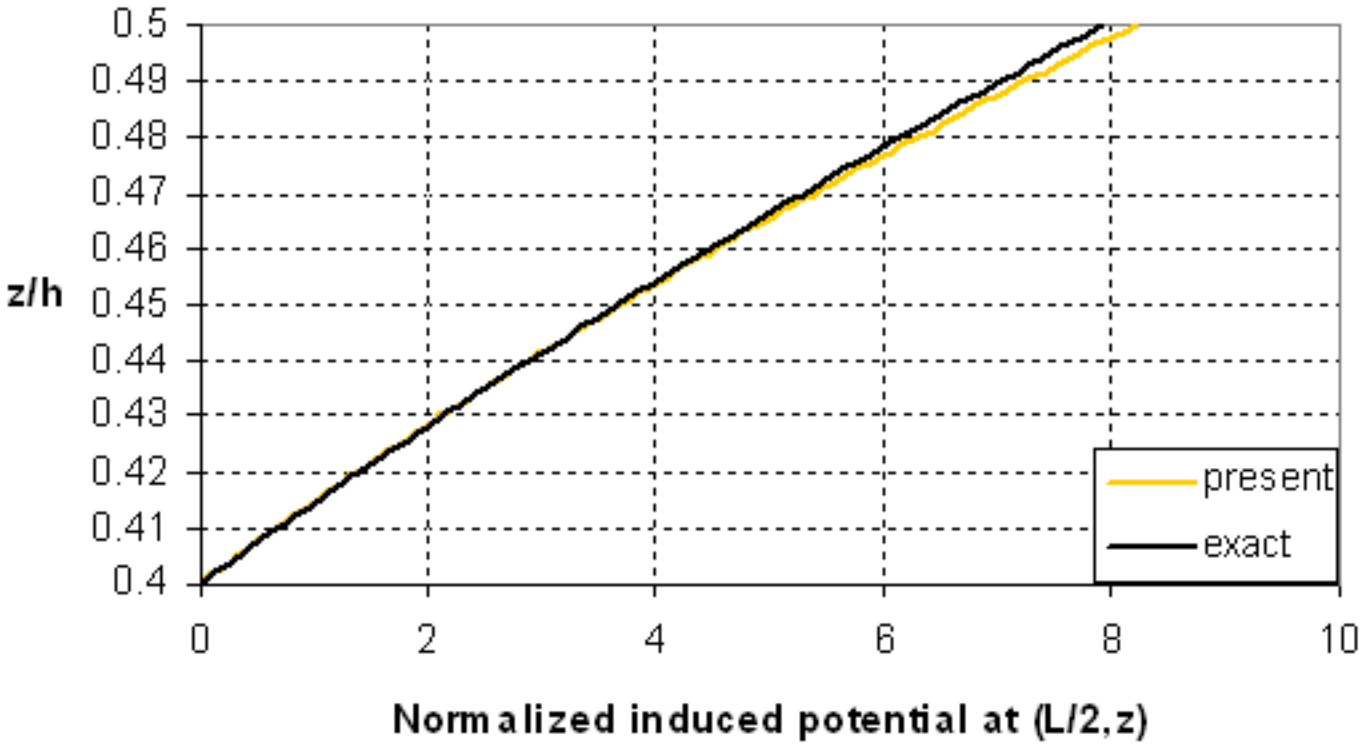

Fig. 6

Click here to download high resolution image

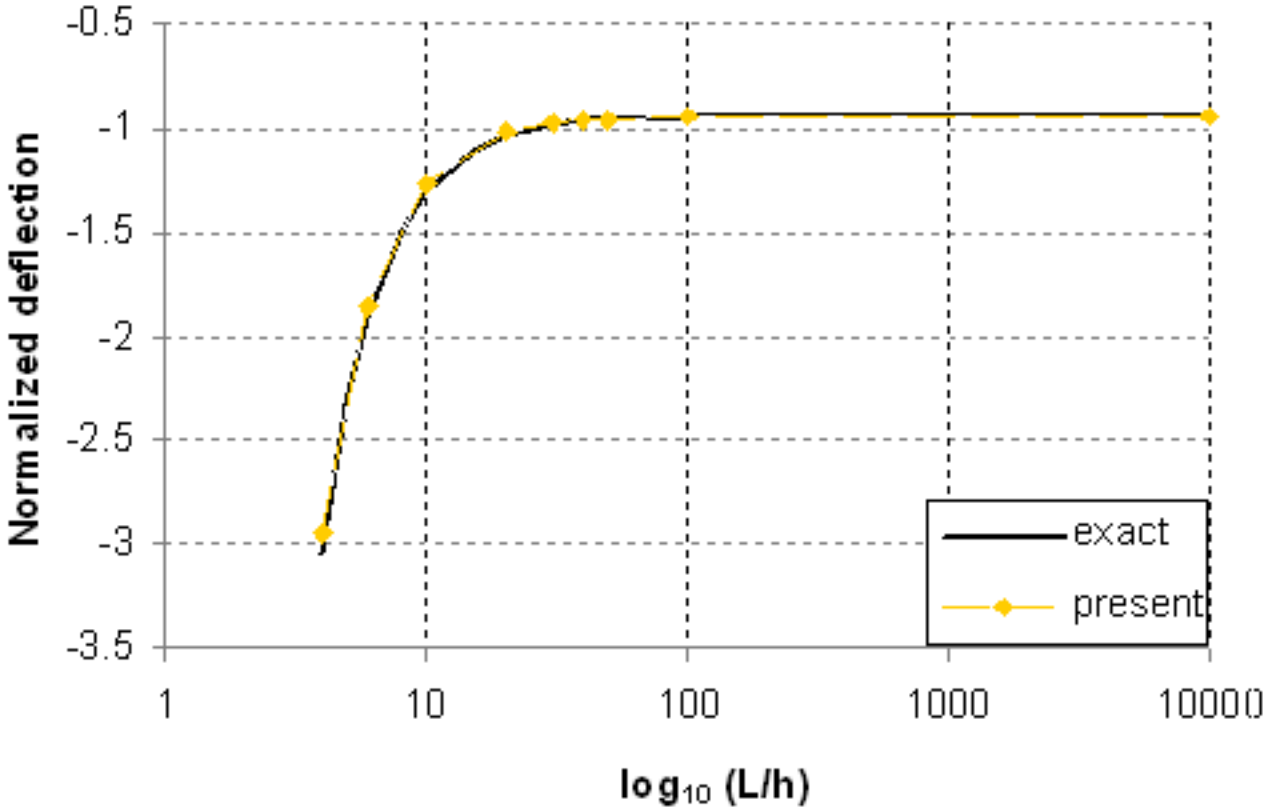

Fig. 7(a)
Click here to download high resolution image

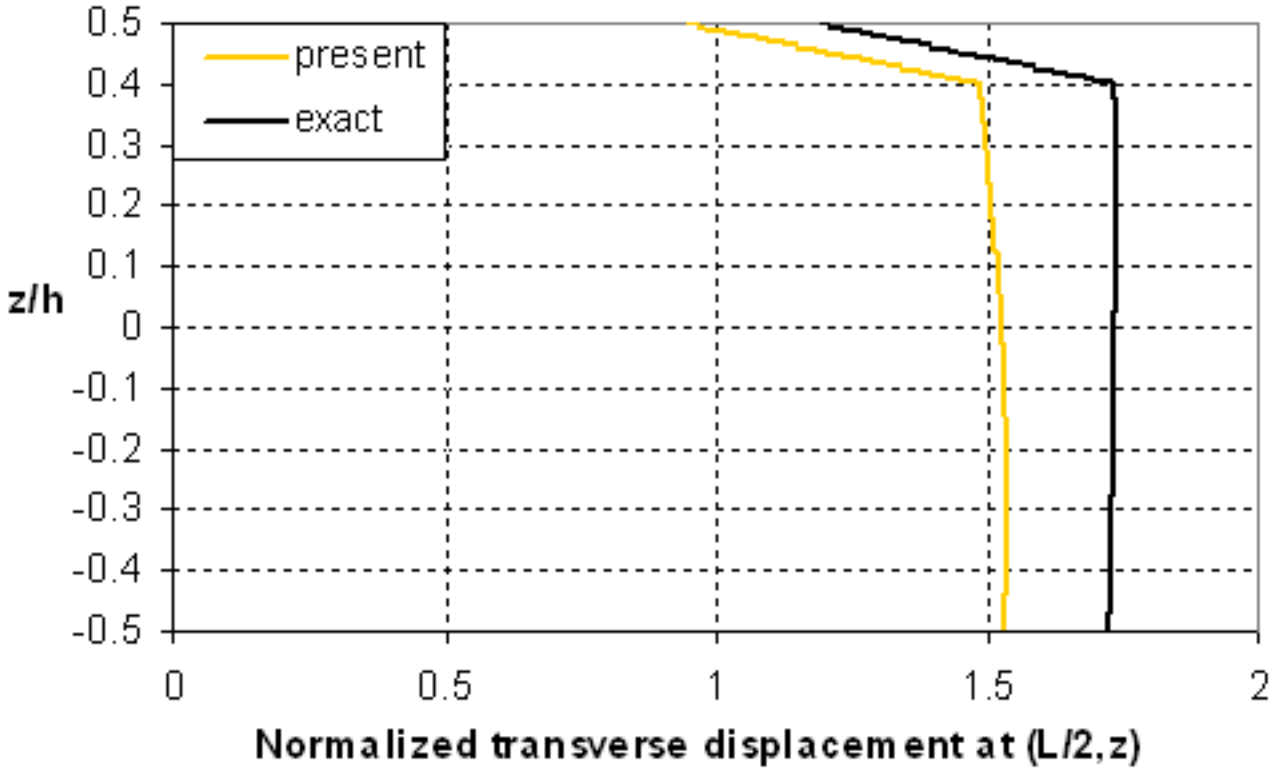

Fig. 7(b)
Click here to download high resolution image

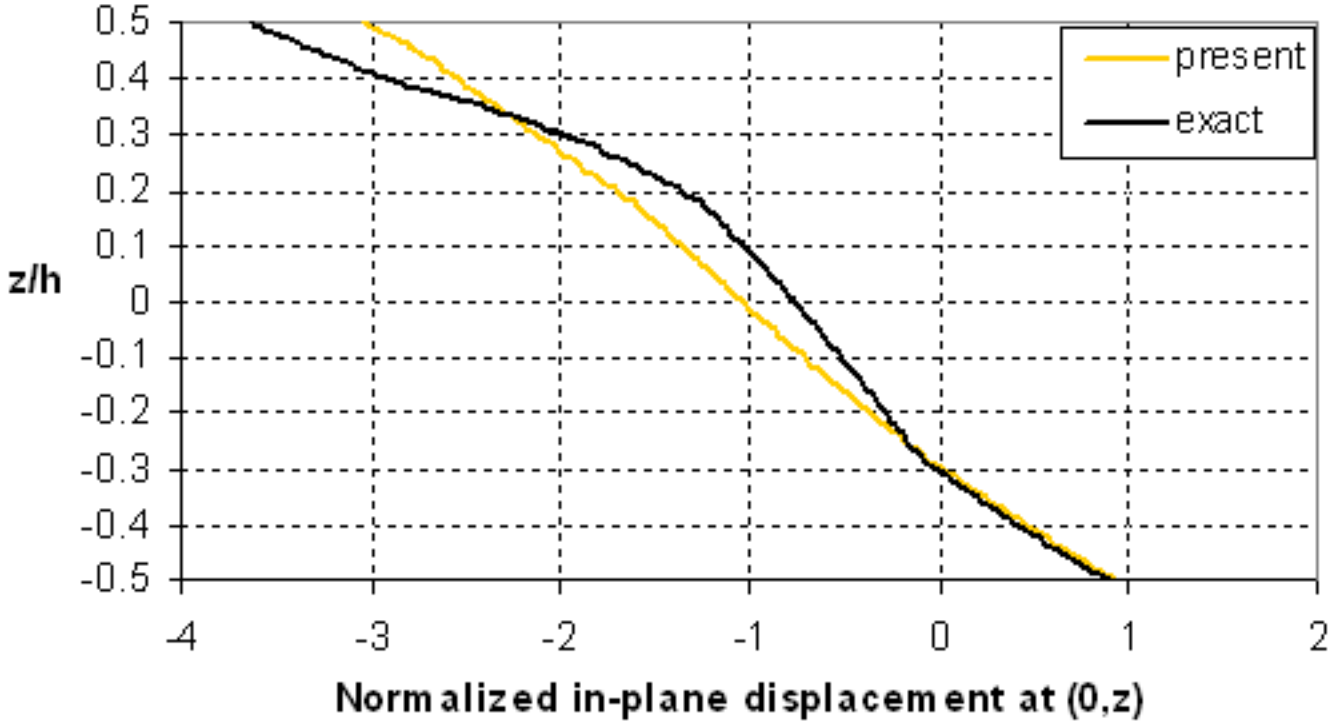

Fig. 7(c)
Click here to download high resolution image

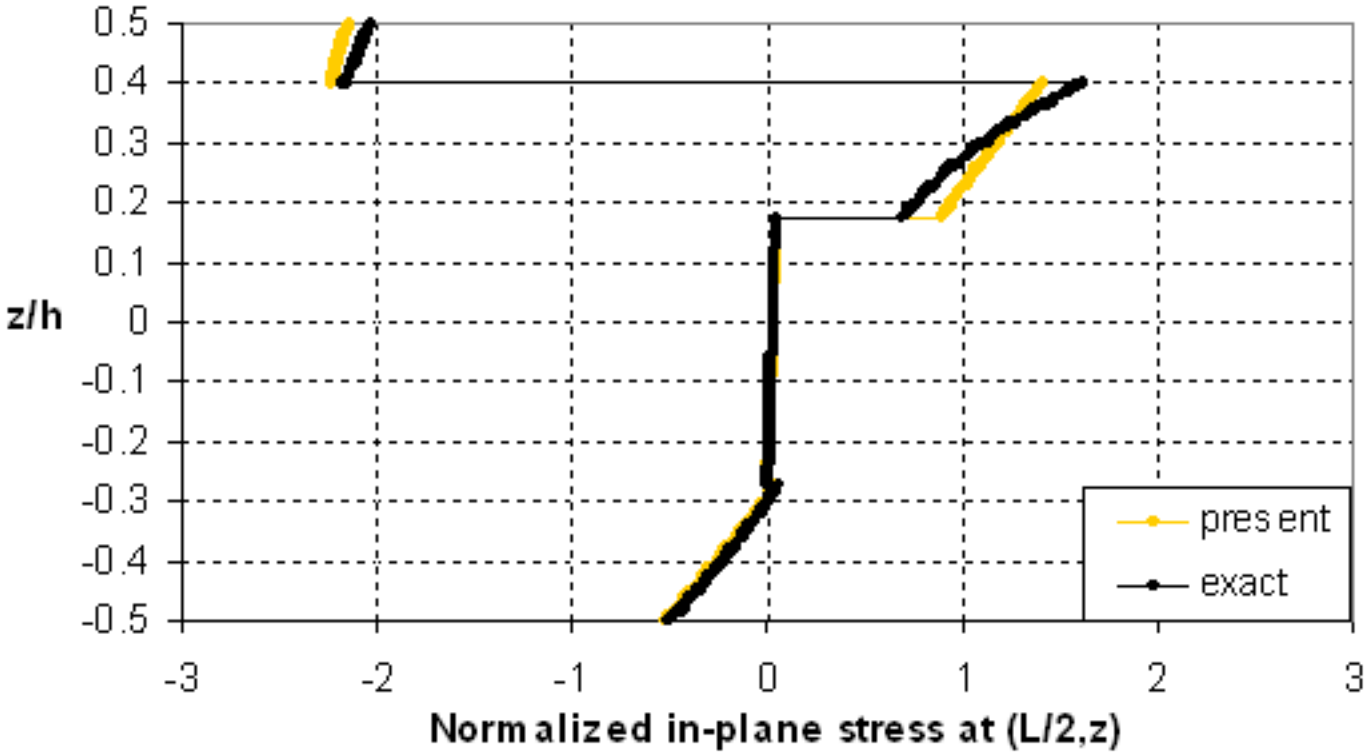

Fig. 7(d)
Click here to download high resolution image

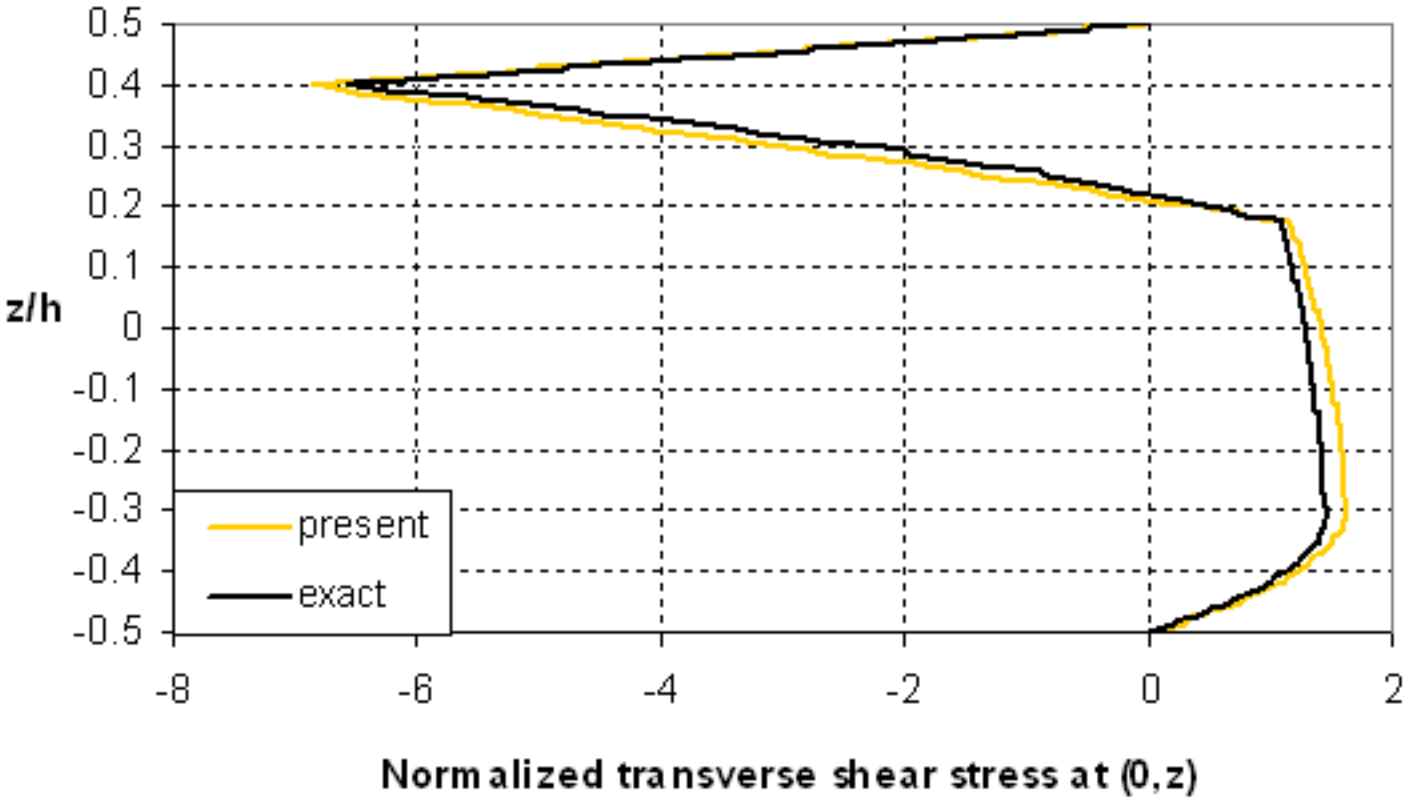

Fig. 7(e)
Click here to download high resolution image

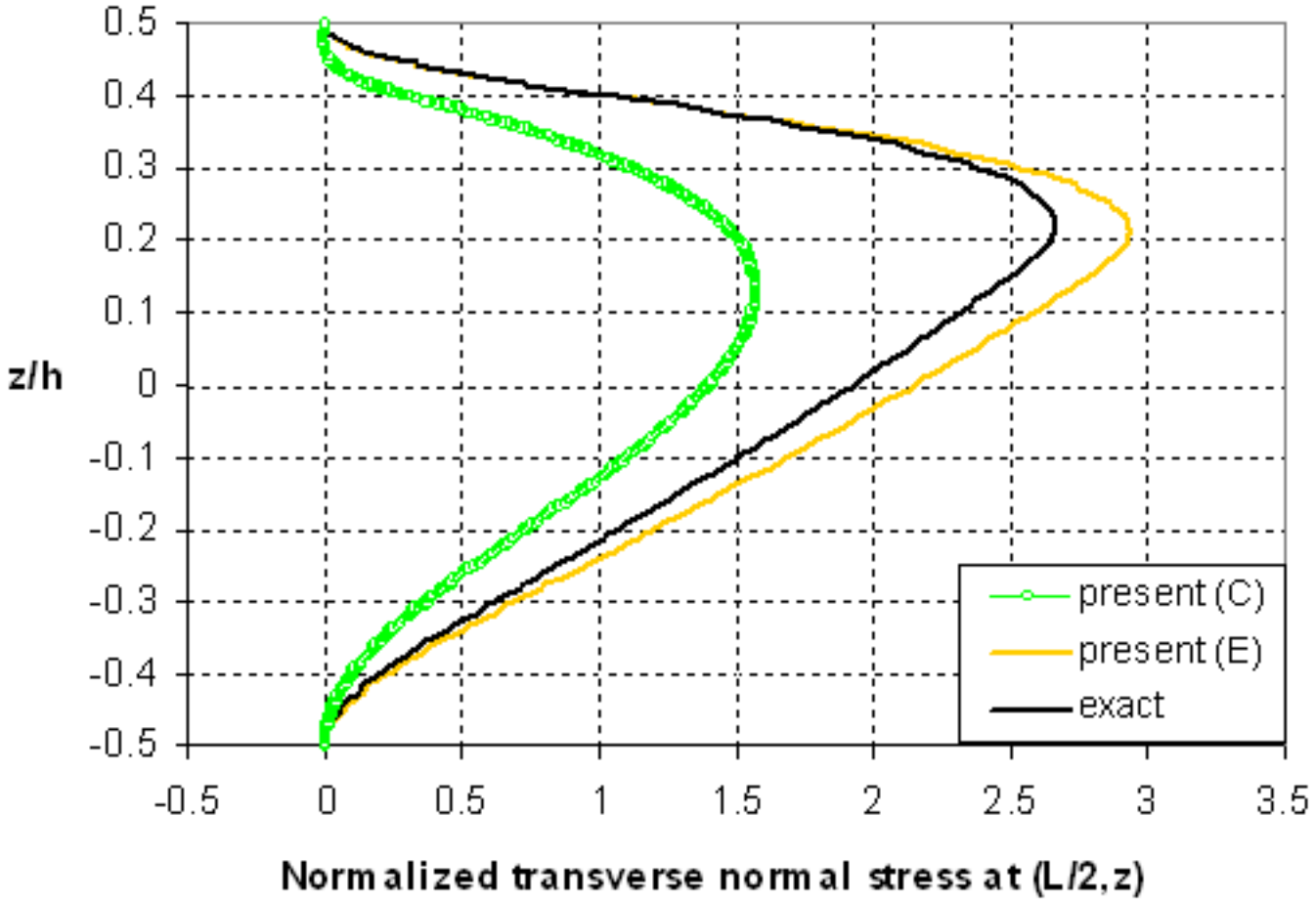

Fig. 7(f)
Click here to download high resolution image

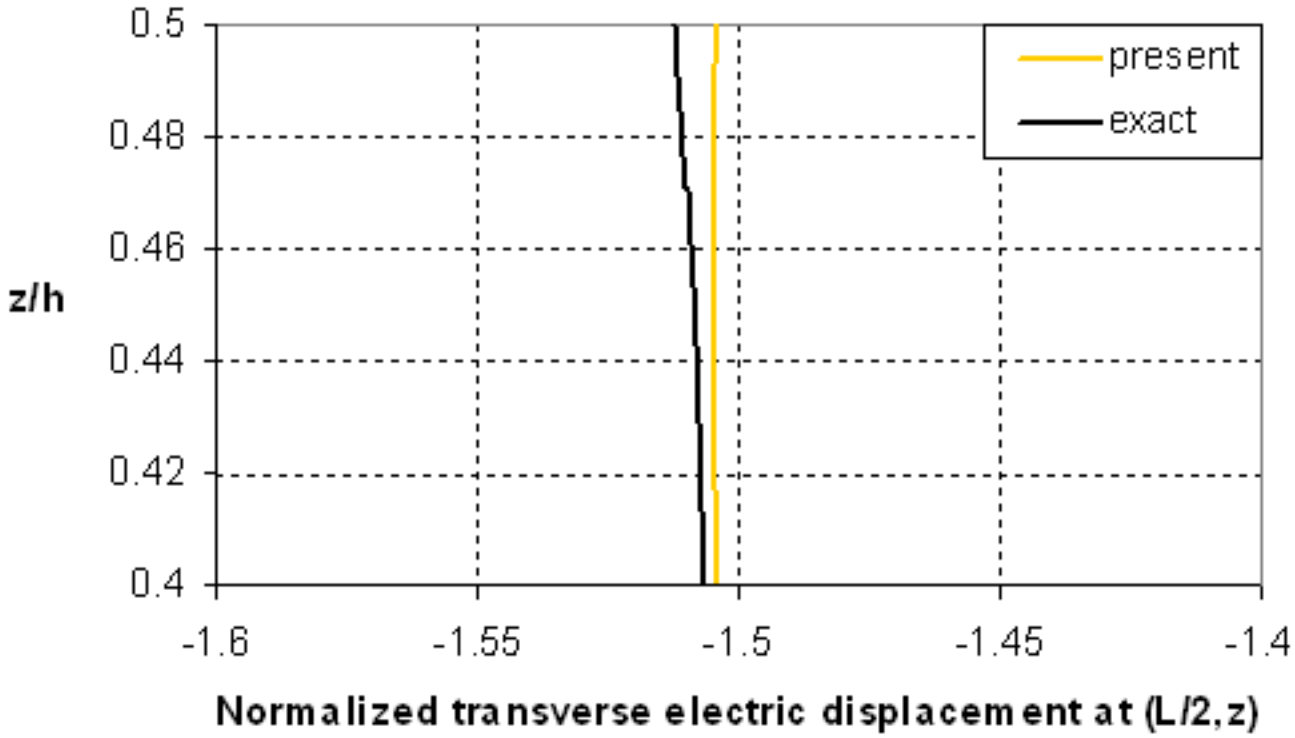

Fig. 8(a)
Click here to download high resolution image

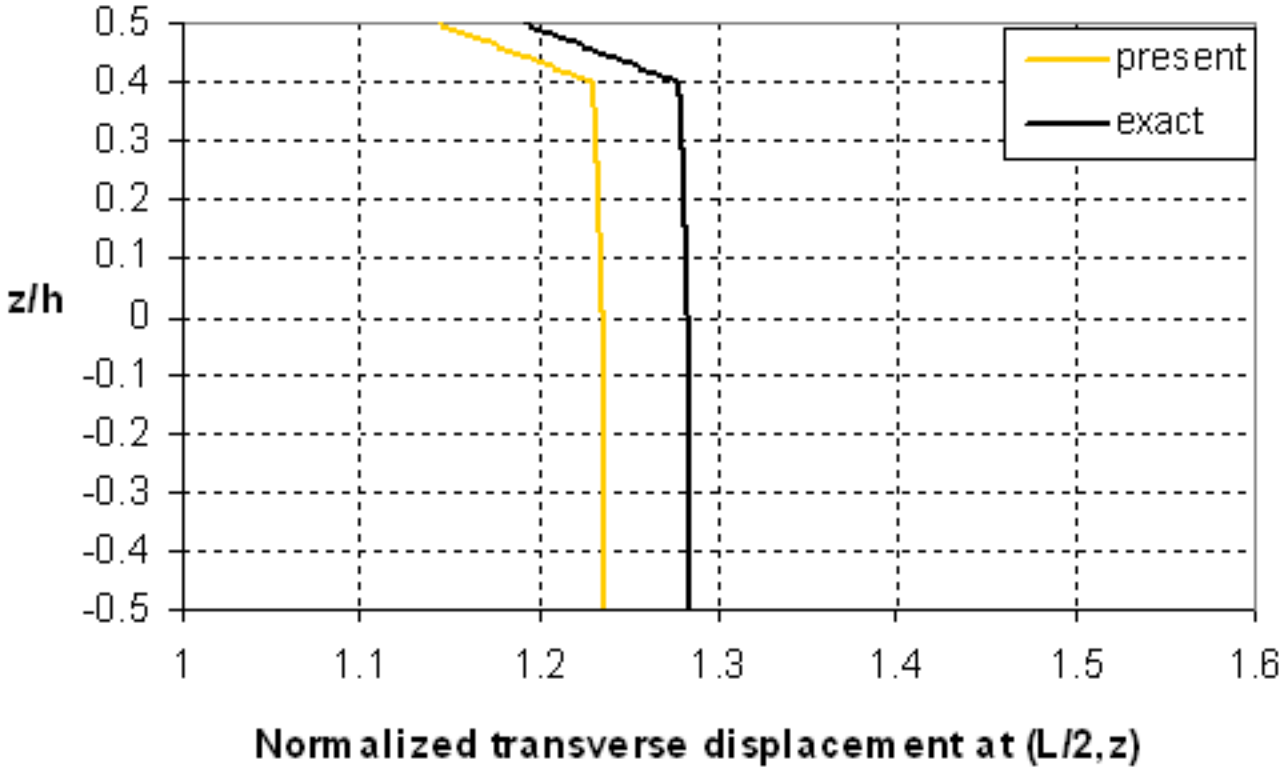

Fig. 8(b)
Click here to download high resolution image

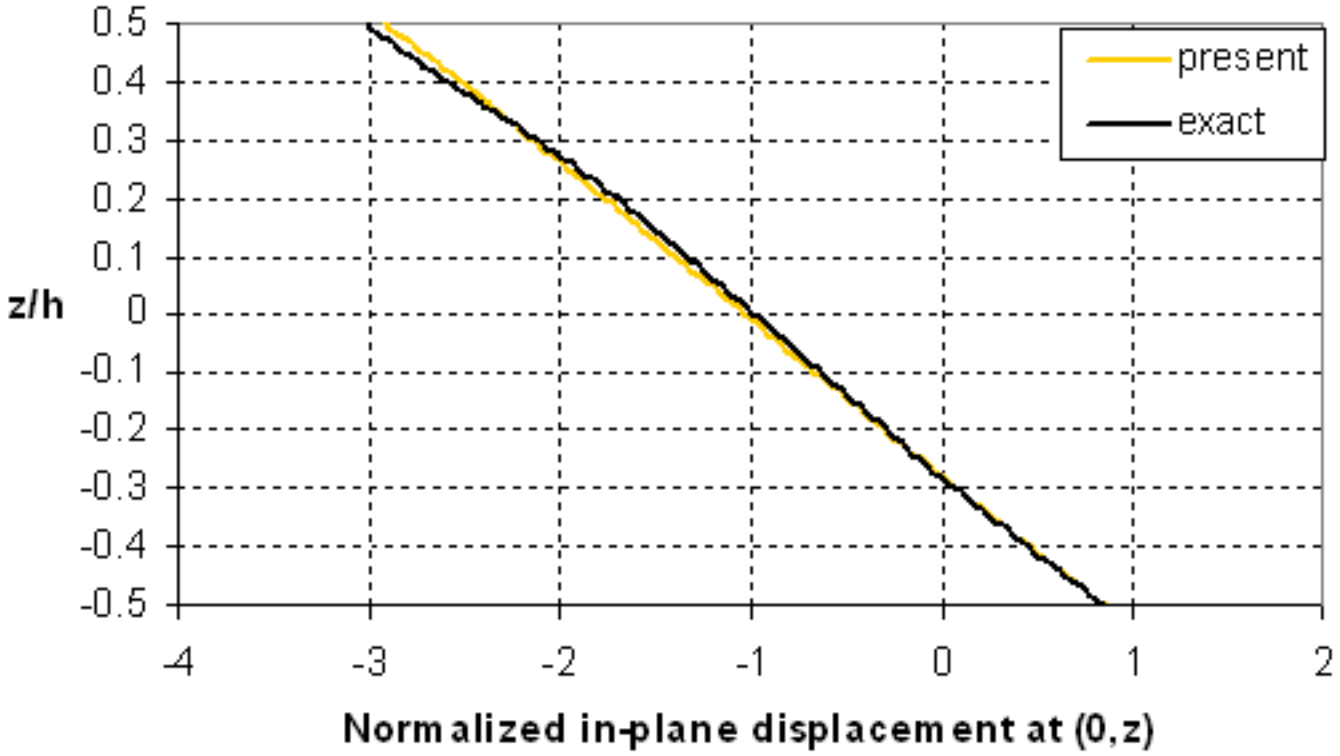

Fig. 8(c)
Click here to download high resolution image

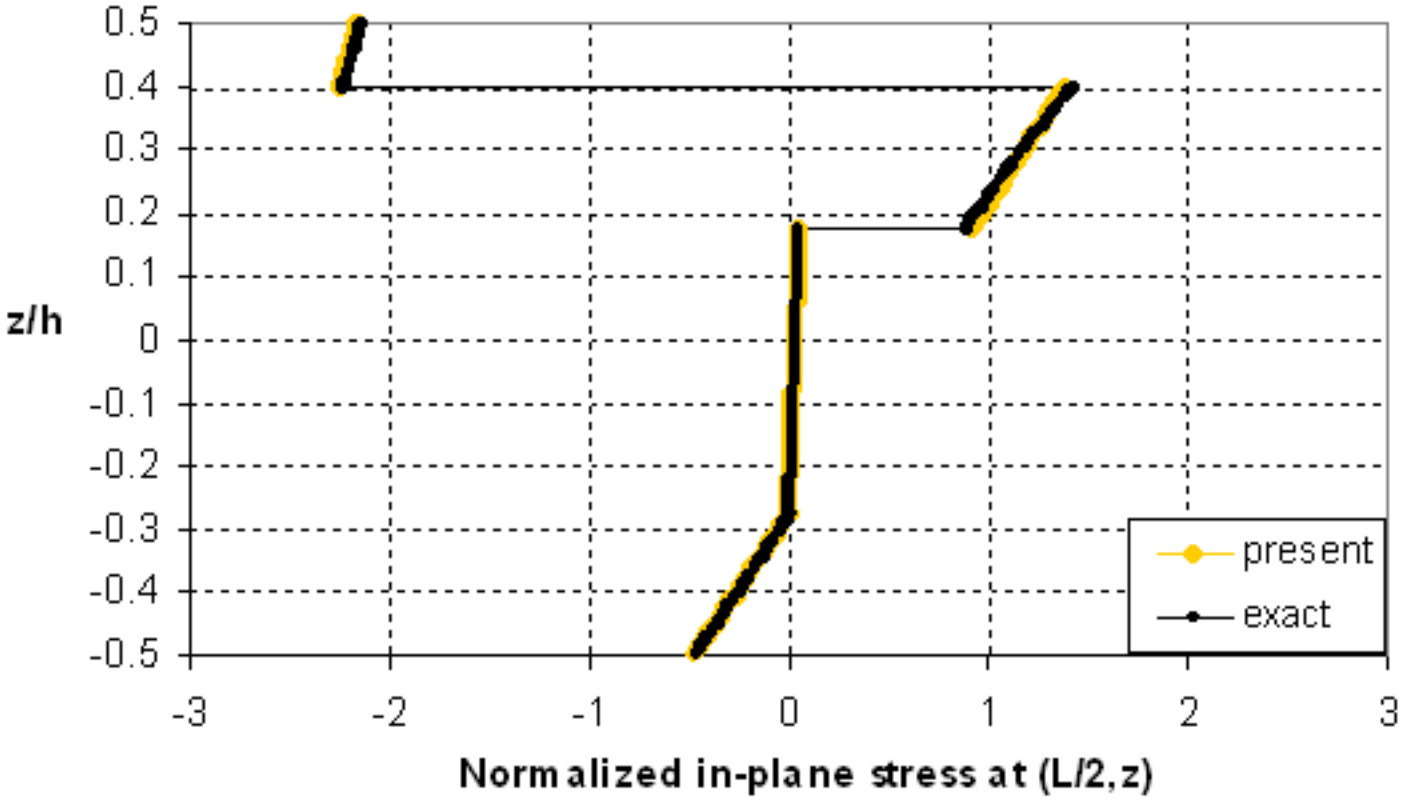

Fig. 8(d)
Click here to download high resolution image

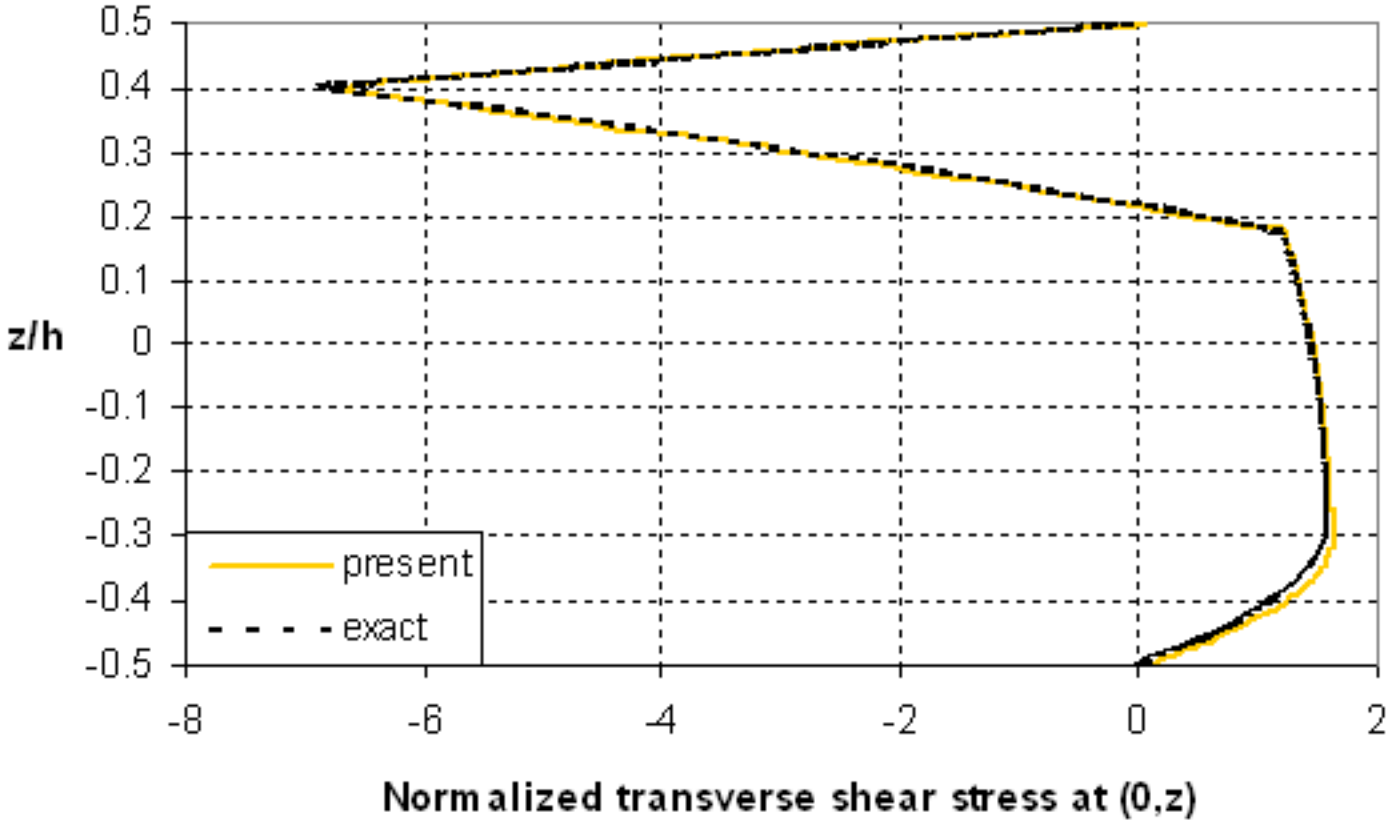

Fig. 8(e)
Click here to download high resolution image

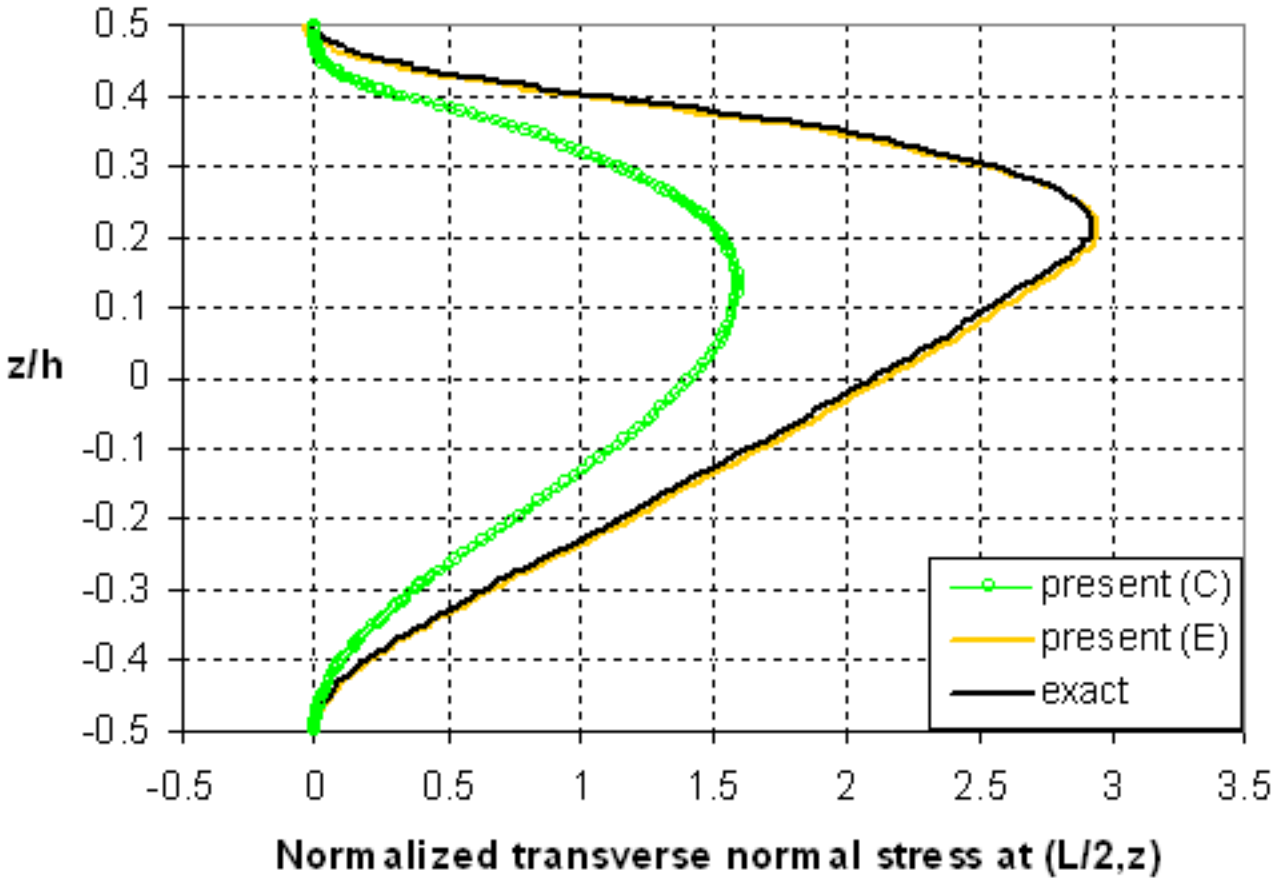

Fig. 8(f)
Click here to download high resolution image

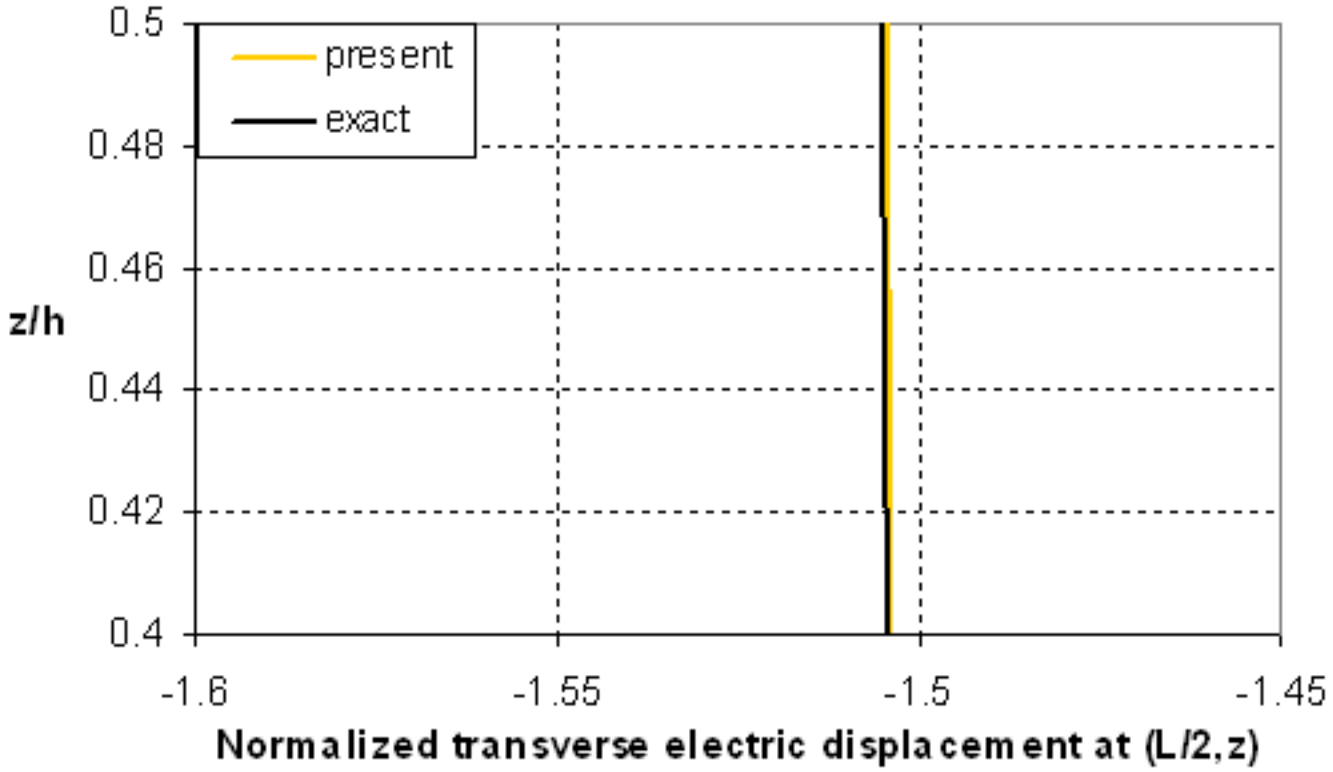

Fig. 9

Click here to download high resolution image

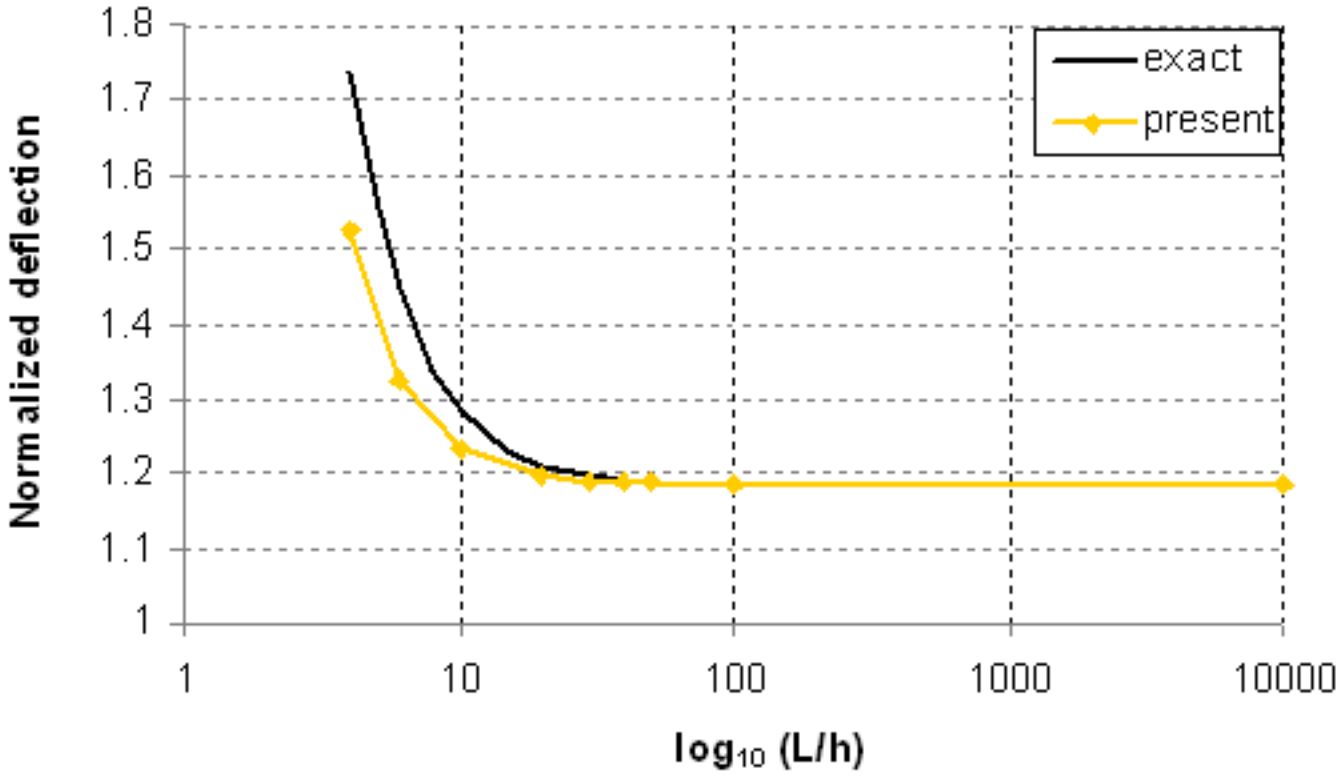

Fig. 10(a)
Click here to download high resolution image

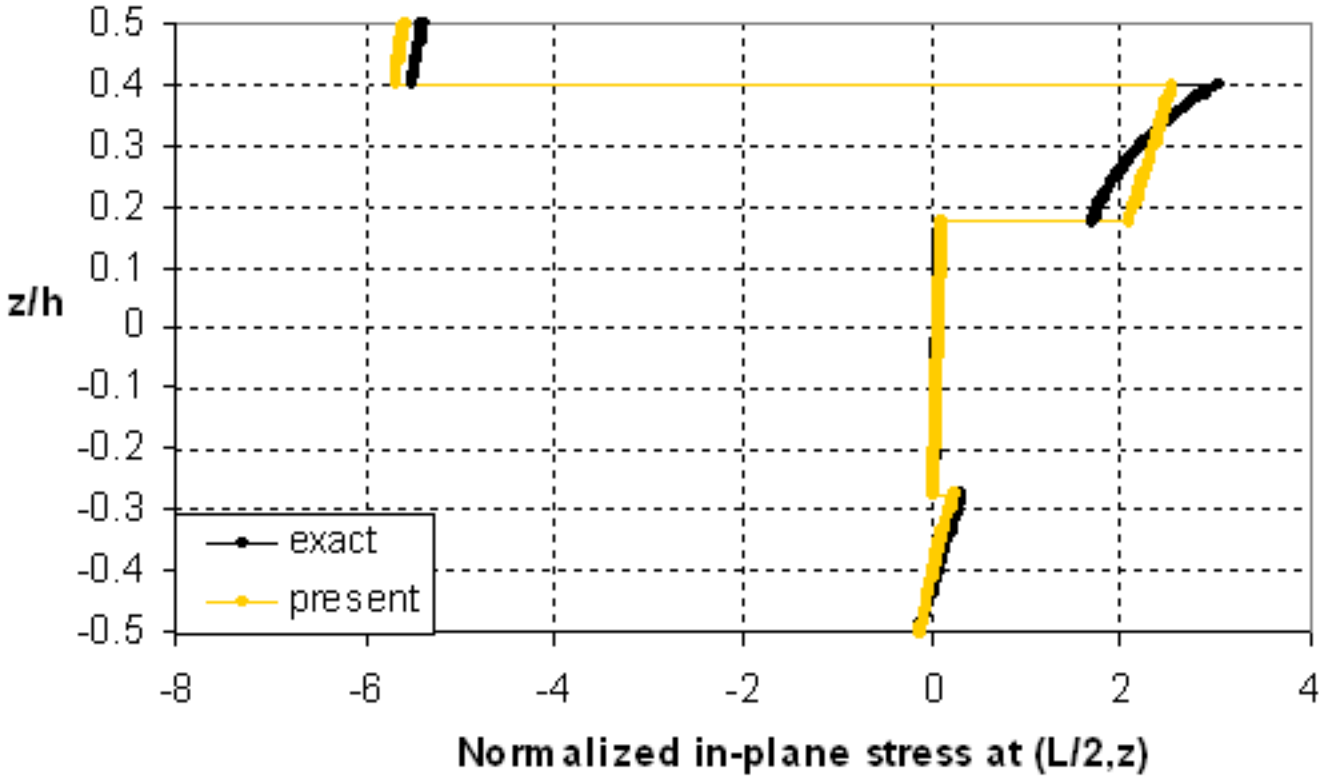

Fig. 10(b)
Click here to download high resolution image

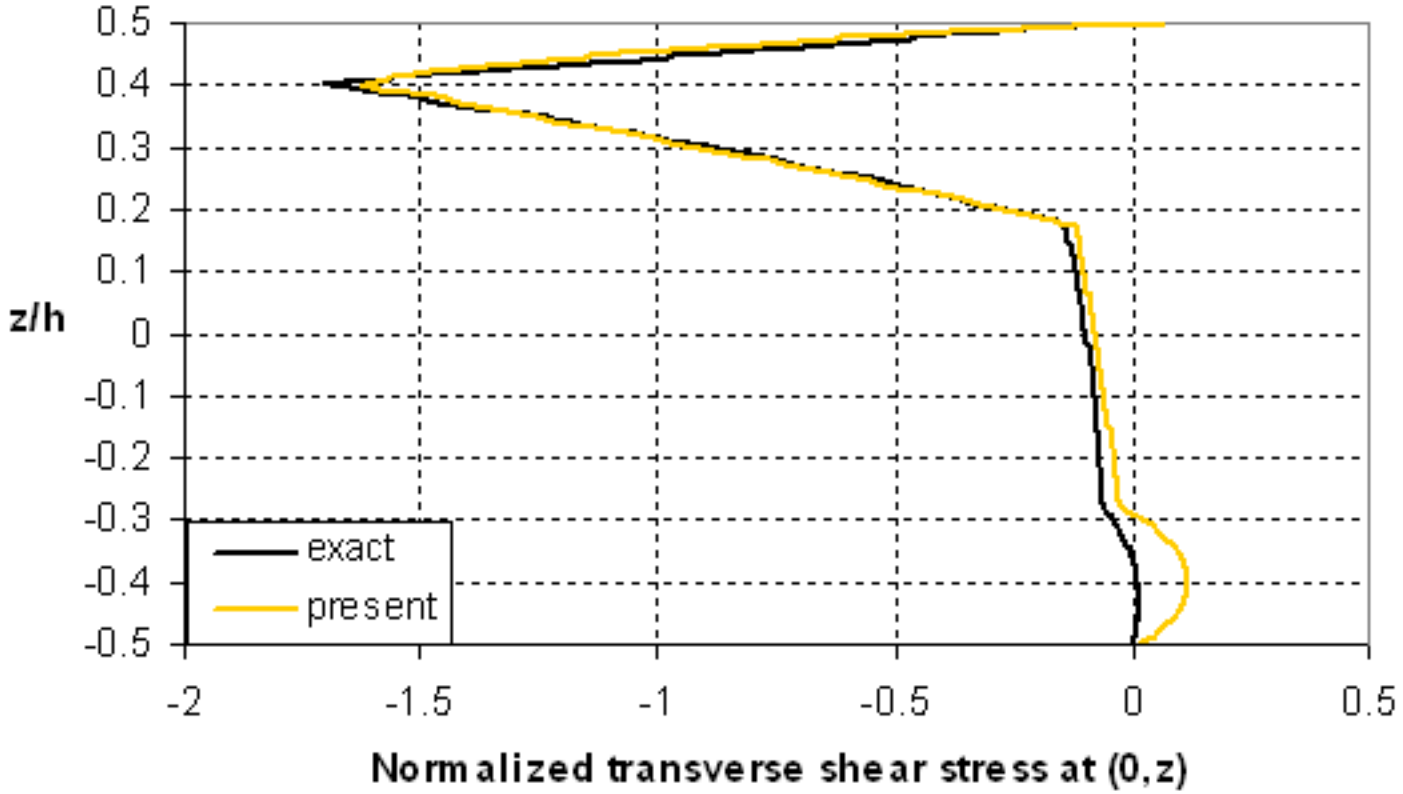

Fig. 10(c)
Click here to download high resolution image

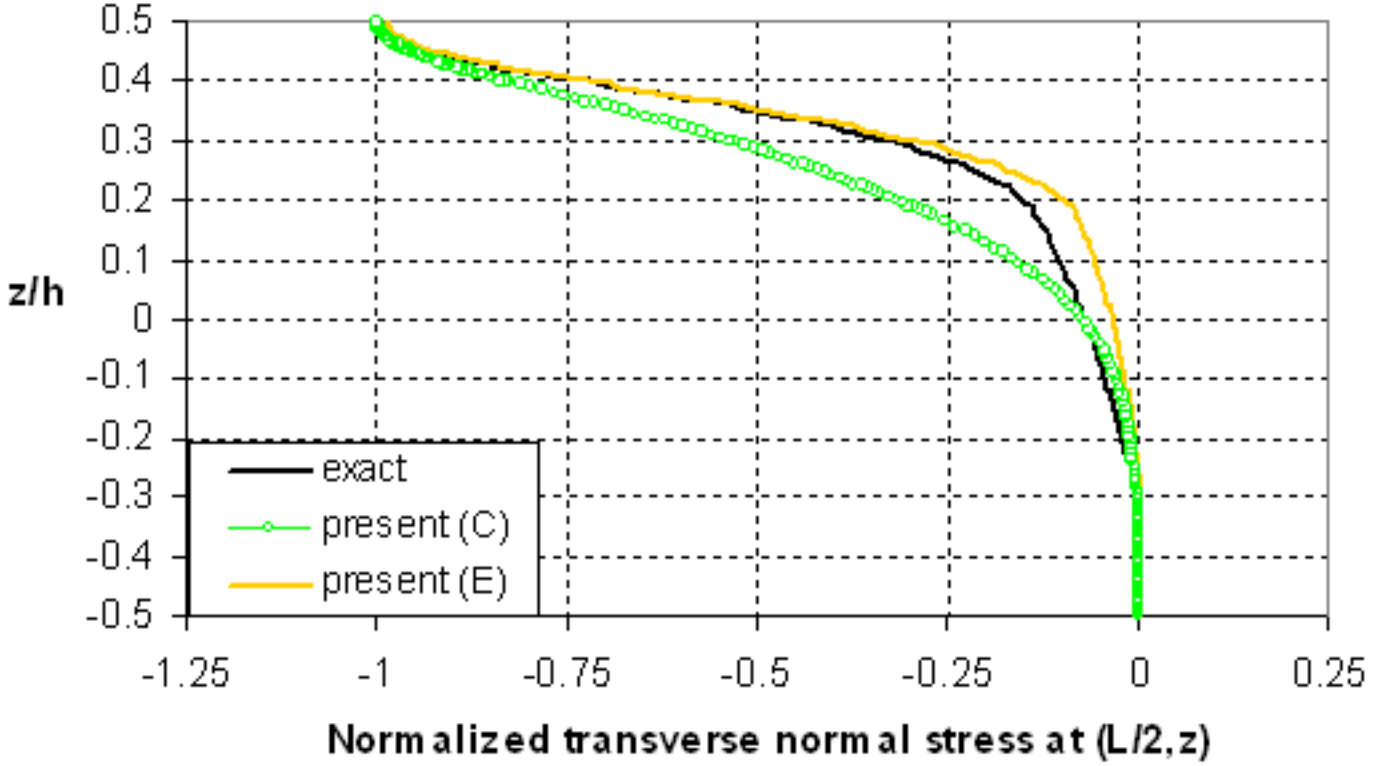

Fig. 10(d)
Click here to download high resolution image

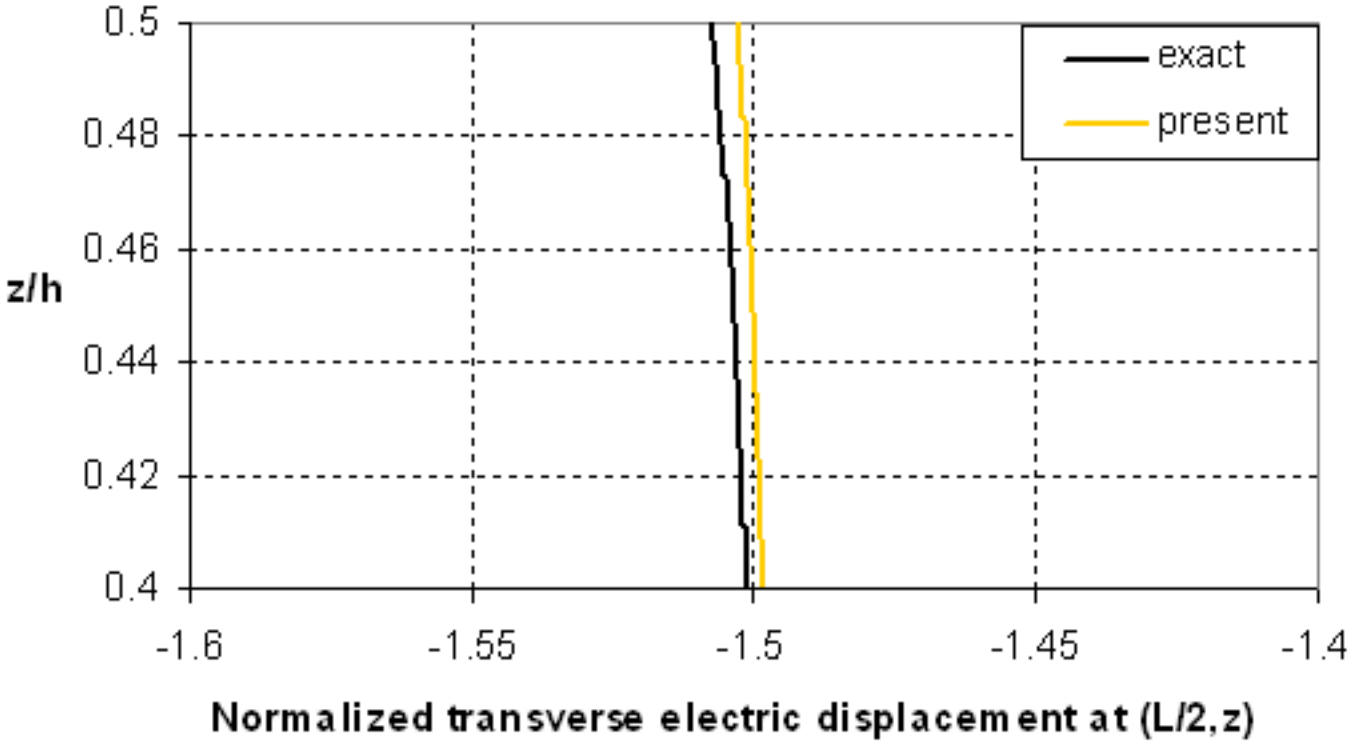

Fig. 11(a)

Click here to download high resolution image

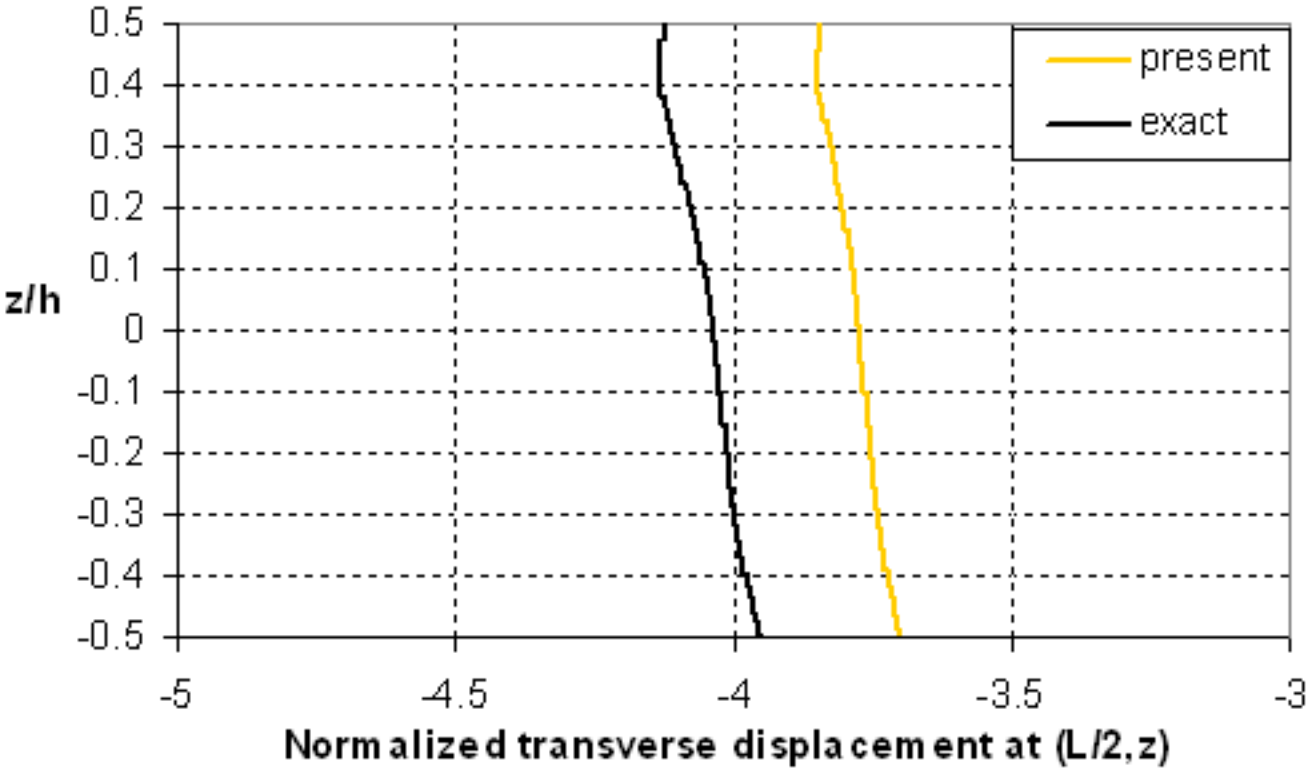

Fig. 11(b)
Click here to download high resolution image

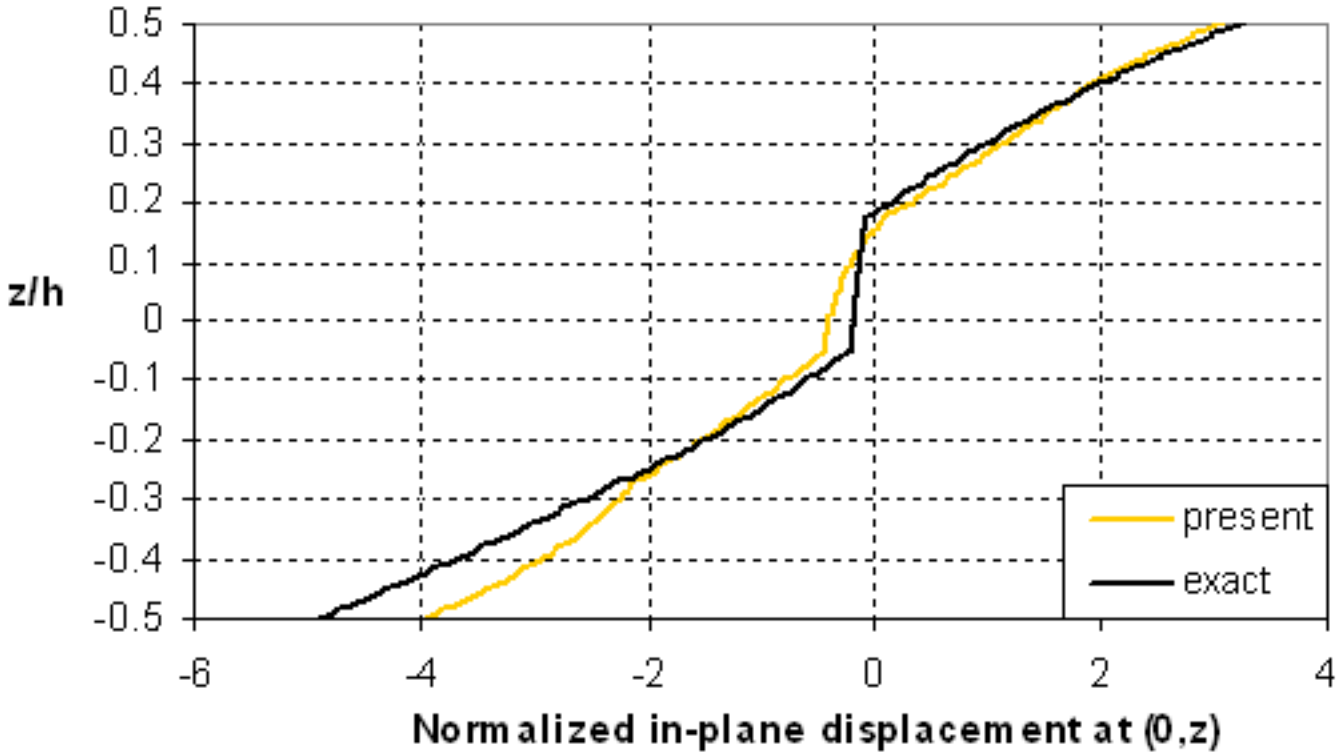

Fig. 11(c)
Click here to download high resolution image

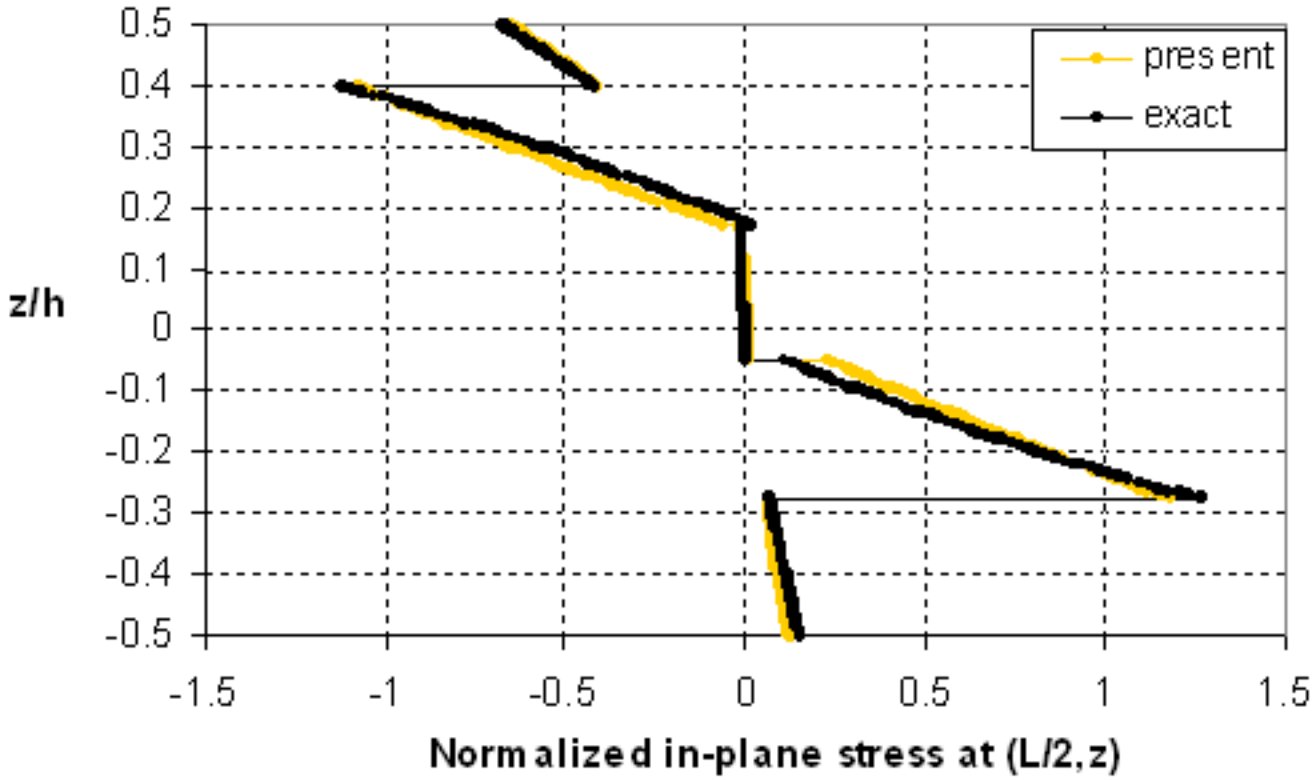

Fig. 11(d)
Click here to download high resolution image

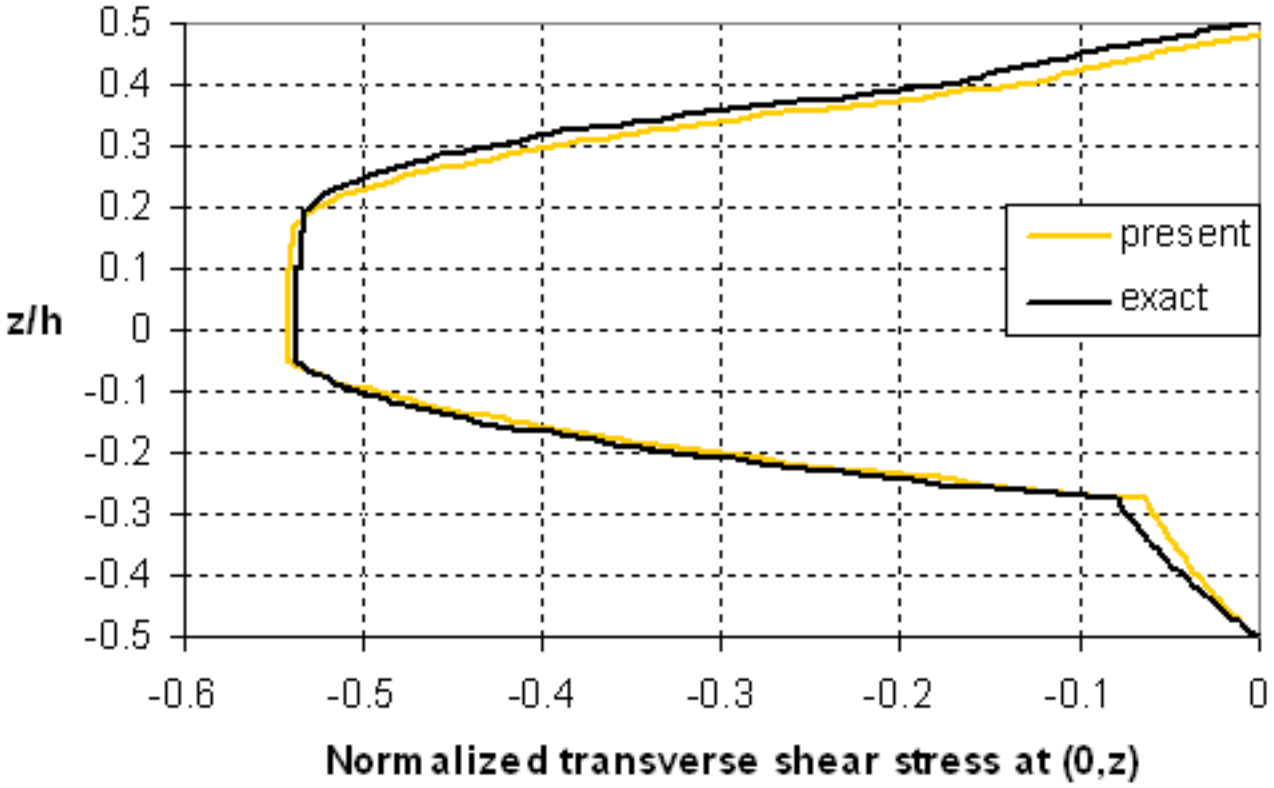

Fig. 11(e)
Click here to download high resolution image

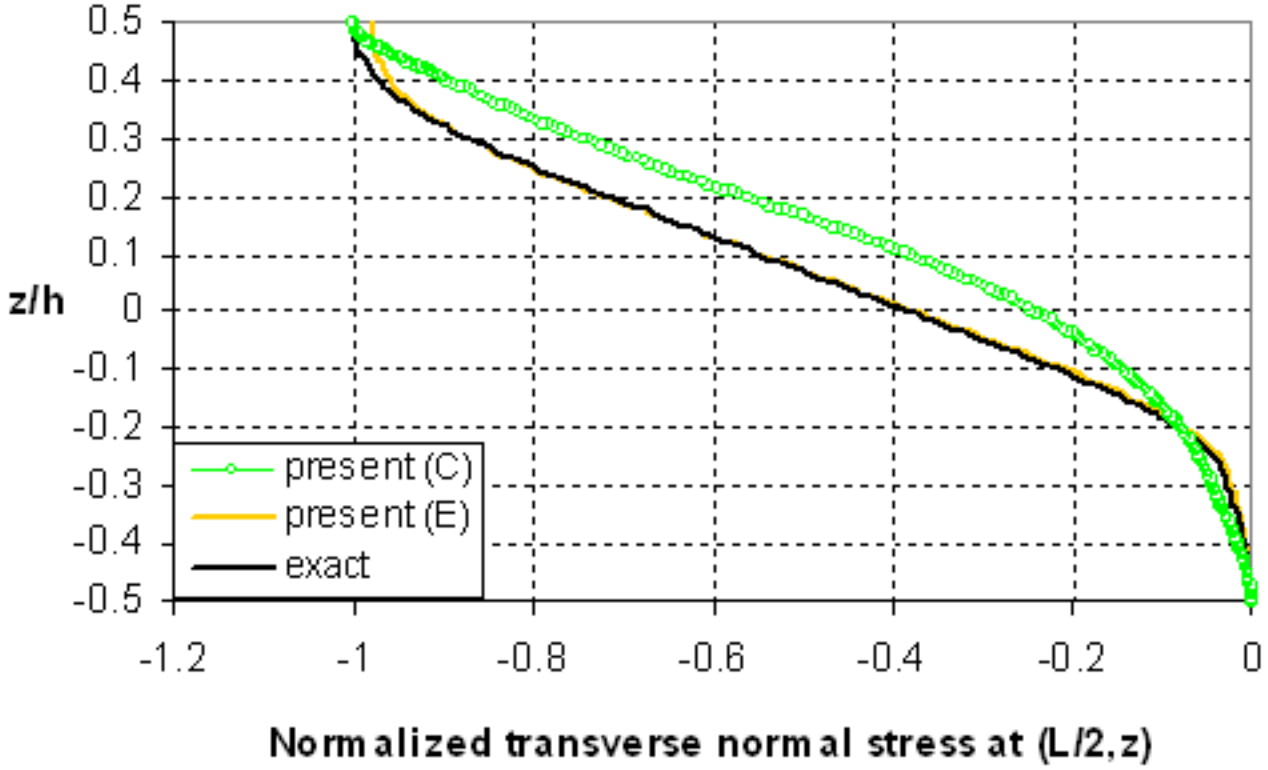

Fig. 11(f)
Click here to download high resolution image

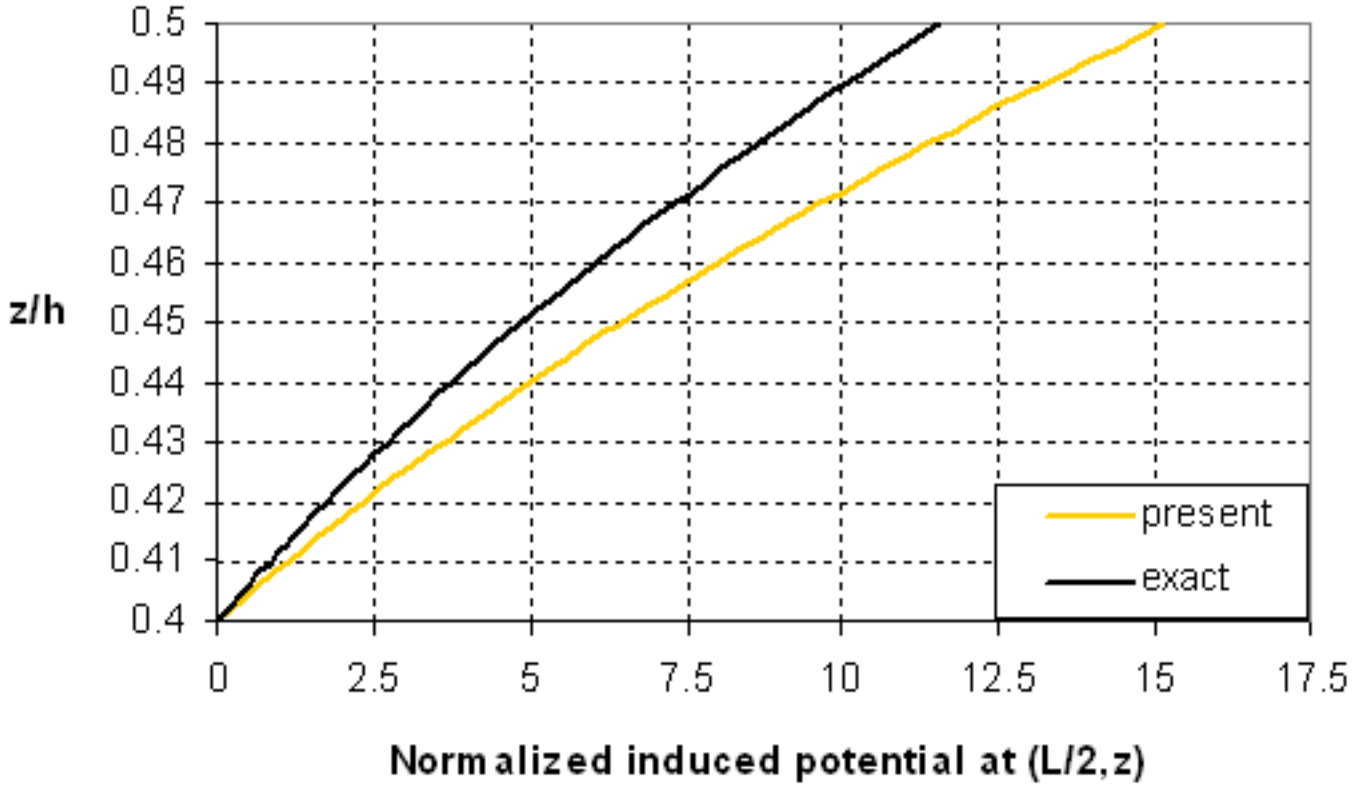

Fig. 12(a)

Click here to download high resolution image

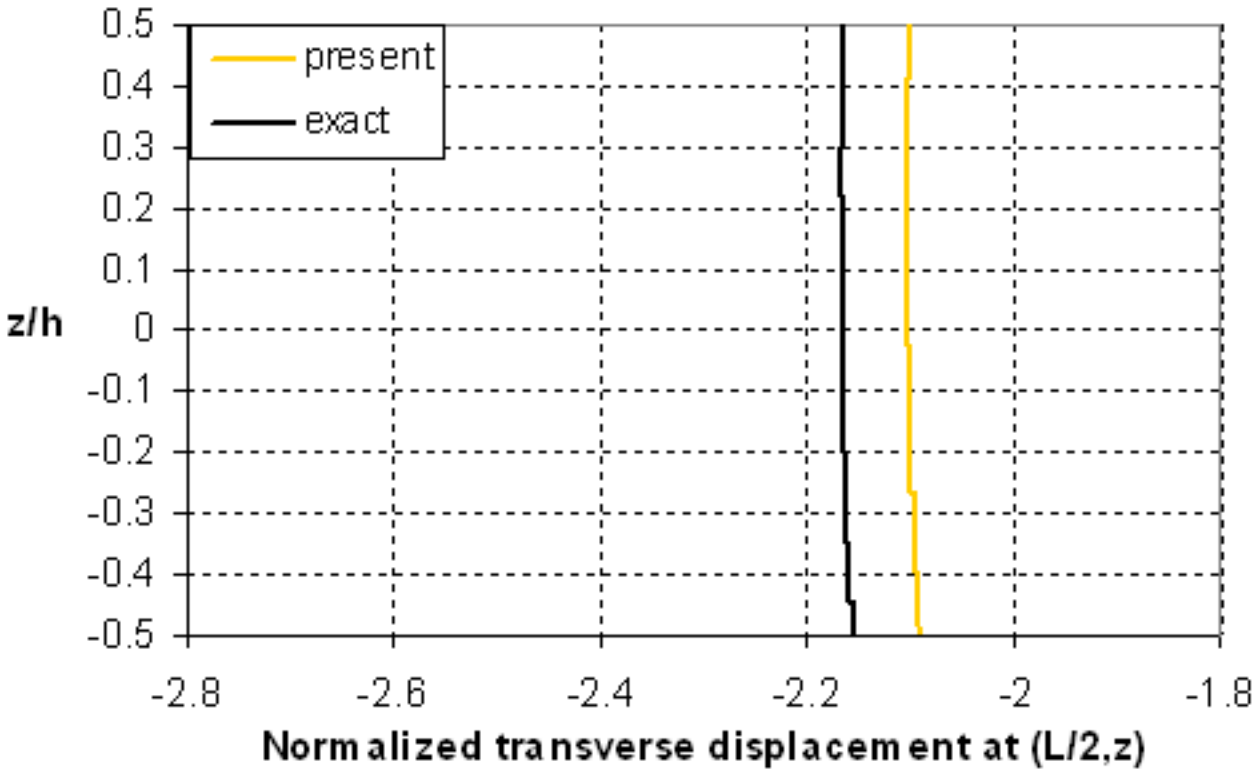

Fig. 12(b)
Click here to download high resolution image

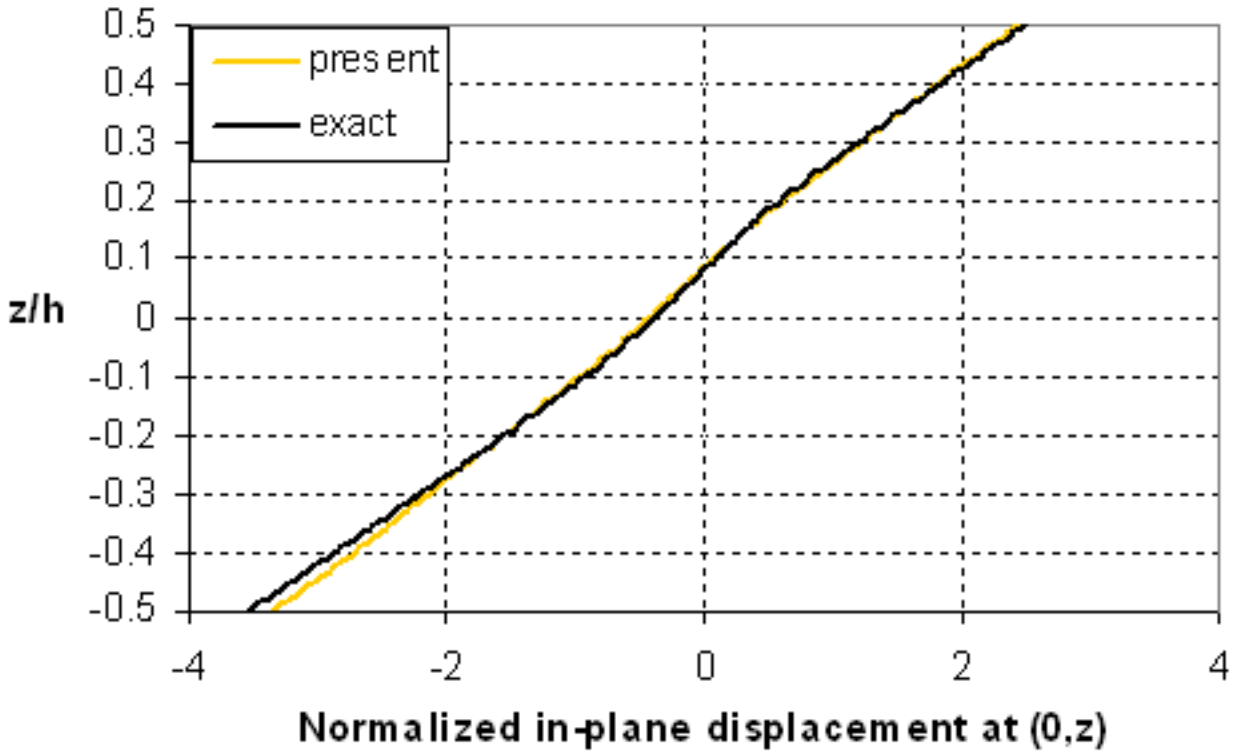

Fig. 12(c)
Click here to download high resolution image

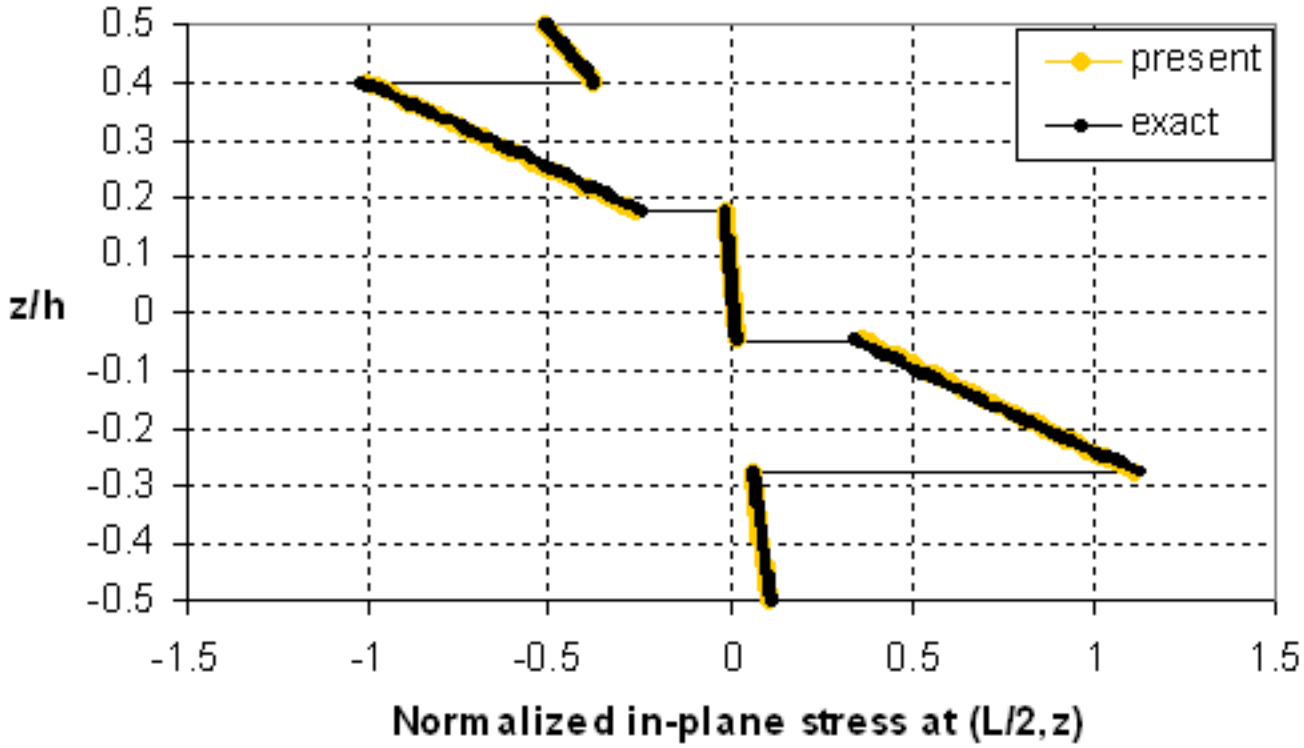

Fig. 12(d)

Click here to download high resolution image

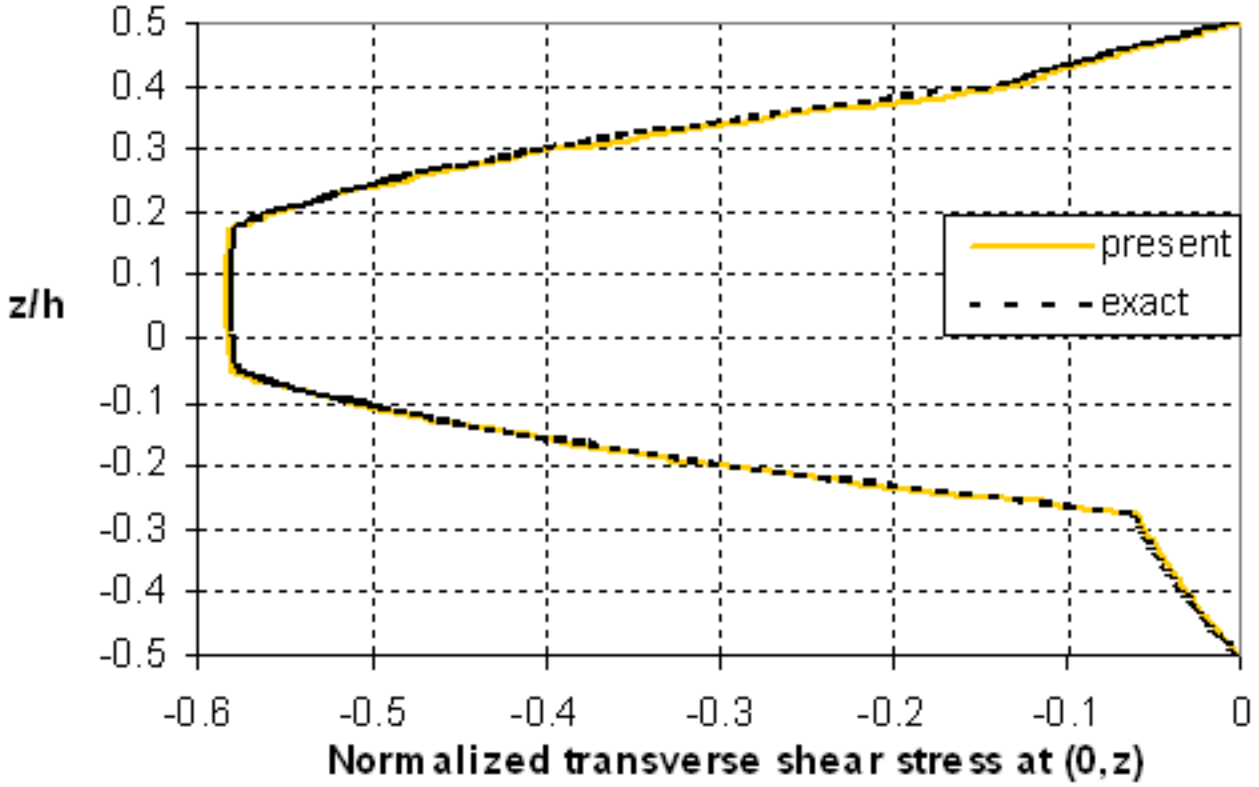

Fig. 12(e)
Click here to download high resolution image

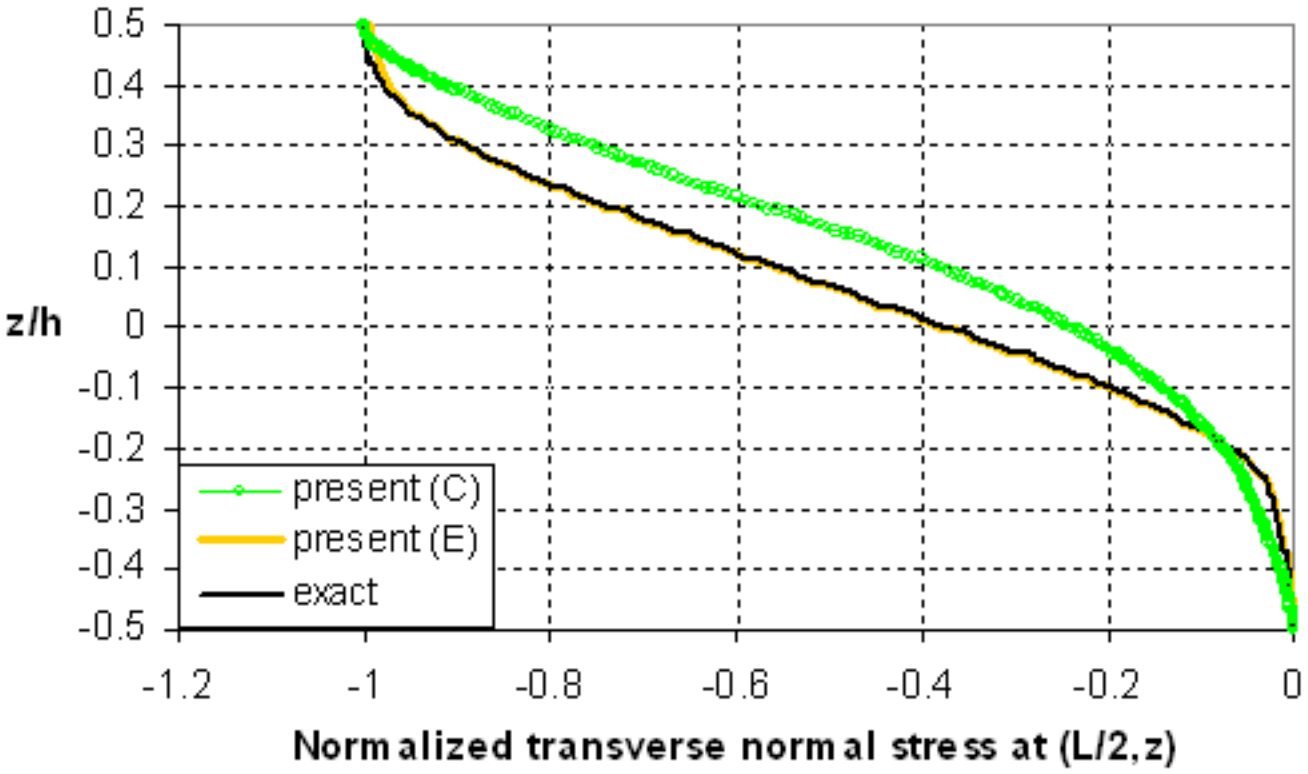

Fig. 12(f)
Click here to download high resolution image

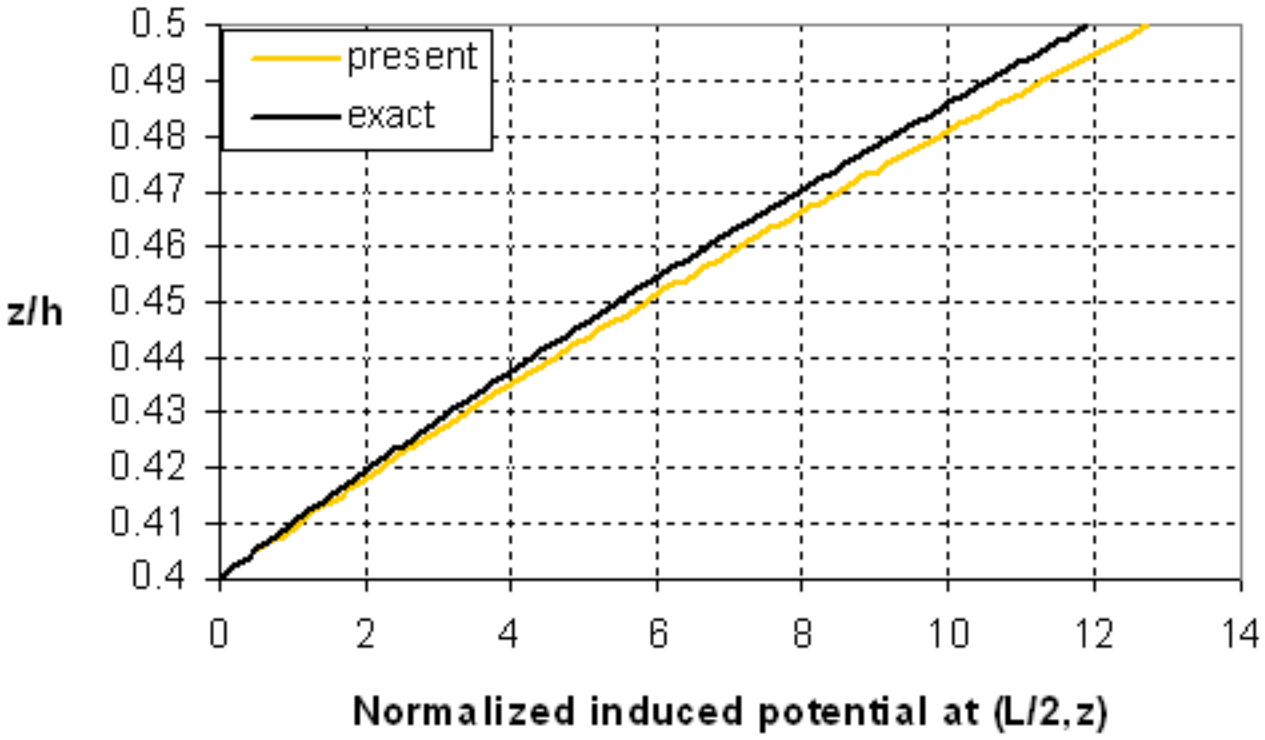

Fig. 13(a)

Click here to download high resolution image

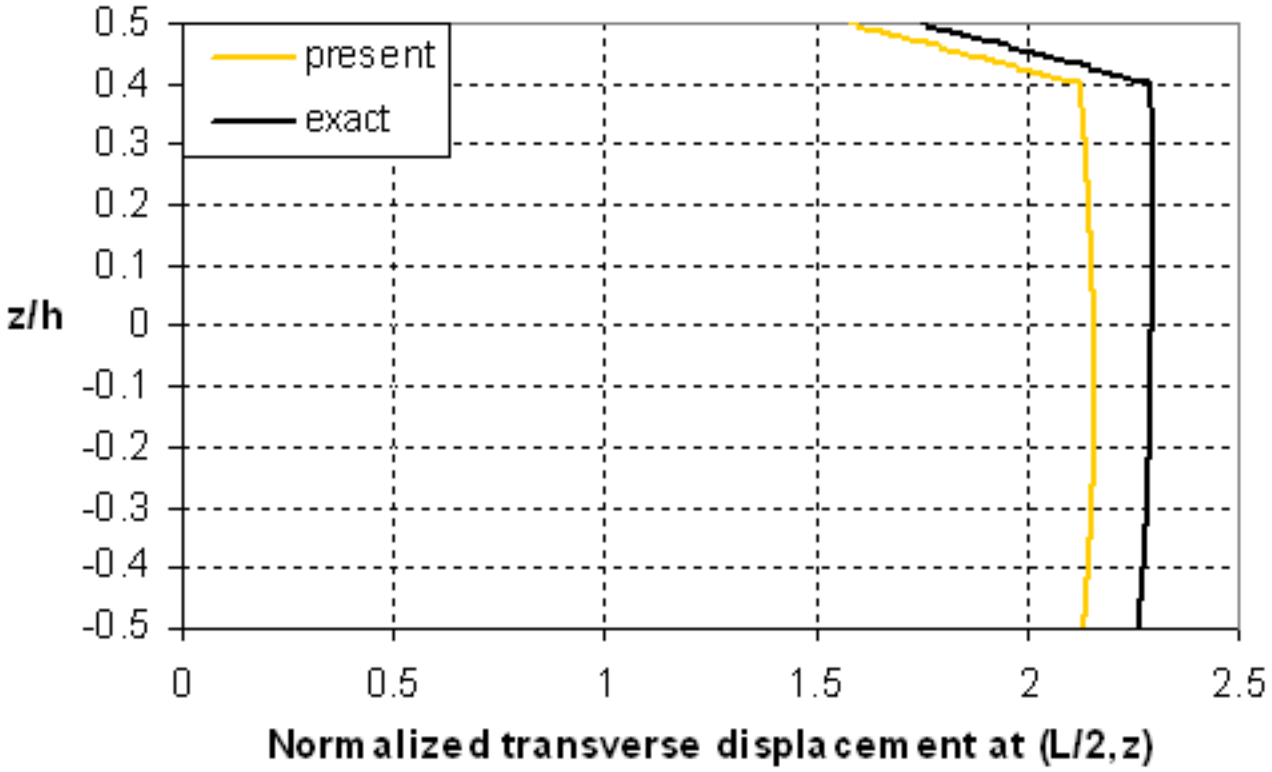

Fig. 13(b)
Click here to download high resolution image

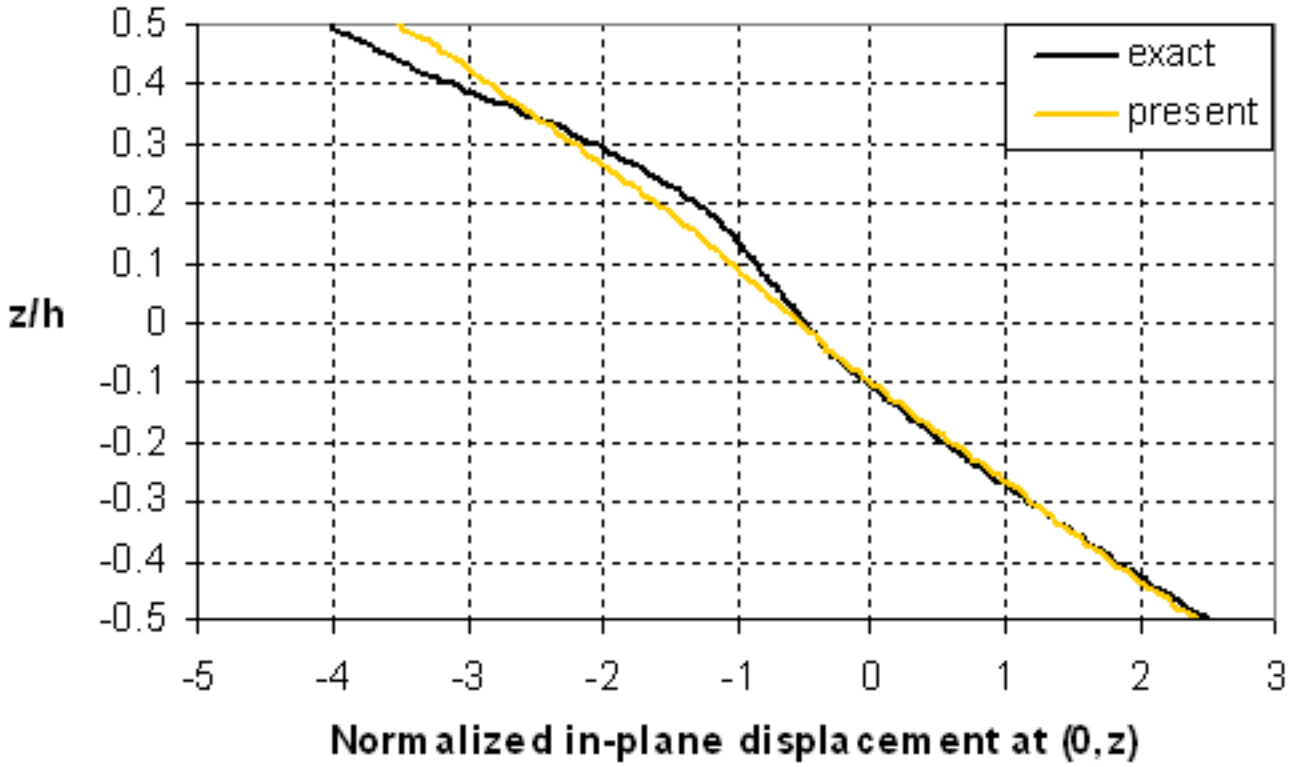

Fig. 13(c)
Click here to download high resolution image

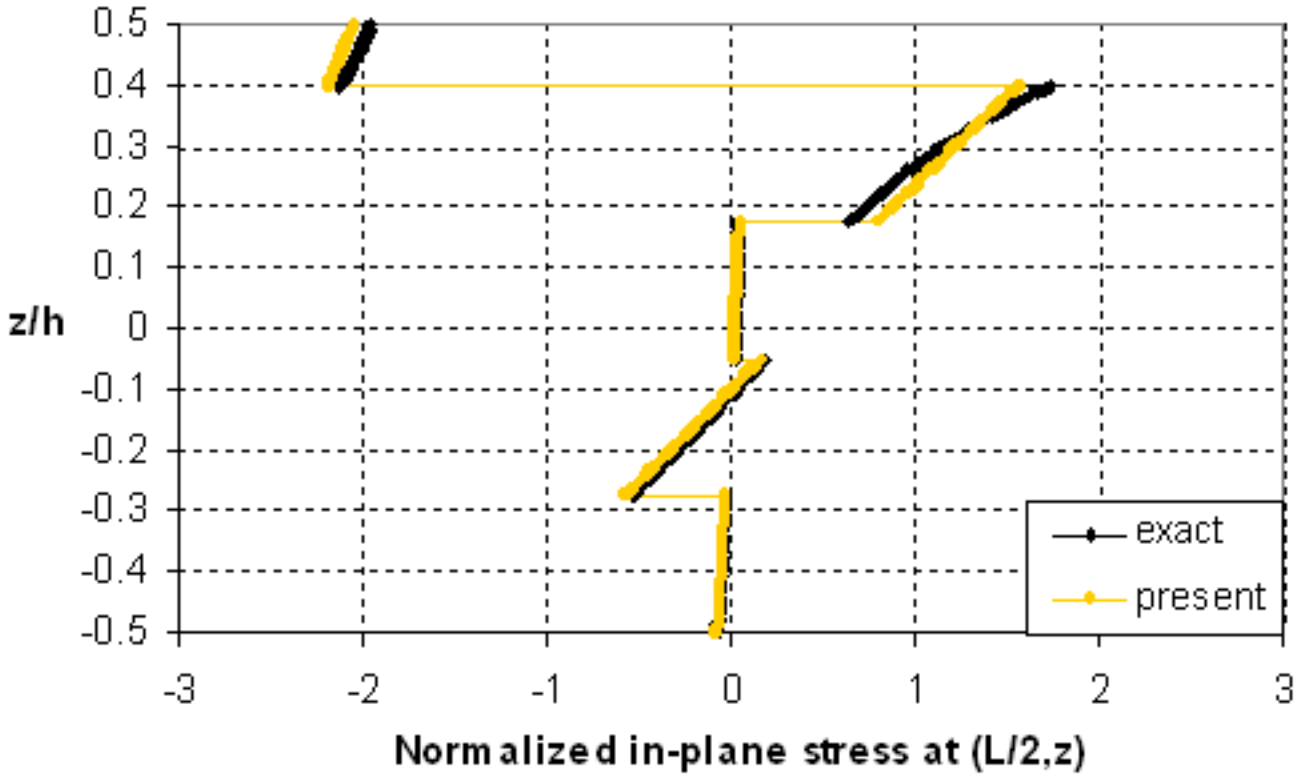

Fig. 13(d)
Click here to download high resolution image

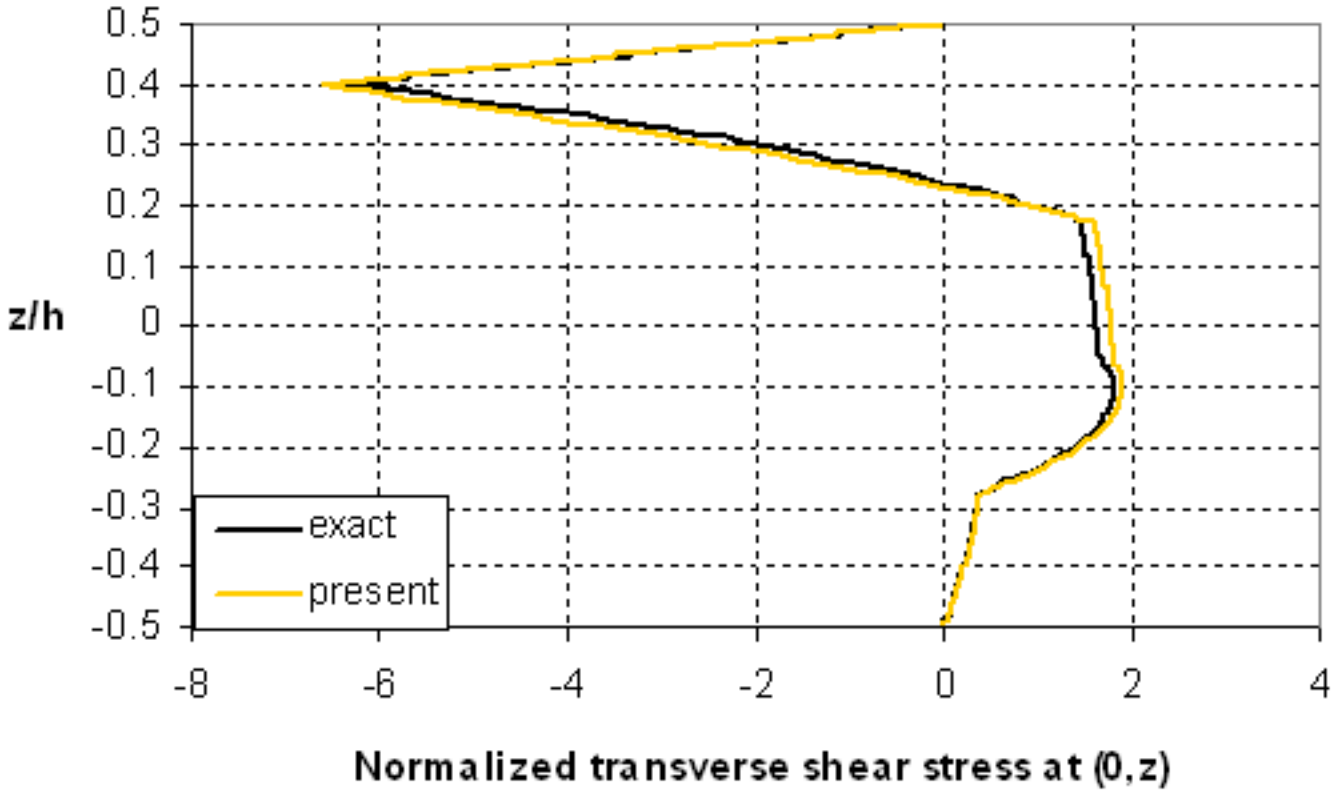

Fig. 13(e)
Click here to download high resolution image

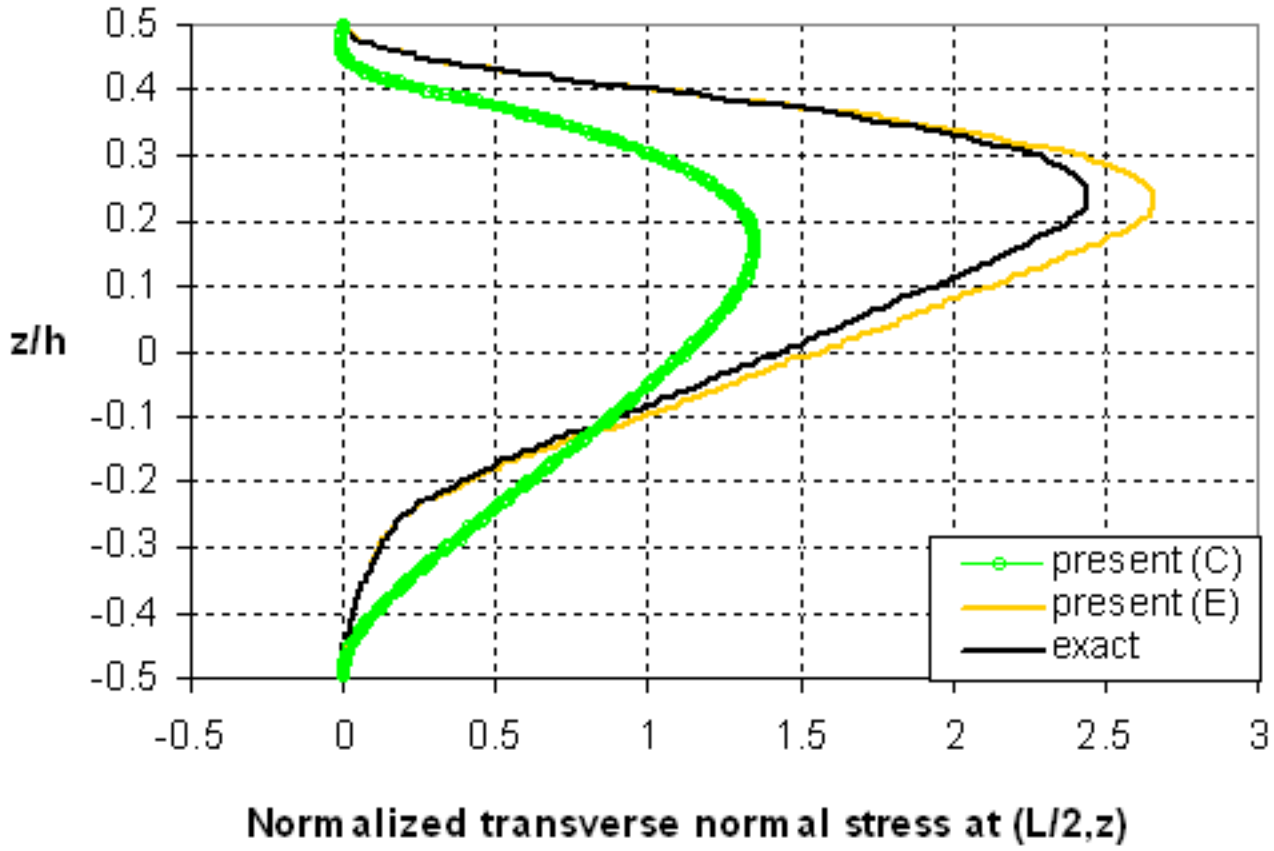

Fig. 13(f)

Click here to download high resolution image

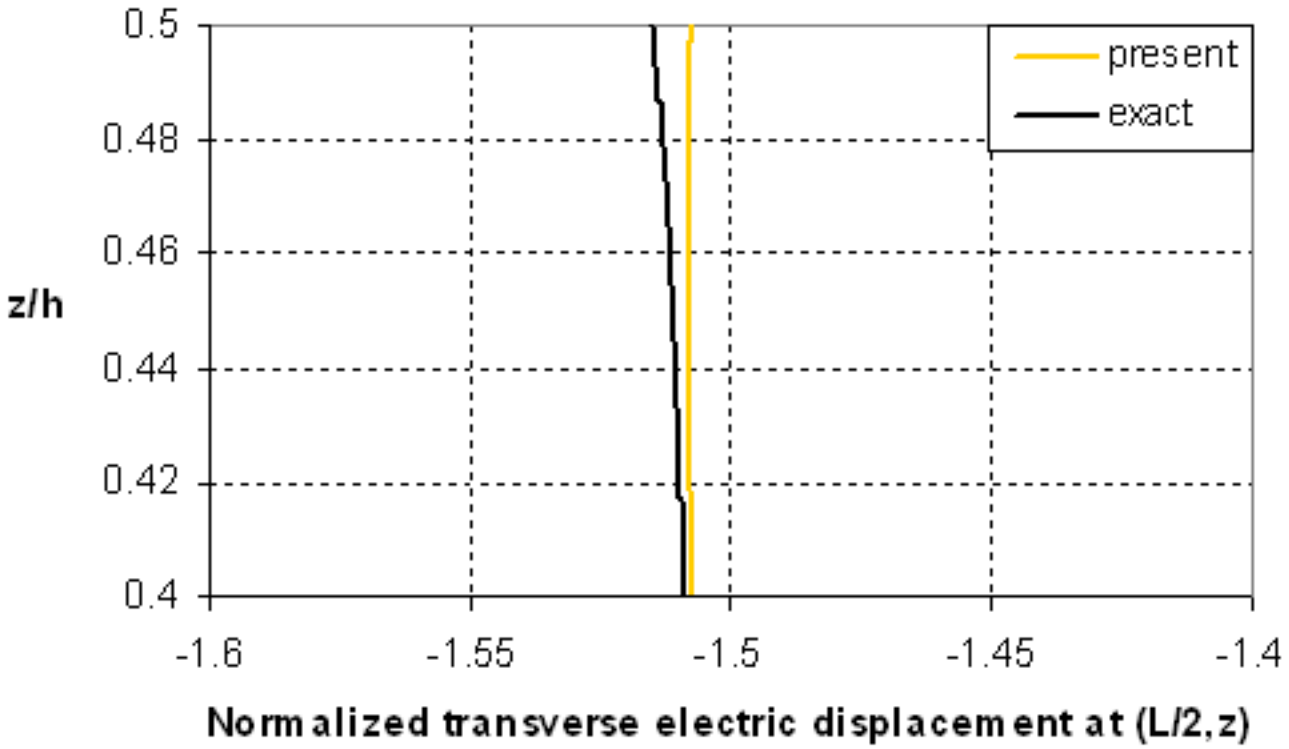

Fig. 14(a)

Click here to download high resolution image

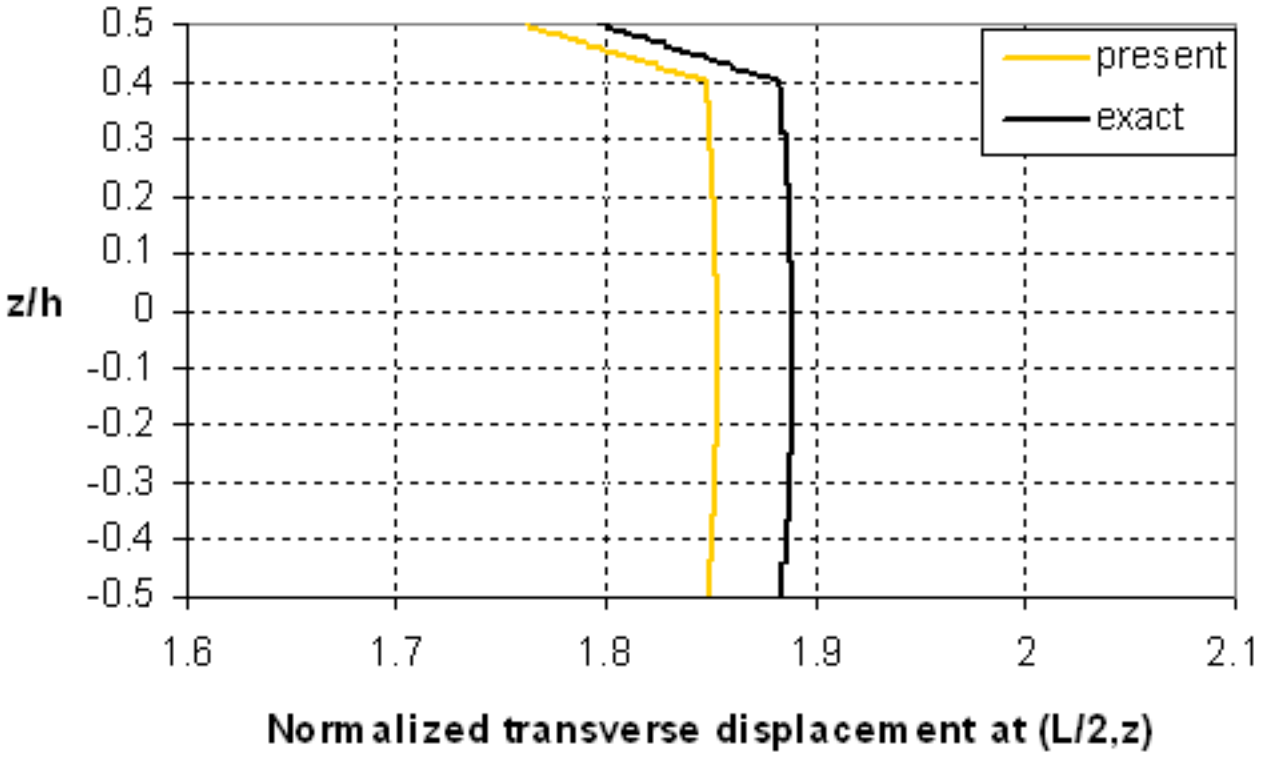

Fig. 14(b)
Click here to download high resolution image

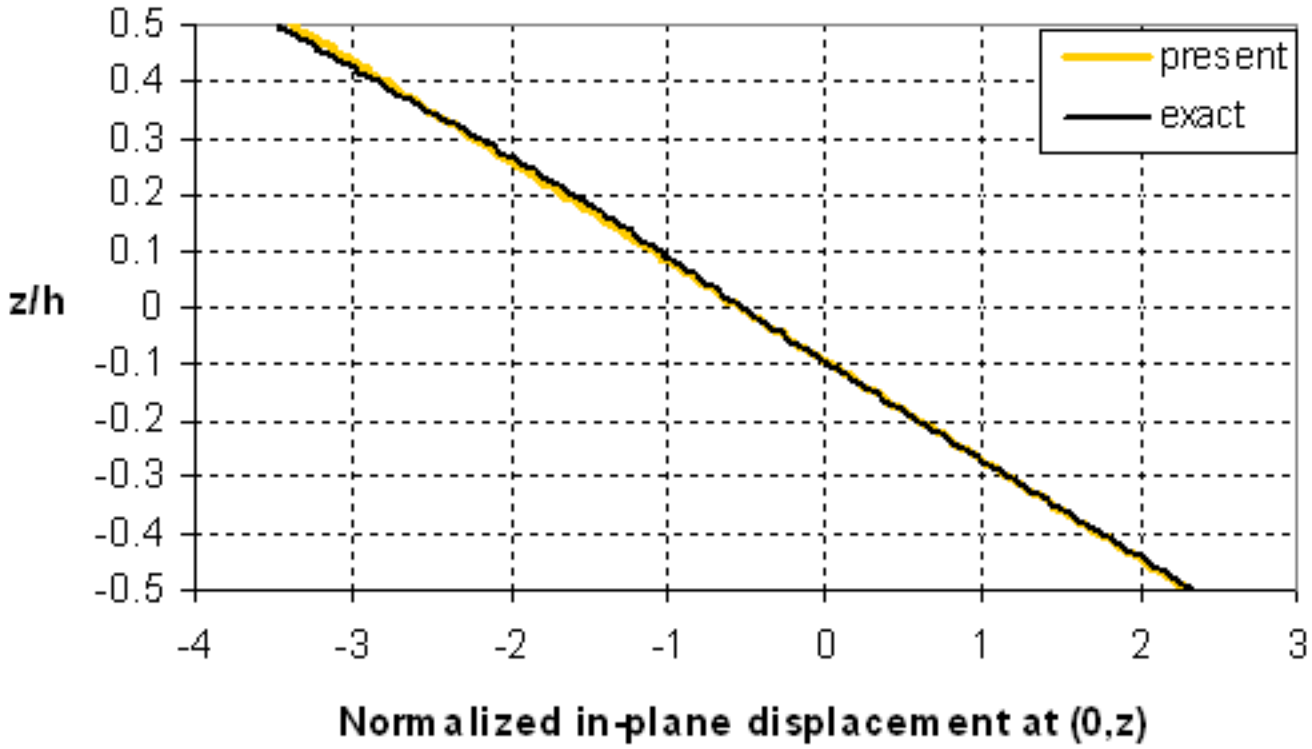

Fig. 14(c)
Click here to download high resolution image

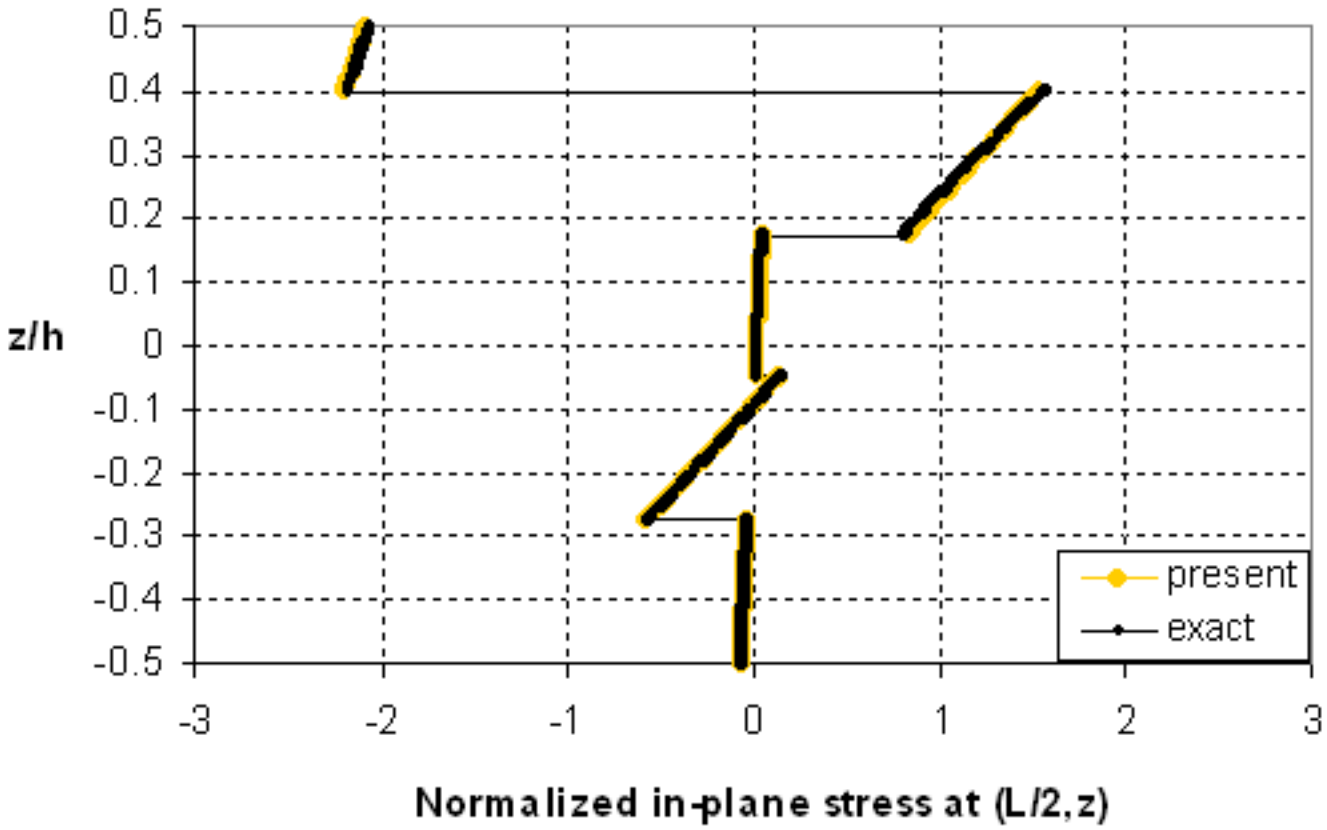

Fig. 14(d)
Click here to download high resolution image

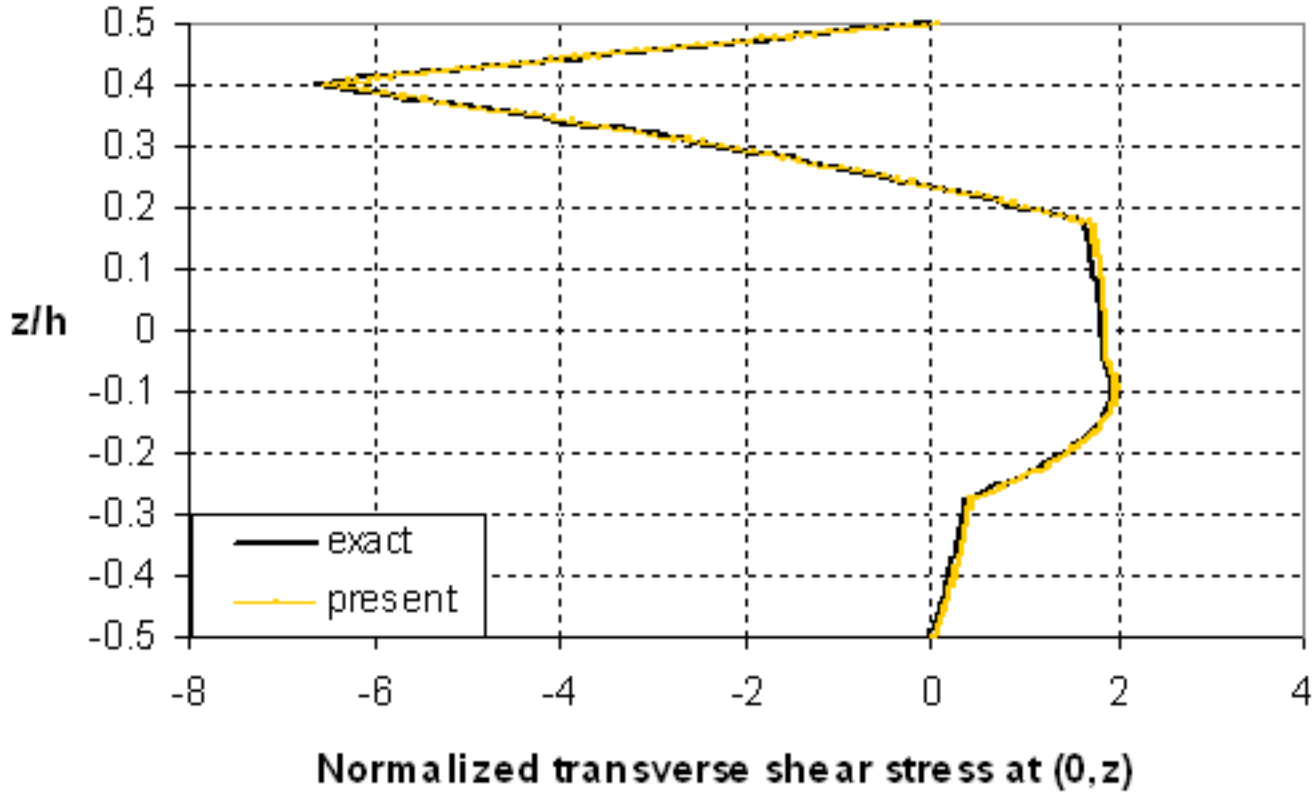

Fig. 14(e)
Click here to download high resolution image

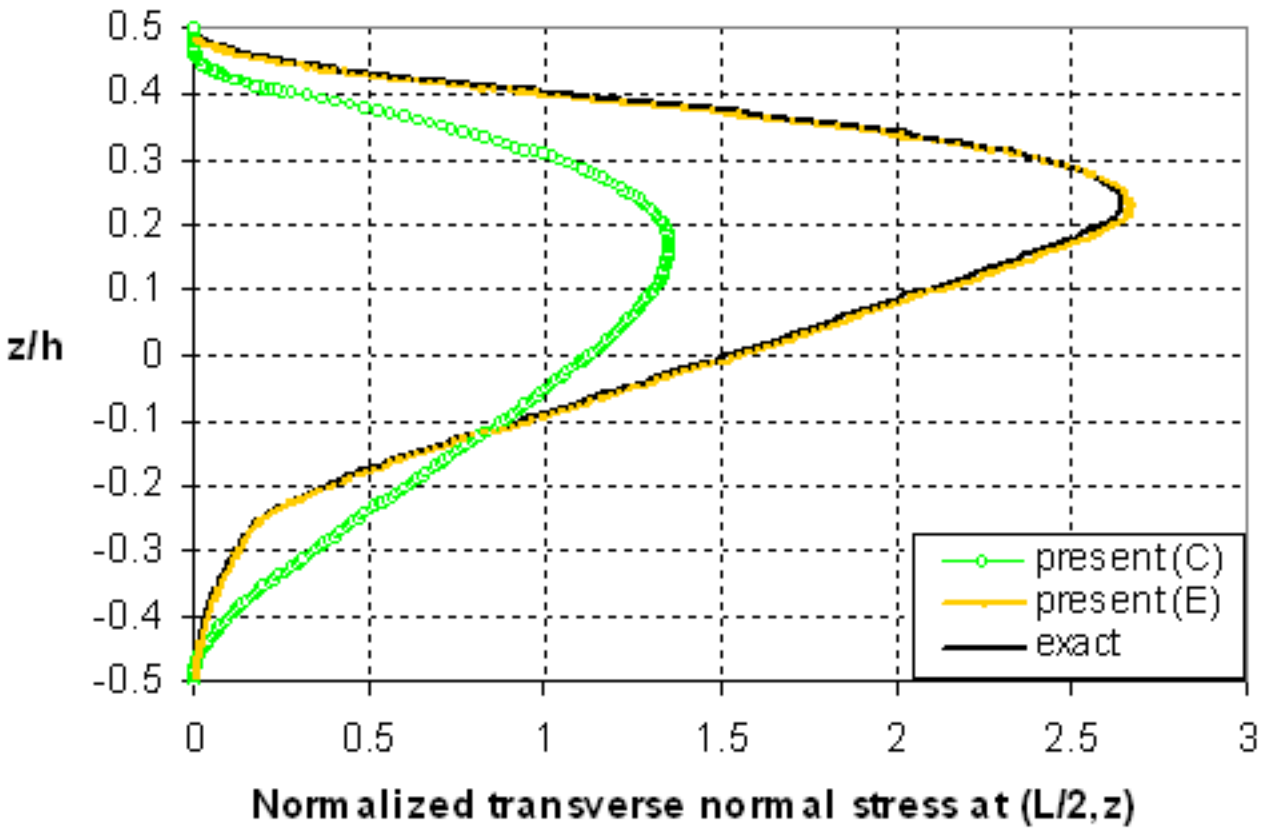

Fig. 14(f)
Click here to download high resolution image

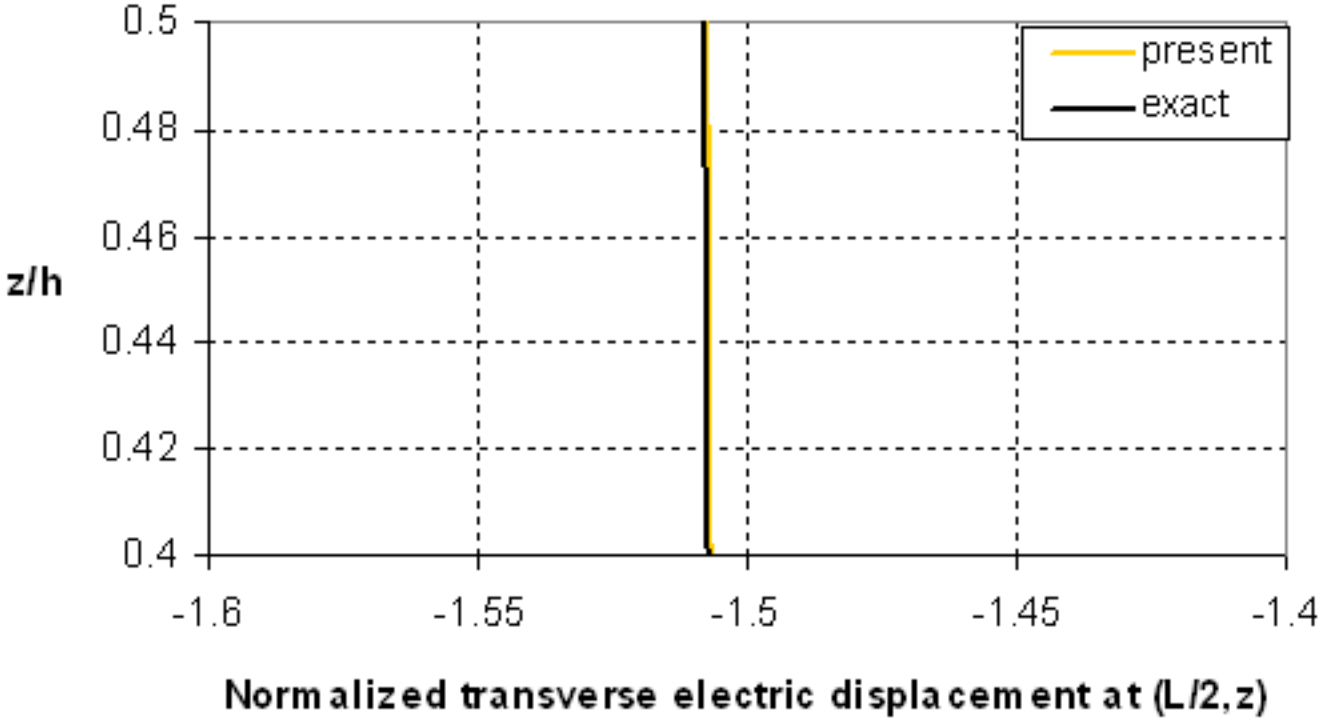

Fig. 15

Click here to download high resolution image

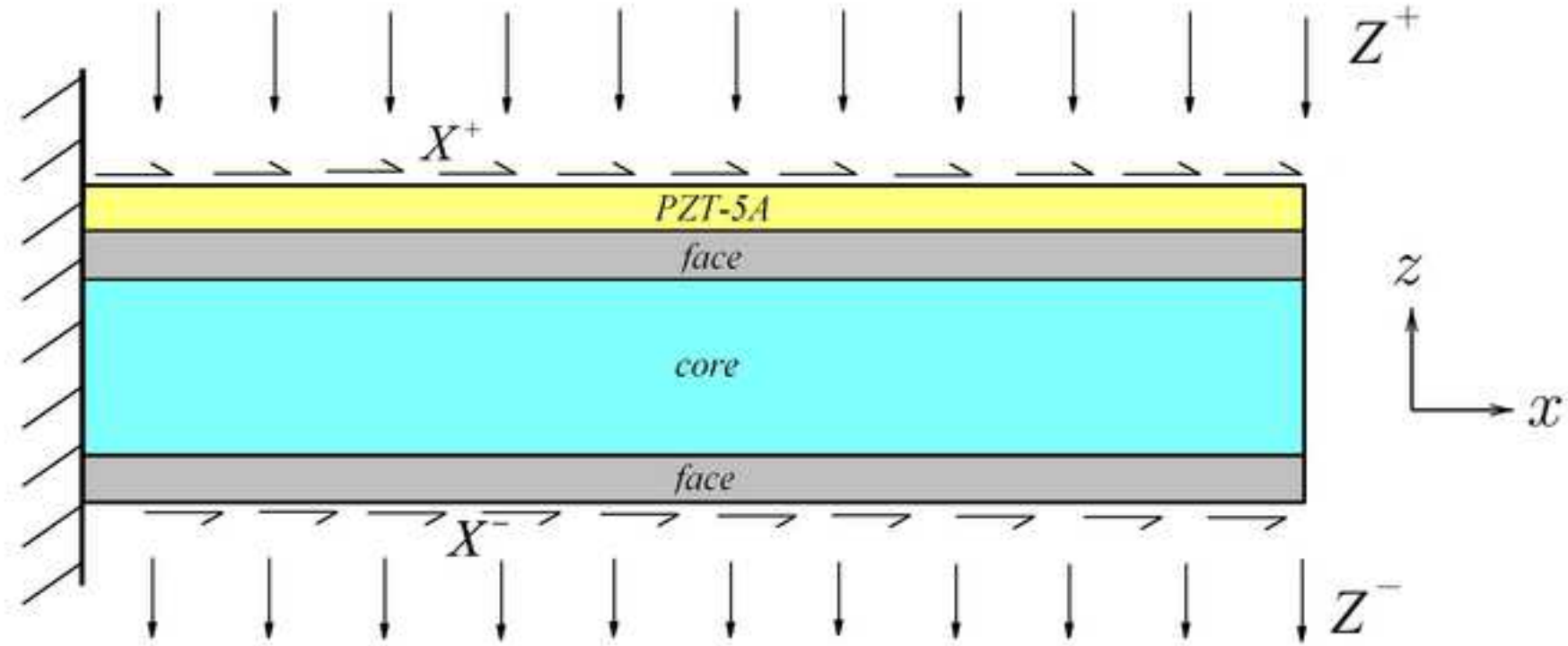

Fig. 16(a)

Click here to download high resolution image

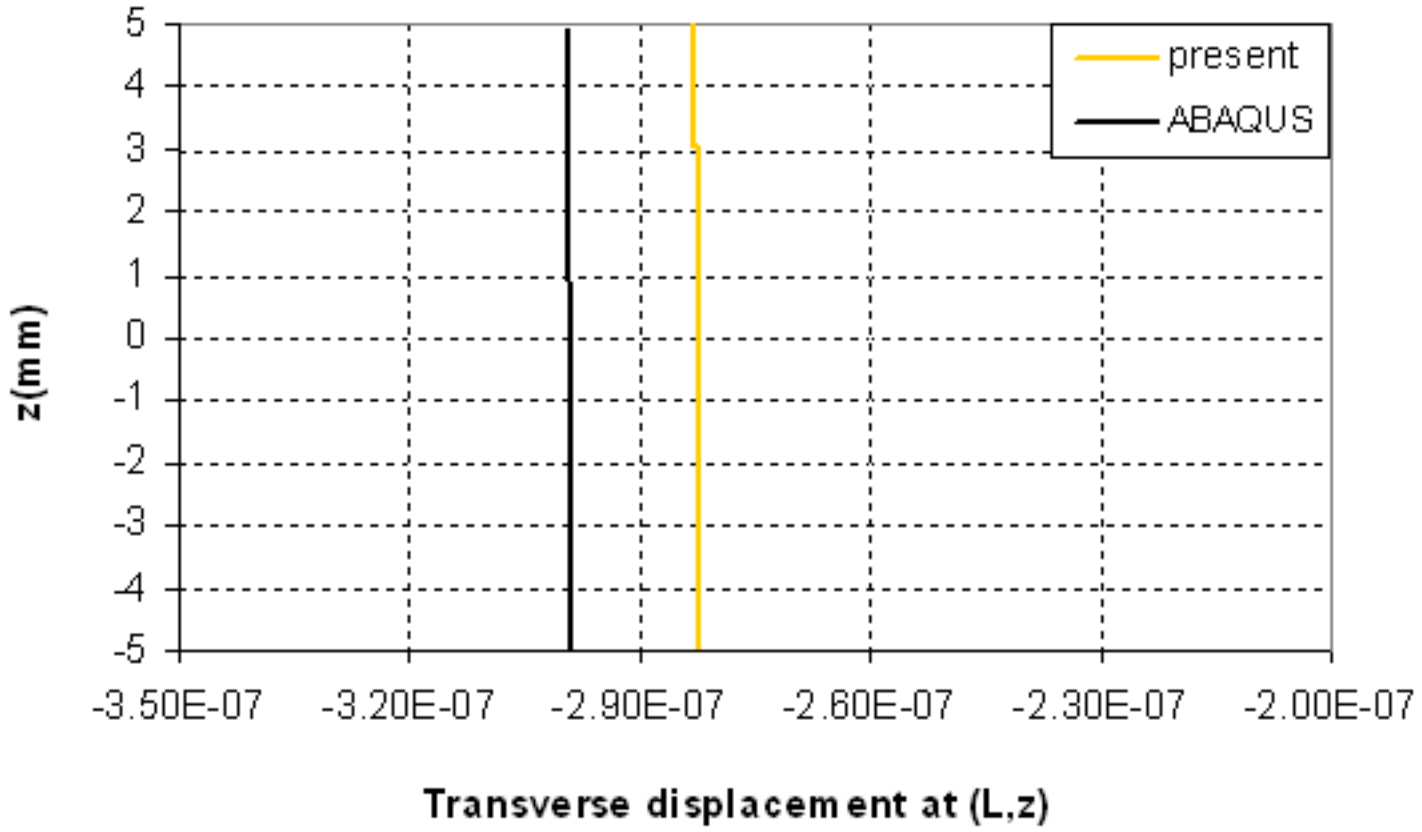

Fig. 16(b)
Click here to download high resolution image

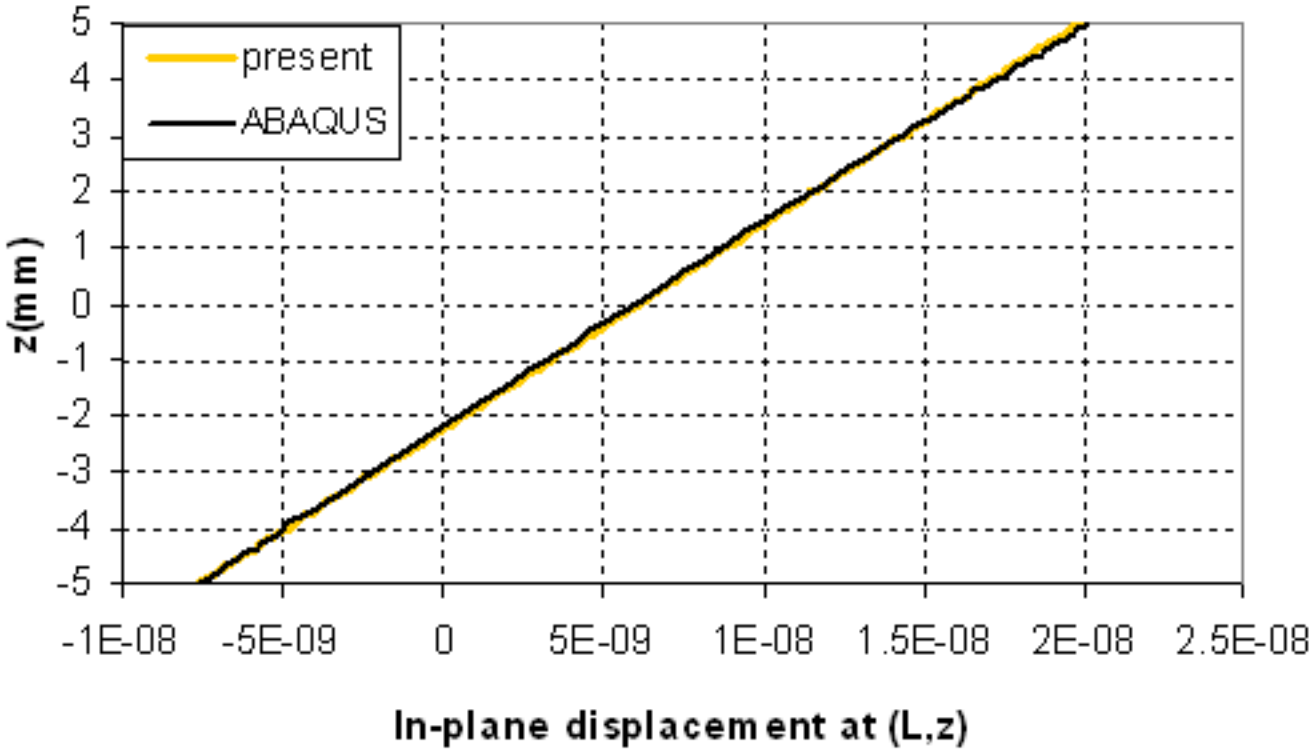

Fig. 16(c)
Click here to download high resolution image

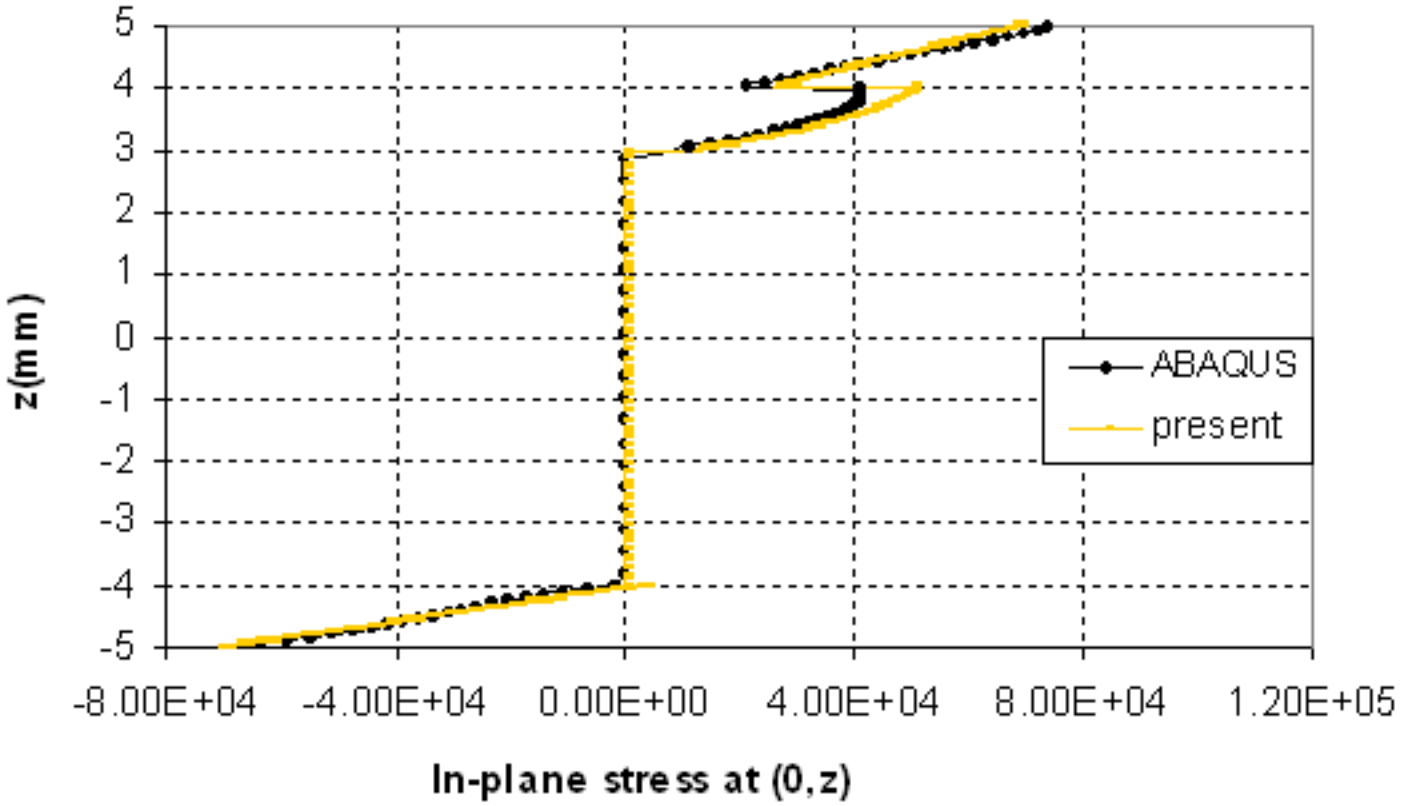

Fig. 16(d)

Click here to download high resolution image

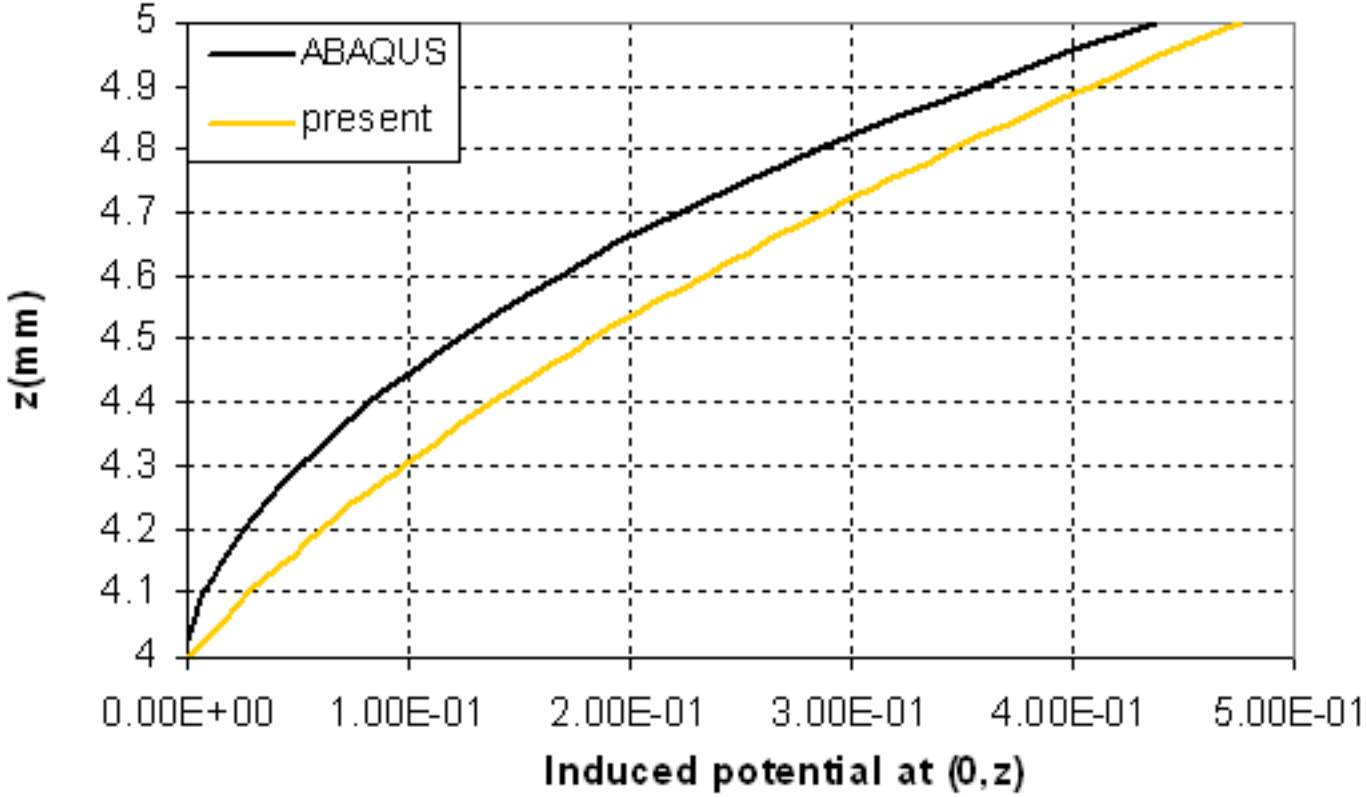

Fig. 17(a)
Click here to download high resolution image

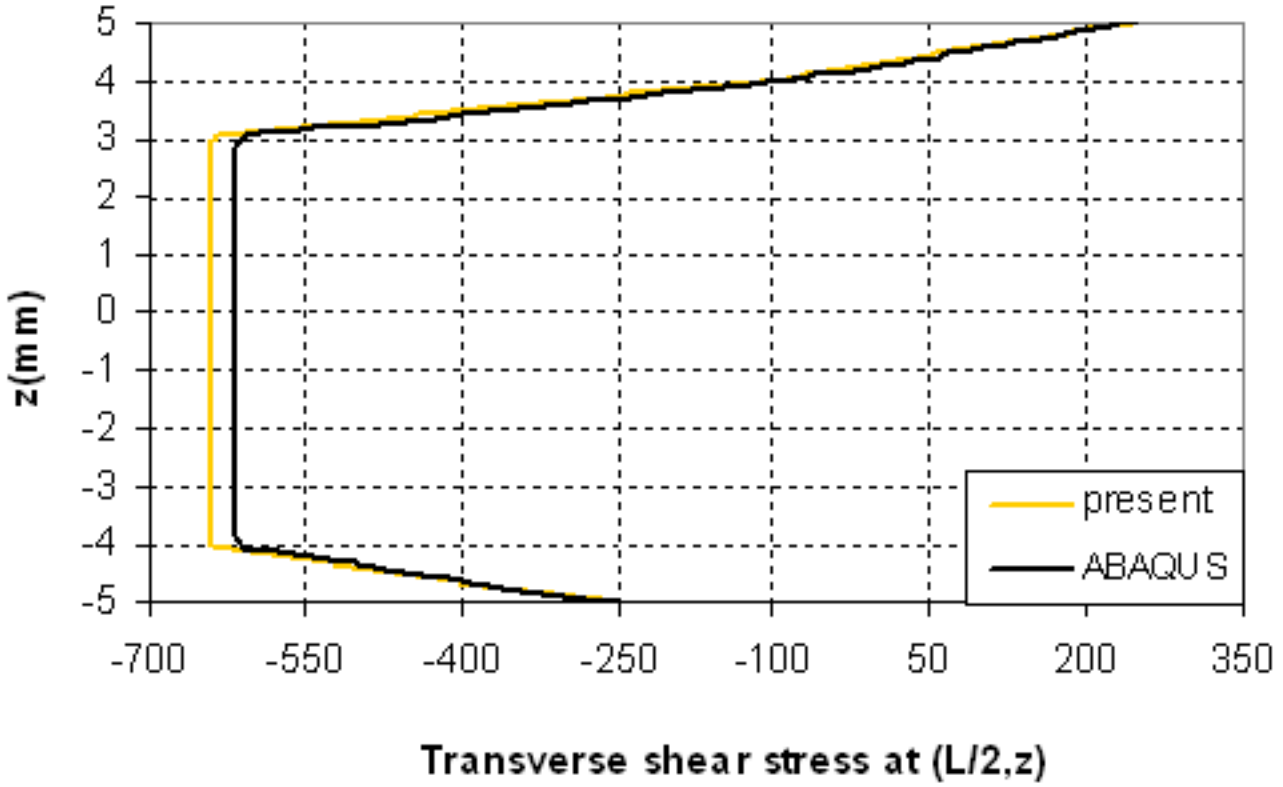

Fig. 17(b)
Click here to download high resolution image

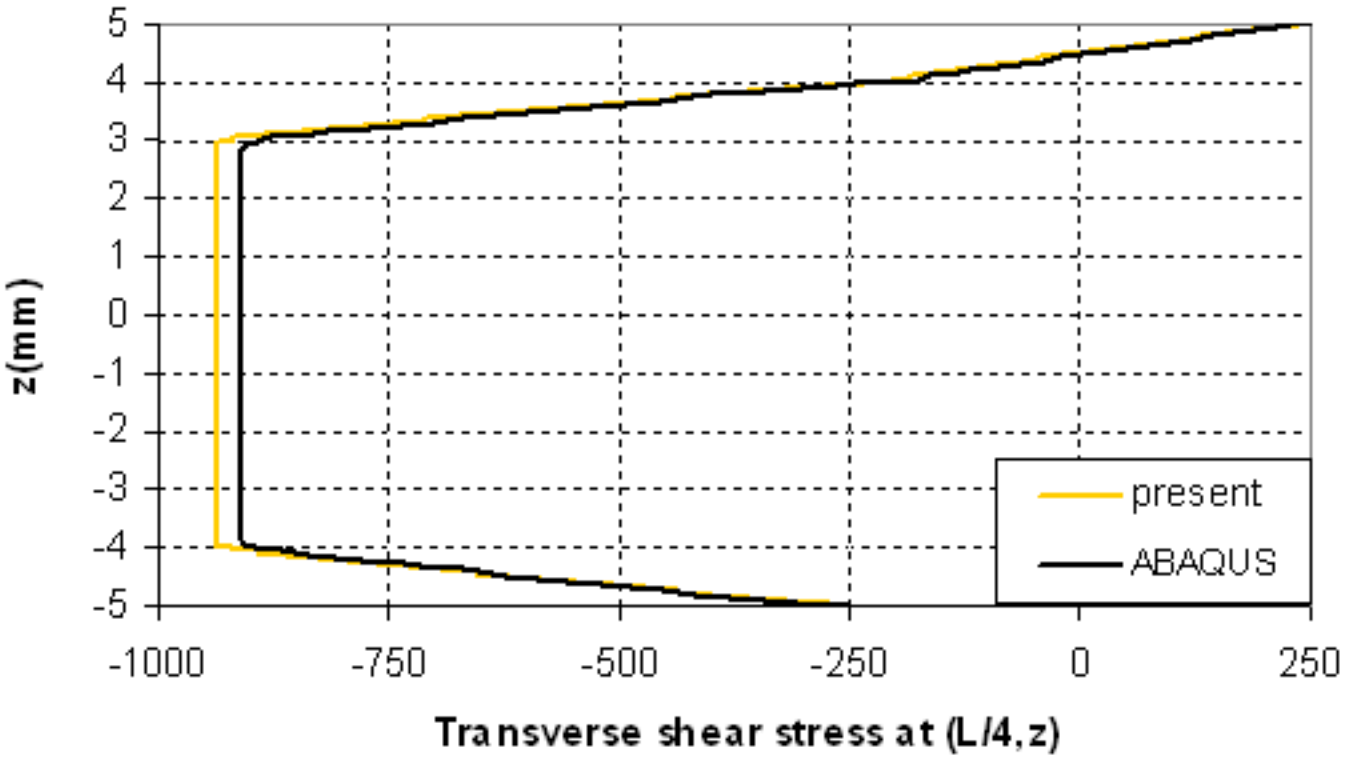

Fig. 17(c)
Click here to download high resolution image

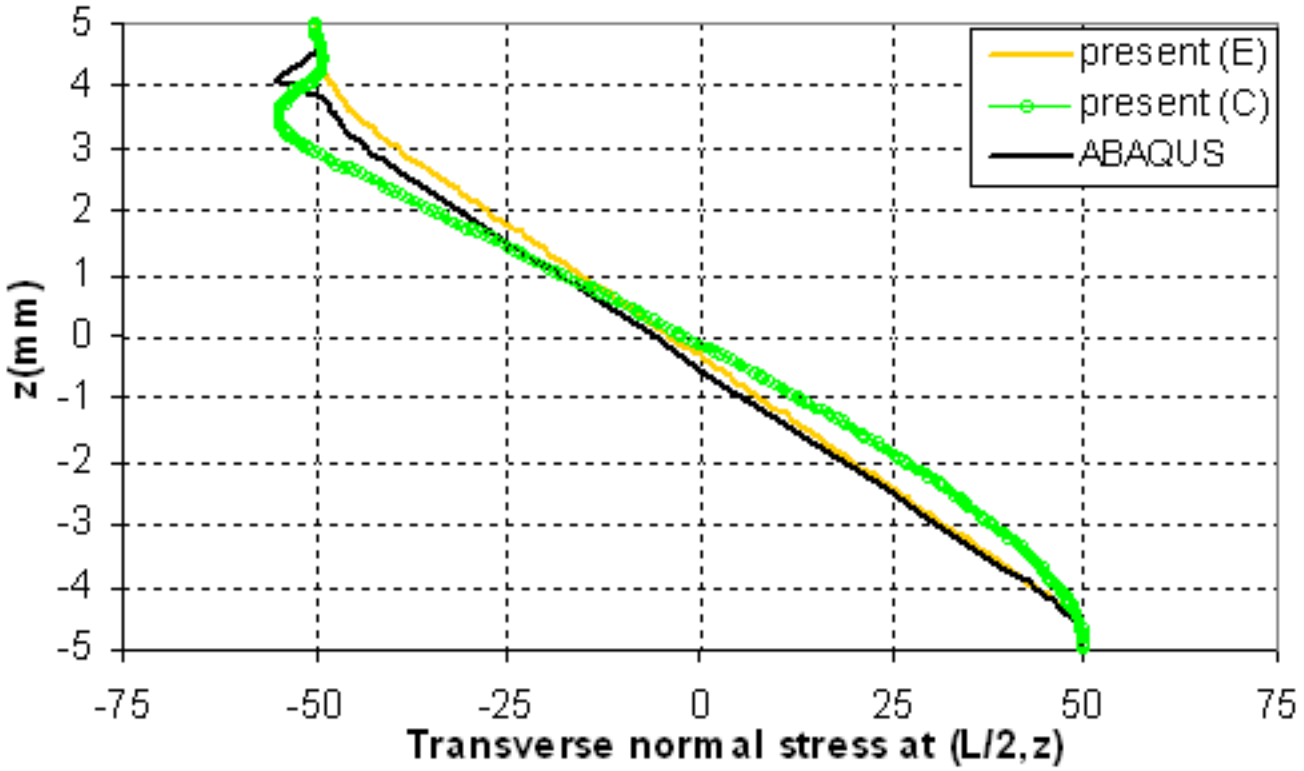

Fig. 17(d)
Click here to download high resolution image

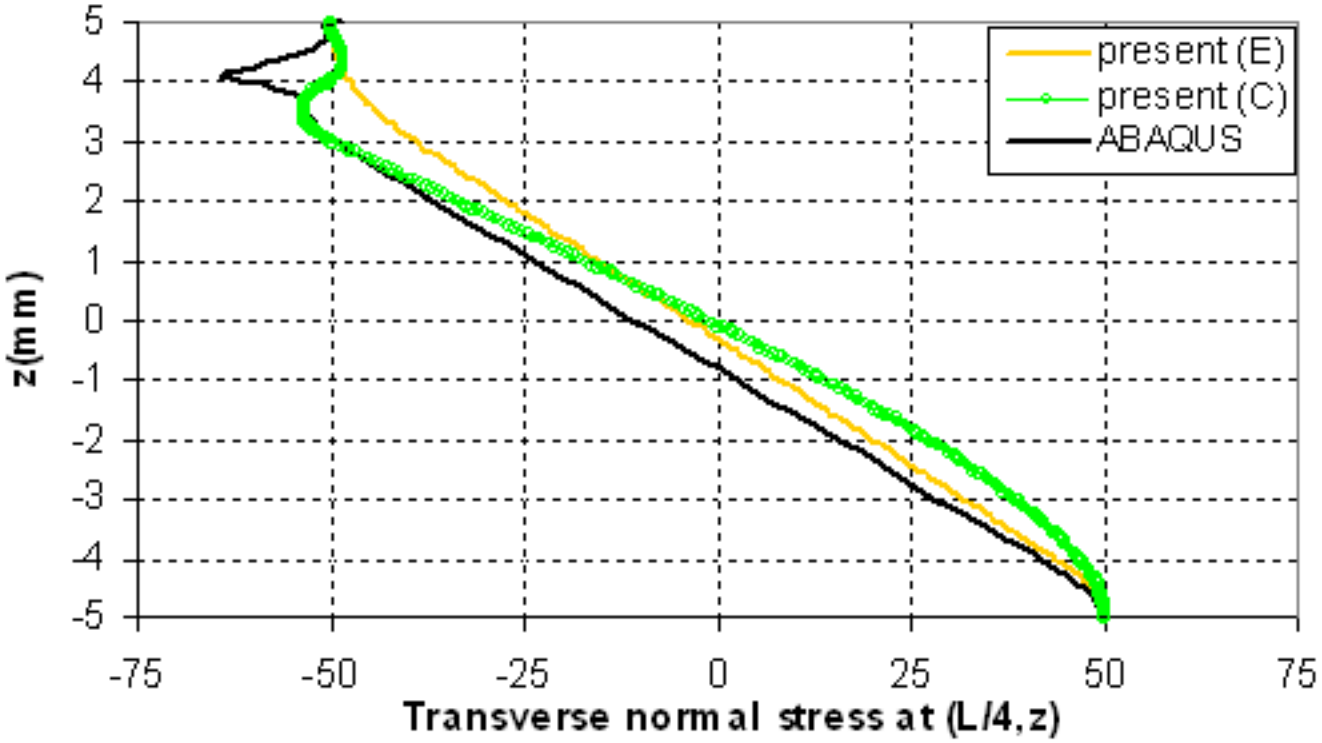

Fig. 18(a)

Click here to download high resolution image

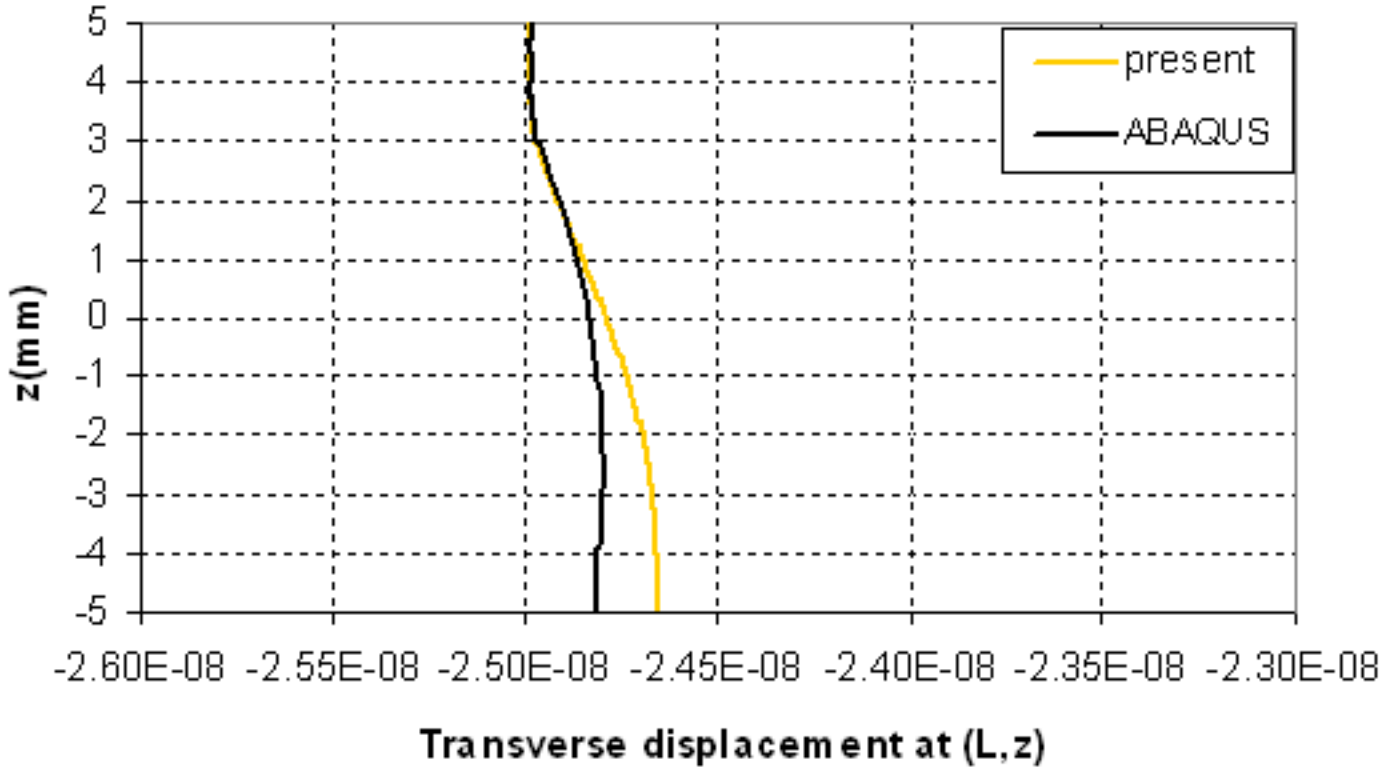

Fig. 18(b)

Click here to download high resolution image

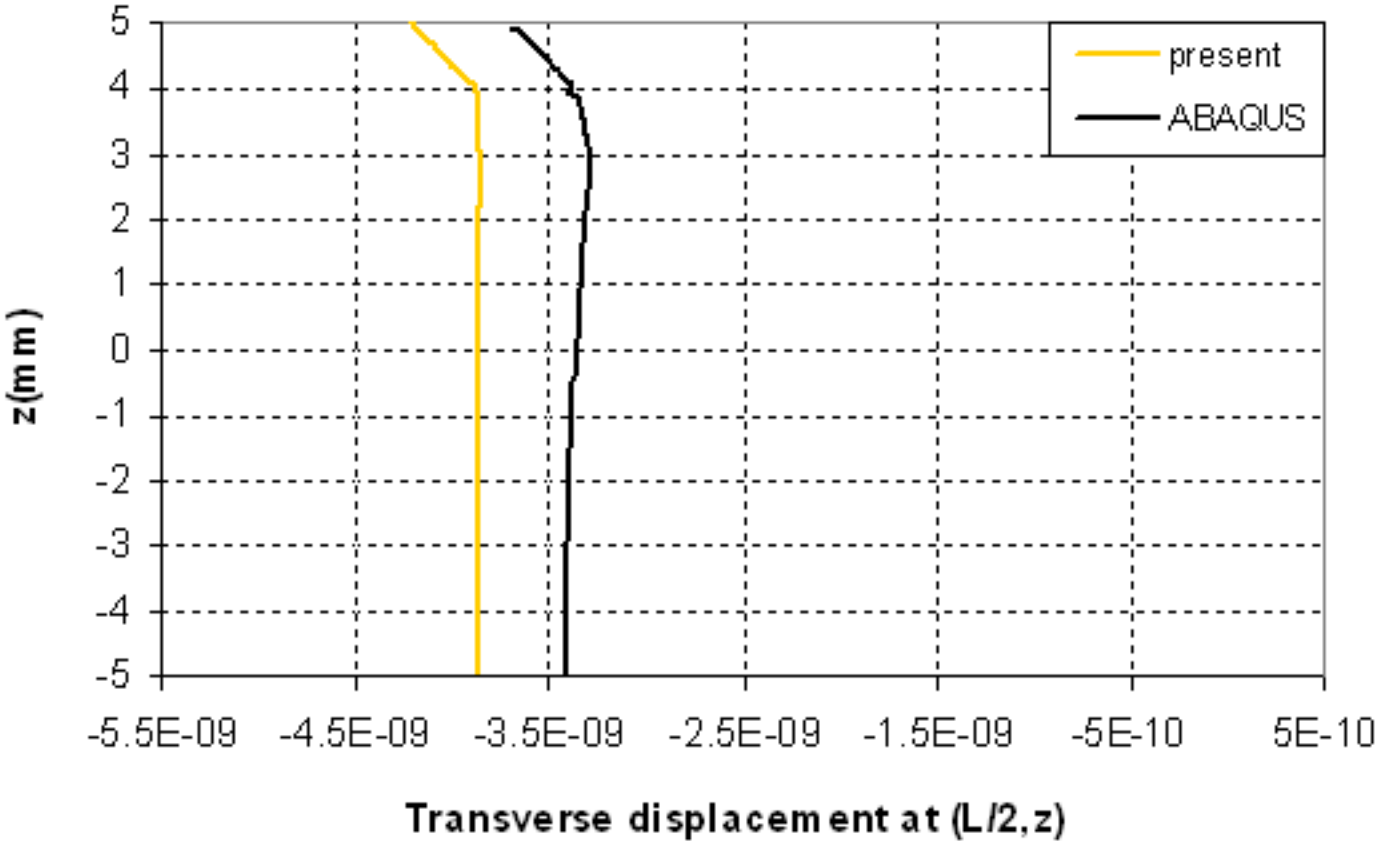

Fig. 18(c)
Click here to download high resolution image

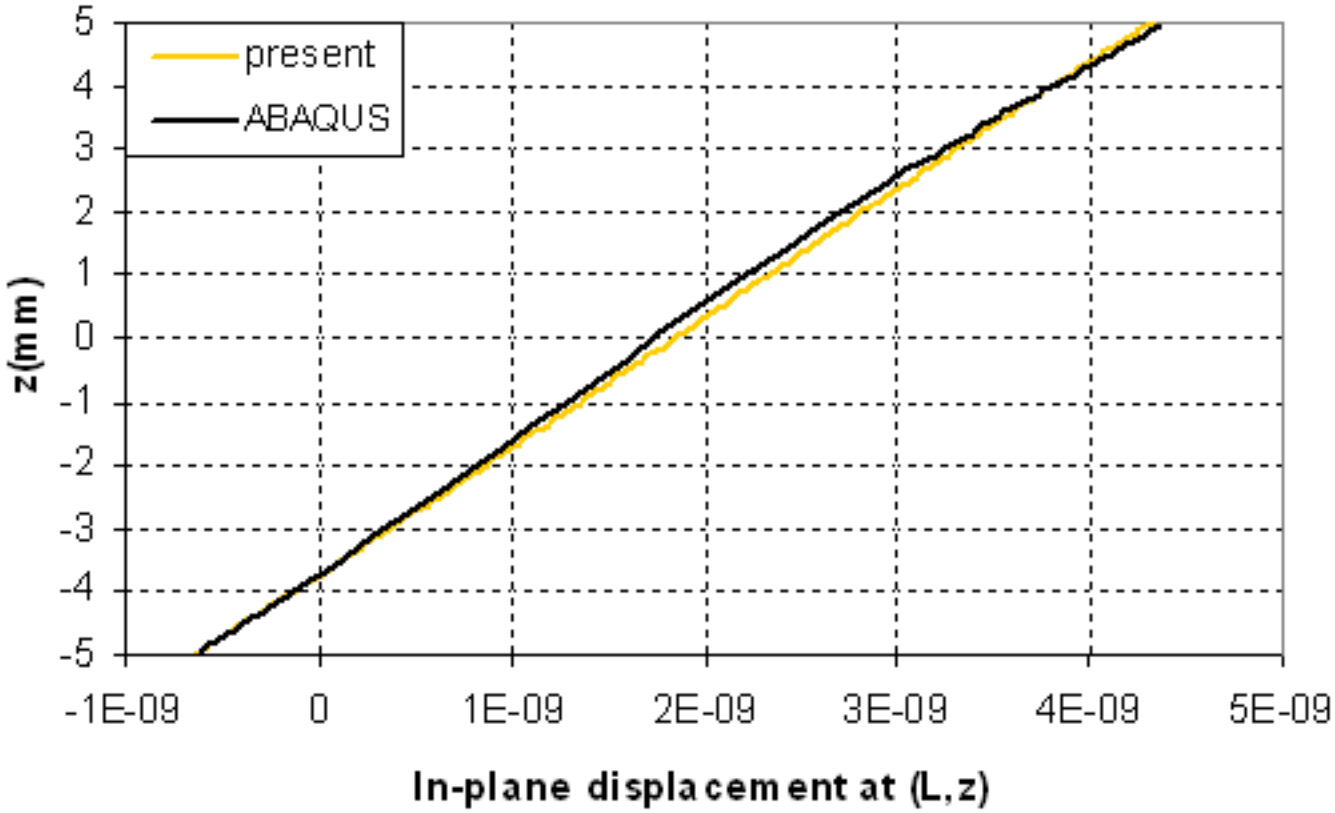

Fig. 18(d)

Click here to download high resolution image

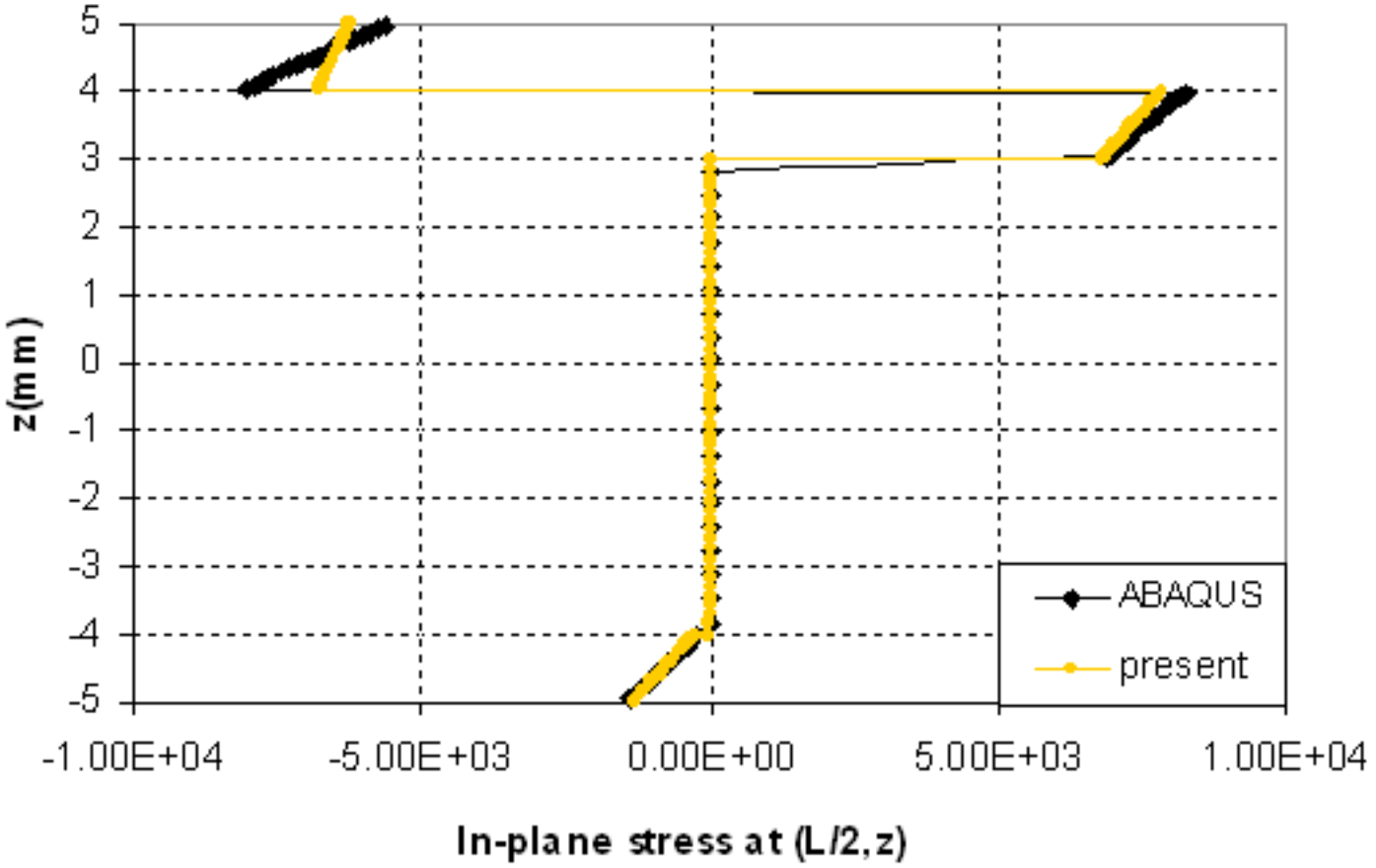

Fig. 18(e)
Click here to download high resolution image

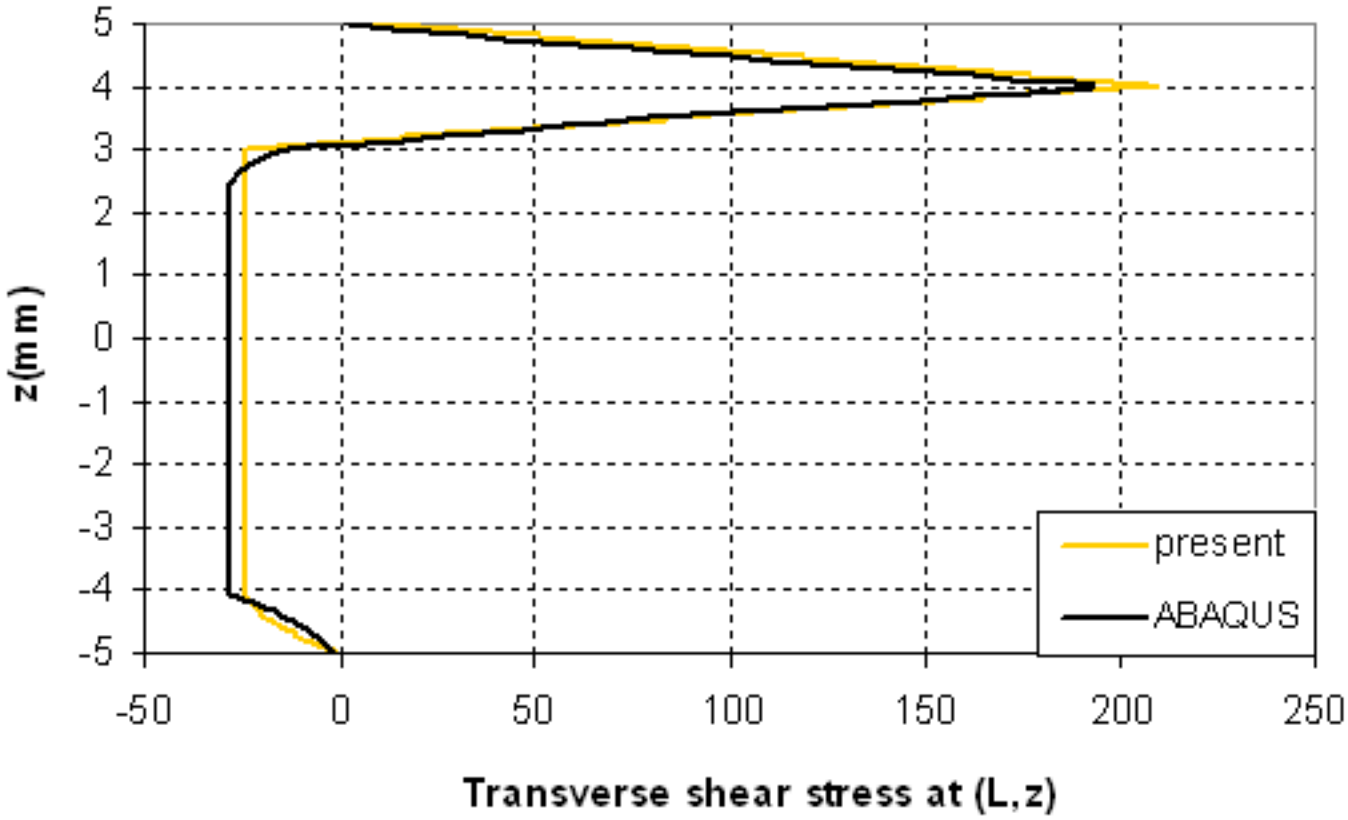

Fig. 18(f)
Click here to download high resolution image

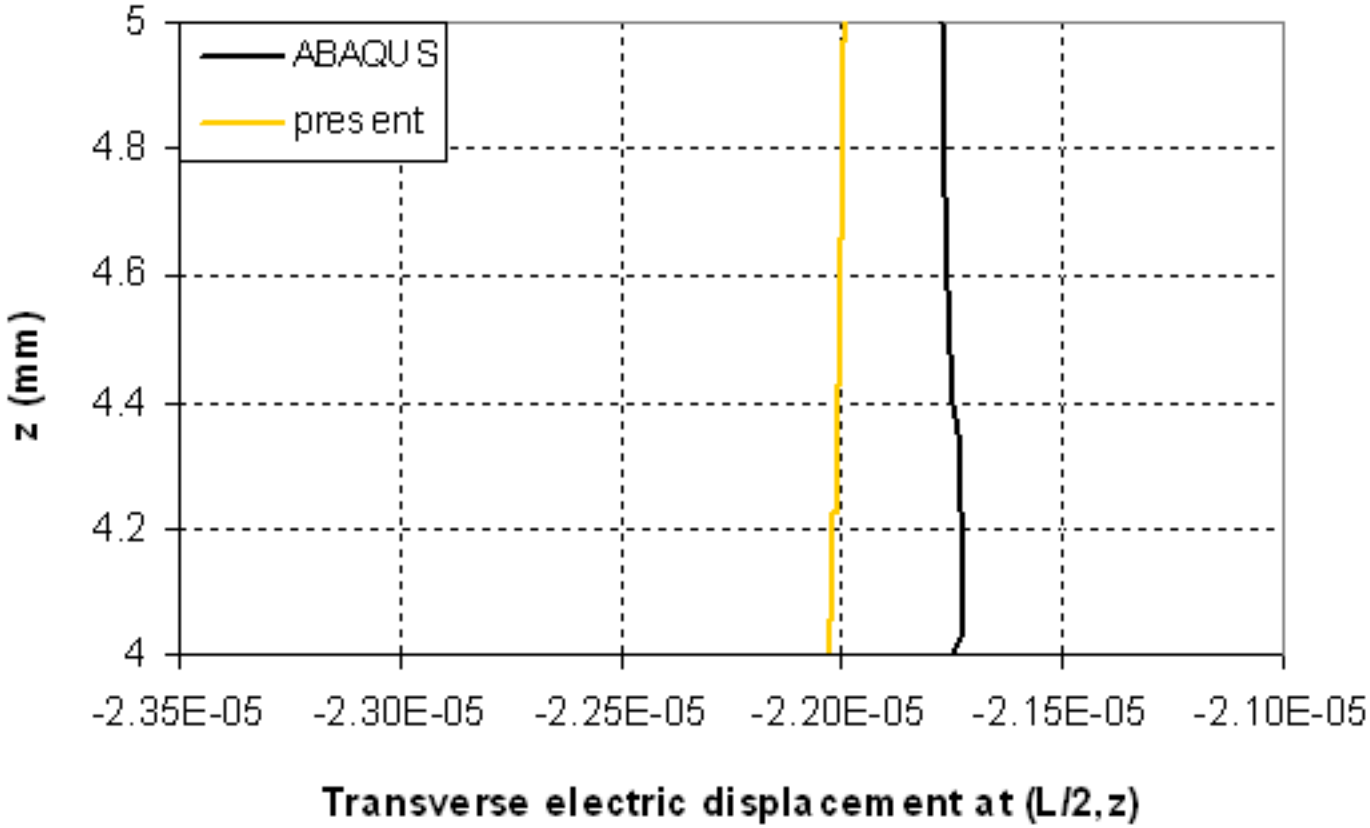

Table 1

Click here to download high resolution image

	No. element					
	2	4	8	12	15	exact
$\bar{w}(0.5L,0)$	-1.2736	-1.2735	-1.2734	-1.2733	-1.2733	-1.2971
$\bar{u}(0,0.5h)$	1.6364	1.6361	1.6360	1.6358	1.6357	1.6797
$\bar{\sigma}_{xx}(0.5L,0.5h)$	-0.3460	-0.3332	-0.3254	-0.3209	-0.3214	-0.3409
$\bar{\sigma}_{xx}(0.5L,0.4^{-}h)$	-0.7228	-0.6984	-0.6933	-0.6943	-0.6953	-0.7065
$\bar{\tau}_{xz}(0,0)$	-0.3957	-0.4249	-0.4325	-0.4340	-0.4345	-0.4343
$\bar{\sigma}_{zz}(0.5L,0)$	-0.3796	-0.5116	-0.5476	-0.5544	-0.5565	-0.5361
$\bar{\phi}(0.5L,0.5h)$	*8.6534*	*8.3200*	*8.2332*	*8.2107*	8.2106	7.9202

Table 2

Click here to download high resolution image

	S	Present	Error (%)	Exact
$\bar{w}(0.5L,0)$	4	-2.9516	3.65	-3.0635
	10	-1.2733	1.83	-1.2971
	100	-0.9441	0.03	-0.9444
$\bar{u}(0,0.5h)$	4	2.2373	9.73	2.4785
	10	1.6357	2.62	1.6797
	100	1.5213	0.03	1.5218
$\bar{\sigma}_{xx}(0.5L,0.5h)$	4	-0.4718	8.21	-0.5140
	10	-0.3214	5.72	-0.3409
	100	-0.3069	0.03	-0.3068
$\bar{\sigma}_{xx}(0.5L,0.4^{-}h)$	4	-0.7447	12.16	-0.8478
	10	-0.6953	1.59	-0.7065
	100	-0.6768	0.06	-0.6764
$\bar{\tau}_{xz}(0,0)$	4	-0.4170	2.63	-0.4063
	10	-0.4345	0.05	-0.4343
	100	-0.4395	0.16	-0.4402
$\bar{\sigma}_{zz}(0.5L,0)$	4	-0.5466 (-0.4012)	2.90 (24.47)	-0.5312
	10	-0.5565 (-0.4084)	2.64 (24.68)	-0.5422
	100	-0.5503 (-0.4323)	1.08 (20.59)	-0.5444
$\bar{\phi}(0.5L,0.5h)$	4	9.4066	19.13	7.8963
	10	8.2106	3.67	7.9202
	100	7.8481	0.45	7.8836

Table 3

Click here to download high resolution image

	No. element					
	2	4	8	12	15	exact
$\tilde{w}(0.5L, 0)$	1.2354	1.2359	1.2359	1.2359	1.2359	1.2837
$\tilde{w}(0.5L, 0.5h)$	1.1429	1.1438	1.1439	1.1439	1.1438	1.1922
$\tilde{u}(0, 0.5h)$	-2.9243	-2.9225	-2.9217	-2.9212	-2.9207	-3.0165
$\tilde{\sigma}_{xx}(0.5L, 0.5h)$	-2.1360	-2.1547	-2.1597	-2.1606	-2.1609	-2.1442
$\tilde{\sigma}_{xx}(0.5L, 0.4^{-}h)$	1.4519	1.4040	1.3908	1.3884	1.3876	1.4286
$\tilde{\tau}_{xz}(0, 0.4h)$	-6.2354	-6.7442	-6.8404	-6.8065	-6.7630	-6.8678
$\max(\tilde{\sigma}_{xx}(0.5L, z))$	1.9963	2.7083	2.9021	2.9386	2.9484	2.9220
$\tilde{D}_z(0.5L, 0.5h)$	-1.5052	-1.5046	-1.5044	-1.5044	-1.5044	-1.5053

Table 4

Click here to download high resolution image

	S	Present	Error	Exact
$\widetilde{w}(0.5L, 0)$	4	1.5266	12.11	1.7370
	10	1.2358	3.73	1.2837
	100	1.1859	0.06	1.1866
$\widetilde{w}(0.5L, 0.5h)$	4	0.9483	20.58	1.1941
	10	1.1438	4.06	1.1922
	100	1.1850	0.05	1.1856
$\widetilde{u}(0, 0.5h)$	4	-3.0369	16.52	-3.6380
	10	-2.9207	3.18	-3.0165
	100	-2.8883	0.04	-2.8896
$\widetilde{\sigma}_{xx}(0.5L, 0.5h)$	4	-2.1374	5.21	-2.0316
	10	-2.1609	0.78	-2.1442
	100	-2.1669	0.01	-2.1672
$\widetilde{\sigma}_{xx}(0.5L, 0.4^{-}h)$	4	1.4093	12.82	1.6166
	10	1.3876	2.87	1.4286
	100	1.3901	0.06	1.3893
$\widetilde{\tau}_{xz}(0, 0.4h)$	4	-6.8617	4.24	-6.5829
	10	-6.7630	1.53	-6.8678
	100	-6.9128	0.20	-6.9266
$\max(\widetilde{\sigma}_{zz}(0.5L, z))$	4	2.9364	10.15	2.6657
	10	2.9484	0.90	2.9220
	100	2.9531	0.77	2.9759
$\widetilde{D}_{z}(0.5L, 0.5h)$	4	-1.5043	0.52	-1.5122
	10	-1.5044	0.06	-1.5053
	100	-1.5039	0.00	-1.5039

Table 5

Click here to download high resolution image

	S	Present	Error (%)	Exact
$\bar{w}(0.5L, 0)$	4	-3.7732	6.49	-4.0352
	10	-2.1014	2.96	-2.1656
	100	-1.7867	0.03	-1.7873
$\bar{u}(0, 0.5h)$	4	3.0682	5.92	3.2611
	10	2.4609	2.01	2.5113
	100	2.3606	0.02	2.3610
$\bar{\sigma}_{xx}(0.5L, 0.5h)$	4	-0.6484	3.48	-0.6718
	10	-0.5128	0.83	-0.5086
	100	-0.4762	0.04	-0.4760
$\bar{\sigma}_{xx}(0.5L, 0.4^{-}h)$	4	-1.0776	3.59	-1.1177
	10	-1.0027	1.28	-1.0157
	100	-0.9943	0.08	-0.9935
$\bar{\tau}_{xz}(0, 0)$	4	-0.5425	0.97	-0.5373
	10	-0.5825	0.54	-0.5794
	100	-0.5877	0.14	-0.5885
$\bar{\sigma}_{zz}(0.5L, 0)$	4	-0.3739 (-0.2395)	1.63 (36.99)	-0.3801
	10	-0.3750 (-0.2381)	0.81 (35.99)	-0.3720
	100	-0.3759 (-0.2819)	1.59 (23.81)	-0.3700
$\bar{\phi}(0.5L, 0.5h)$	4	15.1164	31.11	11.5294
	10	12.7409	6.94	11.9142
	100	11.8757	0.57	11.9436

Table 6

Click here to download high resolution image

		Present	Error	Exact
$\bar{w}(0.5L, 0)$	4	2.1584	5.90	2.2937
	10	1.8534	1.86	1.8886
	100	1.8003	0.03	1.8009
$\bar{w}(0.5L, 0.5h)$	4	1.5810	9.47	1.7464
	10	1.7614	1.99	1.7971
	100	1.7994	0.03	1.8000
$\bar{u}(0, 0.5h)$	4	-3.5170	12.55	-4.0218
	10	-3.3908	2.27	-3.4696
	100	-3.3560	0.03	-3.3571
$\bar{\sigma}_{xx}(0.5L, 0.5h)$	4	-2.0466	4.48	-1.9588
	10	-2.0719	0.66	-2.0584
	100	-2.0783	0.02	-2.0787
$\bar{\sigma}_{xx}(0.5L, 0.4^{-}h)$	4	1.5638	9.82	1.7340
	10	1.5399	2.17	1.5741
	100	1.5419	0.06	1.5409
$\bar{\tau}_{xz}(0, 0.4h)$	4	-6.6259	3.39	-6.4088
	10	-6.5523	1.59	-6.6585
	100	-6.6963	0.20	-6.7097
$\max(\bar{\sigma}_{xx}(0.5L, z))$	4	2.6616	9.07	2.4403
	10	2.6640	0.84	2.6417
	100	2.6655	0.68	2.6837
$\bar{D}_z(0.5L, 0.5h)$	4	-1.5076	0.48	-1.5148
	10	-1.5076	0.05	-1.5083
	100	-1.5071	0.00	-1.5071